ELECTRON DIFFRACTION AND LIQUID CRYSTAL N.M.R. SPECTROSCOPY

Peter Douglas Blair

A thesis presented for the
Degree of Doctor of Philosophy
in the Faculty of Science
of The University of Edinburgh, 1984

EX LIBRIS UNIV. EDINBURGH CHEMISTRY LIBRARY

DECLARATION

I hereby declare that this thesis has been composed by me, and that the work described in it is my own and was carried out at the University of Edinburgh, except where due acknowledgement is made.

SUMMARY

This thesis investigates the validity of the combination of data from Electron Diffraction and Liquid Crystal Nuclear Magnetic Resonance Spectroscopy in the structural analysis of small inorganic molecules.

Electron Diffraction suffers from several major limitations, which are discussed in detail with specific examples. These problems can, to a certain extent, be overcome by the introduction of extra information from alternative sources. A novel source of such structural data is Liquid Crystal Nuclear Magnetic Resonance Spectroscopy. The theory behind this technique, and its practical limitations are discussed.

The physical significance of the structures derived from each technique are different, and the vibrational corrections, to render them compatible, are considered in depth.

A range of compounds containing several N.M.R. active (spin $\frac{1}{2}$) nuclei were prepared, using isotopic enrichment where required. A series of difluorophosphine pseudohalides and difluorophosphine sulphide were investigated by a combination of the two techniques, and the structures compared to previous work and related compounds. The structure of silyl cyanide was determined from Liquid Crystal N.M.R. Spectroscopy alone, and compared to that observed in the gas and solid phases.

The experimental procedures and spectral analysis techniques are reported in detail and the success of the combination of data from the two sources critically analysed.

ACKNOWLEDGMENTS

I should like to express my gratitude to the Science and Engineering Research Council for a grant, to I.C.I. Educational Trust for a scholarship, and to the University of Edinburgh for awarding me the Hope Prize and providing laboratory facilities.

I must thank my supervisor David Rankin for his constant stream of ideas and inspiration, Stephen Cradock, Heather Robertson and Chris Huntley for their words of wisdom, Lawrence Bell and John Millar for running my N.M.R. samples.

Finally, I should like to express my warm thanks to everyone at the University who helped make my time here so enjoyable.

CONTENTS

CHAPTER 1

ELECTRON DIFFRACTION

1.1 Historical Perspective

The first electron diffraction experiments were designed to test the theory propounded by Louis de Broglie[1], that electrons should exhibit wave-like properties. One such experiment was performed by Davisson and Germer[2] in the Bell Telephone Laboratories, New York, in 1927, where they studied the scattering of a beam of electrons from crystals of nickel. The resulting pattern showed striking similarities to that obtained using X-rays as the incident beam.

Meanwhile in Britain, experiments by Thomson and Reid[3] were providing further verification of the theory of wave-particle duality. They studied the diffraction pattern of electron beams of high energy, up to 60 kV, passing through thin films of aluminium, gold, platinum and celluloid, using a photographic plate as detector. If electrons are wavelike in nature, then the product $D\sqrt{P}$ should be constant, where P is the accelerating potential and D the diameter of the observed scattering ring. The experiment showed that this was in fact the case. It is interesting to note[4] in this context that while G.P. Thomson was to receive the Nobel Prize for proving that the electron could be treated as a wave, it had previously been presented to his father, J.J. Thomson, for showing that the electron was a particle.

It was using essentially a Thomson-type apparatus that Mark and Weirl[5] carried out the pioneering gas-phase electron diffraction (E.D.) experiments, studying carbon tetrachloride and a variety of simple di- and triatomics. E.D. apparatus in use today maintain basically the same lay-out, but incorporate several important improvements.

Initially there was scepticism as to the value of E.D. as a structural technique. The pertinent information is superimposed on a structureless background, contributed by atomic scattering, dependent approximately on the fourth power of the scattering angle, and beyond the resolution imposed by conventional photographic detection techniques. Trendelenburg[6] copied his diffraction plates using a rotating heart-shaped sector device to subtract much of this background, but it was not until Debye[7] suggested inserting a similar sector between the scattering zone and the photographic plate, effectively reducing the exposure time at smaller scattering angles, that E.D. emerged as a viable structural technique. Alternative data collection methods[8,9], such as the solid state counting techniques often employed in X-ray crystallography, have so far proved impractical because of the long data accumulation times and large amounts of sample required.

Over the years, inconsistencies have been minimised with improvements in scattering theory and the consideration of vibrational effects. High vacuum techniques and the accuracy of modern methods of tracing the photographic

plates by microdensitometry have increased definition while powerful computers have simplified the calculations, such that the structures of molecules with more than fifty atoms have now been refined[10].

Despite certain limitations (see Chapter 1.7), E.D. retains an advantage over microwave spectroscopy by not requiring permanent dipoles or isotopic substitution for a complete structural determination. Several atoms, notably fluorine and phosphorus, only possess a single isotope, and compounds containing these atoms form a substantial proportion of those studied in this thesis. Thus, in this case, the logical structural technique to utilise was gas-phase Electron Diffraction.

1.2 Theory

De Broglie's postulate[1] of wave-particle duality bestows on the electron a wavelength corresponding to:

$$\lambda = \frac{h}{p} = \frac{h}{mv} \qquad (1.1)$$

The kinetic energy of an electron accelerated through a potential, V, is calculated from:

$$\tfrac{1}{2}mv^2 = eV \qquad (1.2)$$

These combine to give:

$$\lambda = \frac{h}{\sqrt{2\ meV}} \qquad (1.3)$$

The high accelerating potential used in the E.D. experiment, around 50 kV, results in an electron velocity approaching that of light, and so relativistic corrections must be applied[11].

The total energy of the particle is given by:

$$W = M_o C^2 + eV \qquad (1.4)$$

and from the general equation[12]:

$$W^2 - p^2c^2 = M_o{}^2C^4 \qquad (1.5)$$

The relativistic wavelength can be calculated:

$$p = \frac{1}{C}\sqrt{W^2 - M_o{}^2C^4}$$

$$= M_oC\sqrt{\left(1 + \frac{eV}{M_oC^2}\right)^2 - 1}$$

$$\Rightarrow \quad \lambda = \frac{h}{M_oC\sqrt{\left(1 + \frac{eV}{M_oC^2}\right)^2 - 1}} \qquad (1.6)$$

Using an accelerating potential of 50 kV this gives an electron wavelength of 5.4 pm; about an order of magnitude less than interatomic separations, the optimum for observing interference and diffraction effects.

If the electron beam passes through a gaseous sample of the compound under investigation, then the total observed scattered intensity depends on contributions from atomic and molecular scattering processes, both

elastic and inelastic, coherent and incoherent. The inelastic scattering[13], which is practically negligible at the electron accelerating potentials used[14], and the incoherent scattering, arising from double collisions and extraneous scattering from residual gas in the chamber or reflections from the walls of the apparatus, are later deducted as a smooth background.

The theory of atomic and molecular scattering is based on the early work of Rutherford[15], Debye[16] and Ehrenfest[17]. If the scattering from a point charge is considered then the scattered intensity is given by:

$$I(\theta) = \frac{I^o}{R^2} |f(\theta)|^2 \qquad (1.7)$$

where θ is the scattering angle and I^o the incident beam intensity.

The atomic scattering amplitude, $f(\theta)$, calculated assuming the first Born approximation[18] is given by:

$$f(\theta) = \frac{2}{a_o} \frac{Z - F}{S^2} \qquad (1.8)$$

where a_o is the Bohr radius, Z the atomic number and F the atomic form factor as used in X-ray diffraction. The convenient parameter, S, is introduced where:

$$S = \frac{4\pi}{\lambda} \sin\left(\frac{\theta}{2}\right) \qquad (1.9)$$

which is independent of the apparatus utilised and so allows comparison of data from diverse sources.

It has been found that this approximate approach is not valid[19] when considering nuclei of large atomic number. In this case the scattering amplitude must be considered as a complex quantity:

$$f(\theta) = |f(\theta)| \; e^{i\eta(\theta)} \qquad (1.10)$$

Values for this quantity may be calculated using the partial wave method[20] or by direct numerical solution of the Schroedinger equation[21] for an electron in a spherically symmetric force field.

Molecular scattering intensities are calculated using the independent atom approximation[22]. If a rigid molecular structure of N atoms is considered then combining (1.7) and (1.10) gives:

$$I(S) = \frac{I^o}{R^2} \sum_{i \neq j}^{N} |f_i||f_j| \cos(\eta_i - \eta_j) \frac{\sin(r_{ij}.S)}{r_{ij}.S} \qquad (1.11)$$

Since the period of vibration of the molecule is several orders of magnitude greater than the time of interaction with the electron, this result must be averaged over the expectation value of the sin term[23]. If a distorted Gaussian distribution of expectation values is considered[24] which correspond to the ground state of a Morse oscillator[25] then the equation for the scattered intensity (1.11) becomes:

$$I(S) = \frac{I^o}{R^2} \sum \frac{1}{r_{ij}.S} |f_i||f_j| \cos(\eta_i - \eta_j) \exp(-\tfrac{1}{2}u_{ij}^2 S^2). \sin[(r_{ij} - \frac{u_{ij}^2}{r_{ij}} - K_{ij}S^2).S] \quad (1.12)$$

where u_{ij}^2 = mean square amplitude of vibration

r_{ij} = mean distance between the atoms i and j

$K_{ij} = \frac{au^4}{6}$

The Morse anharmonicity, a, is usually assumed to be 200 pm^{-1} for bonded atom pairs, and otherwise zero. The terms f_i and η_i have been tabulated by several groups[26]; in Edinburgh those of Schäfer et al[27] are used.

If the function representing the scattered intensity is Fourier transformed then the resulting radial distribution curve[28] is a useful visual aid to structure determination. The position of the resulting peaks is dependent on interatomic separation while their shape depends on the vibrations[29]. In Russia the radial distribution curves are used for direct refinement by a regularisation method[30], but this approach has no comrades in the west and is inherently less accurate than conventional analysis.

1.3 The Edinburgh Apparatus

The Edinburgh University Electron Diffraction Apparatus (see Figure 1.1) was imported from Cornell University[31] in 1977.

The main chamber[32] is constructed of non-magnetic stainless steel, aluminium and brass, with lead-glass viewing windows in strategic positions. An array of rotary and oil diffusion pumps maintain the main chamber at a pressure down to 4.0×10^{-7} torr.

The electron gun consists of a pointed tungsten filament from which thermionically emitted electrons are accelerated through a potential of around 50 kV. The beam is collimated and focussed by the mechanical adjustment of two magnetic lenses and beam diameters of 0.3 mm are typical.

The sample under investigation is introduced via an aluminium nozzle of 0.3 mm internal diameter. This is aligned so as to form a stream of molecules perpendicular to the electron beam, which are adsorbed on the activated carbon coating of a cryogenic pump directly opposite. The nozzle has two positions which effectively correspond to short and long camera lengths, for observing wide and narrow angle scattering respectively (see Figure 1.2). The focussing and positioning of the electron beam relative to the inlet nozzle are monitored on a fluorescent screen incorporated in the camera.

Figure 1.1 The University of Edinburgh Electron Diffraction Apparatus

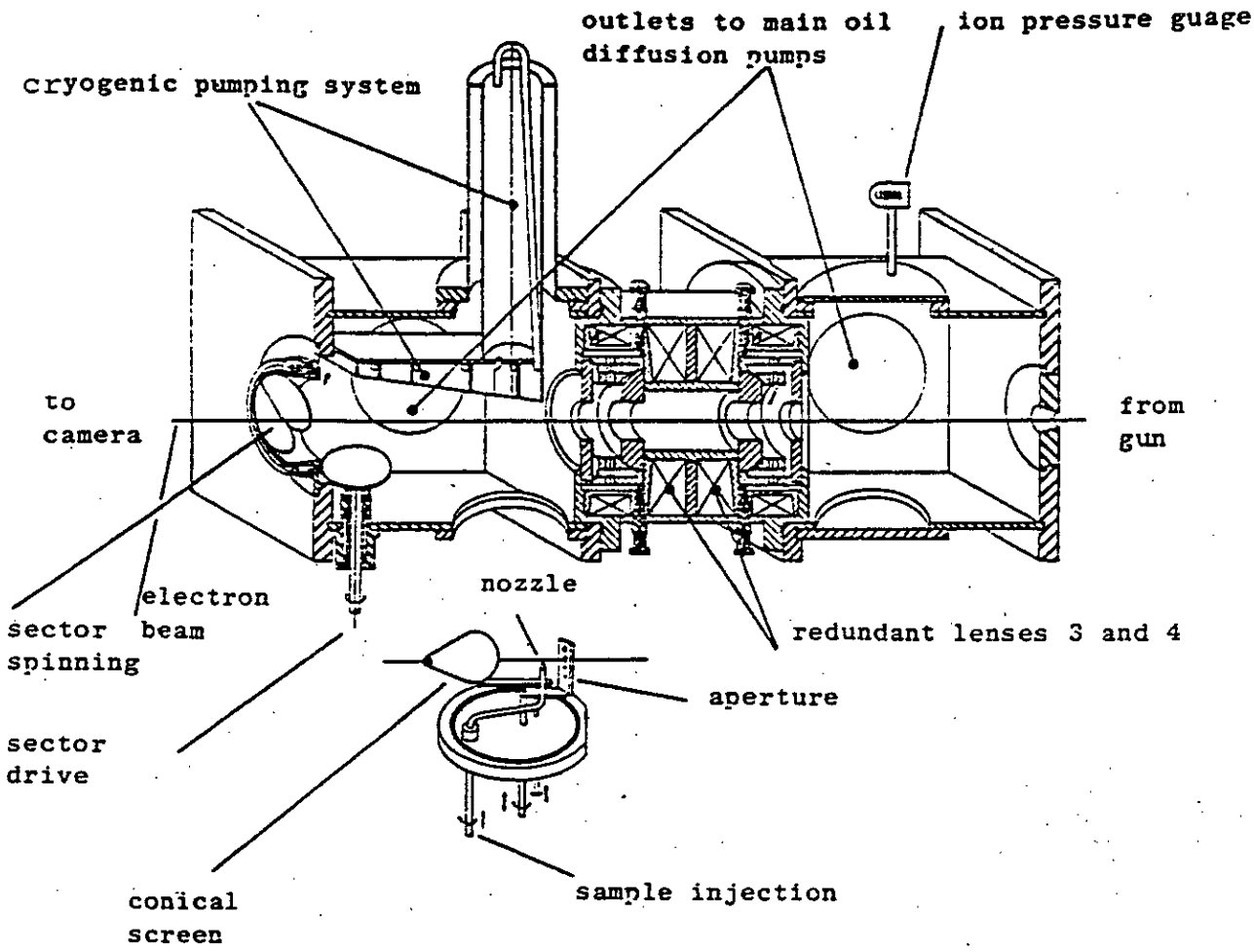

Figure 1.2 Schematic Representation of the Camera Distances

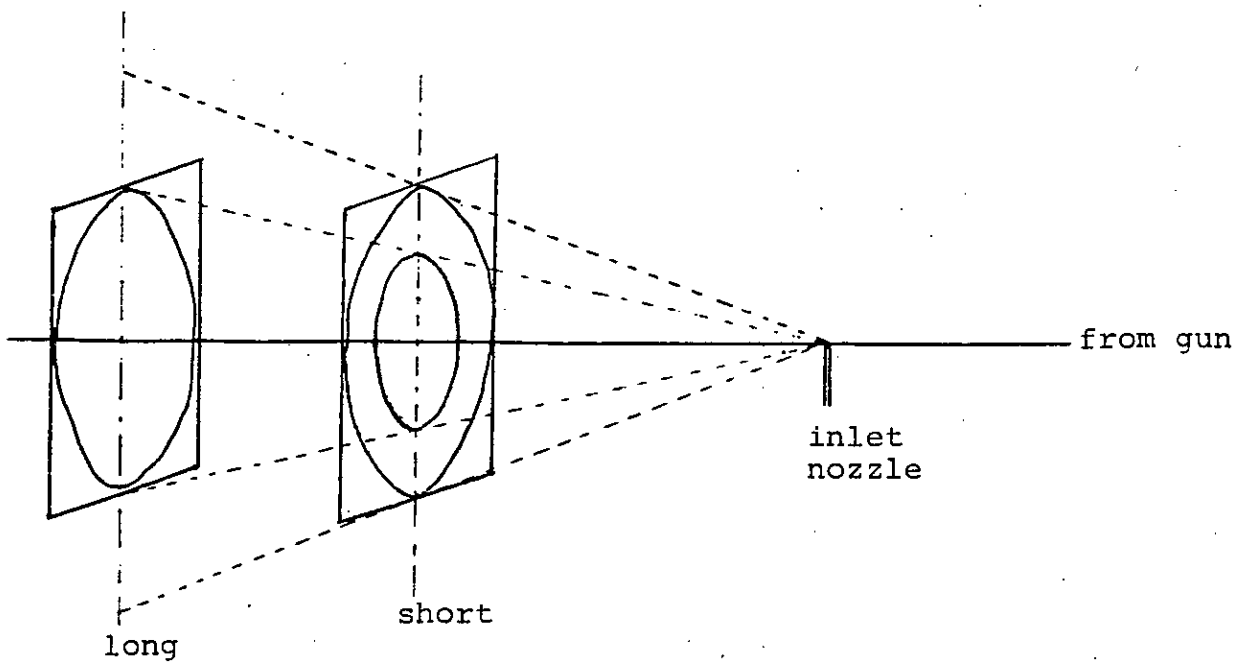

Between the inlet nozzle and the camera, lies the rotating sector. This is a heart-shaped device of accurately determined shape, which effectively decreases the exposure at small scattering angles by subtracting a known function proportional to the fourth power of the scattering angle. This ensures that the scattered intensity reaching the camera only varies over a range that lies well within the resolution of the photographic emulsion.

The design of the camera is particularly elegant in its simplicity; it can contain up to ten Kodak Electron Image plates which are dropped into place in turn under gravity. This efficient system enables the collection of sufficient data for a complete structural determination in a single run.

1.4 Experimental Details

The compound under investigation is prepared on a vacuum line and the purity checked by Infrared and possibly also Nuclear Magnetic Resonance Spectroscopy. Depending on the scattering power of the sample, around 300 mg are required for a structural determination.

The Electron Diffraction apparatus is pumped down to a steady state with the camera, containing ten unexposed photographic plates, attached.

In order to calibrate each run, benzene is introduced for the first two exposures. The structure of benzene is accurately known[33] and therefore the exact camera length and electron wavelength for that particular run can be precisely determined.

A tap ampoule, containing the sample frozen down in liquid nitrogen, is now attached to the inlet of the apparatus and degassed. Depending upon the volatility of the compound under study the ampoule is either allowed to warm up to room temperature or kept cool in an ice or slush bath. The inlet nozzle is always at room temperature as opposed to some Electron Diffraction apparatus[34] which have the facility to heat the nozzle in order to look at less volatile compounds.

Three sample exposures at the first camera distance are taken, bracketted around an exposure time calculated based on previous experience, the relevant atomic scattering factors, the apparent strength of the electron beam and the increase in pressure in the scattering chamber, as monitored on an ion gauge, as the sample is introduced.

At this point the inlet nozzle is swivelled into the second camera distance, the alignment rechecked and a further three sample, followed by two benzene, plates are exposed.

The exposed plates are removed from the camera in total darkness and developed for twelve minutes in Kodak D19/D19R developer solution with nitrogen bubble burst agitation at 20°C, washed for one minute in cold running water and then fixed for twenty minutes in Kodafix solution. After thorough washing in cold water, the plates are immersed in Kodak Photo-Flo solution and left to dry, they are then ready to be traced by microdensitometry.

Table 1.1 Electron Diffraction Experimental Details

Compound	Sample Temp./K	Camera Height/mm	Δs nm^{-1}	s_{min} nm^{-1}	Weighting Points min	Weighting Points max	nm^{-1}	Correlation	Scale Factor
PF_2CN	273	1000	1	7	17	52	73	0.330	0.928(18)
	273	250	4	52	70	230	292	0.475	1.054(22)
PF_2NCS	273	285.5	2	20	50	120	146	0.130	0.893(4)
	273	128.4	4	64	70	280	344	0.058	0.765(10)
PF_2NCO	273	285.3	2	20	40	126	146	0.408	0.818(4)
	273	128.4	4	60	70	320	344	0.123	0.778(17)
PF_2HS	228	999.8	1	10	22	62	75	-0.025	0.721(5)
	228	500.1	2	28	42	138	156	0.496	0.830(4)
	228	250.1	4	72	93	265	300	0.429	0.620(17)
SiH_3CN	273	285.4	2	28	34	124	138	0.400	0.769(14)
	300	128.4	4	76	100	220	284	-0.150	0.799(19)

The experimental details for each compound studied in this thesis are listed in Table 1.1. Compounds where there are three camera heights recorded were run in Manchester prior to the installation of the Edinburgh E.D. apparatus. In these cases the plates have been retraced by the new microdensitometry service at Daresbury (see Chapter 1.5). The maximum and minimum measurements at each camera distance are denoted by S_{max} and S_{min} respectively, with observations taken at intervals of Δ s (see Equation 1.9).

W_1 and W_2 represent the lower and upper limits of the trapezoidal weighting function, the off-diagonal elements of which (see Chapter 1.6) are given by the correlation factor. The scale factor is a term by which the scattered intensities are scaled to fit the theoretical curve.

1.5 Microdensitometry

The image on an exposed Electron Diffraction plate appears as a set of concentric rings (see Figure 1.3). In the early days this pattern would be analysed by eye[35], but the plates have for long now been traced by microdensitometry.

Figure 1.3 A Typical Benzene Plate (Short)

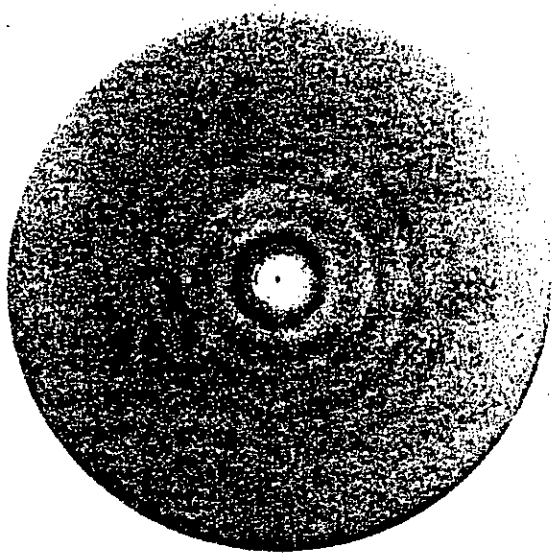

Until recently at Edinburgh a Jarrell-Ash double beam spinning microphotometer was used[36], but this machine has now been rendered obsolete with the inauguration in 1981 of the S.E.R.C. Microdensitometry service at Daresbury. Plates are now sent there to be traced on a Joyce-Loebl Microdensitometer 6[37].

Initially the benzene plates are traced using estimated values for the electron wavelength and the short and long camera distances. These estimates result in scaling errors in the benzene parameters and the precise values can be calculated from:

$$\lambda = \frac{\lambda in.139.70}{r(C-C)} \qquad (1.13)$$

$$S = \frac{Sin.r(C-C)}{r(C-C)_S} \qquad (1.14)$$

$$L = \frac{Lin.r(C-C)}{r(C-C)_L} \qquad (1.15)$$

where S and L stand for the short and long camera distances and 139.70 pm is the accepted carbon-carbon bondlength in benzene[33].

In tracing the sample plates, the corrected electron wavelength and camera distances, and the approximate co-ordinates of the centre of the diffraction pattern are input to a computer. This automatically finds the exact centre and then controls the microdensitometer's X and Y drives, measuring the optical density five times at each of one thousand points spaced equally round a ring of constant S value (see Equation 1.9). The machine scans the entire plate at rings with radii increasing corresponding to integer values of ΔS. After every five rings are traced, the density of a fixed region of exposed plate is rechecked to ensure that there is no drift in the calibration. A final outer clear unexposed ring is measured as a background to subtract for the inherent optical density of the photographic plate.

The output consists of a list of numbers corresponding to the average optical densities for each ring. Each density is measured with an accuracy of ±0.002 D, and so

the mean density of each ring, being measured five thousand times, has an accuracy of better than ±0.0001 D.

Apart from the greatly increased sensitivity, there are several major improvements in this system compared with that used previously. Any flaws in the diffraction pattern caused for example by cracks in the plate or specks in the photographic emulsion can be omitted by the simple expedient of programming the computer to ignore a certain angular sector of the plate. Secondly, the fact that measurements are only taken at the area of interest, that is at predetermined integral values of ΔS, makes it unnecessary to interpolate between points, thus reducing correlations between observations.

On the inception of the Daresbury service, several trial experiments were undertaken on benzene plates to check the effect of possible sources of experimental error in the tracing procedure. These included false centering of the plate, missing out sectors of plate, and defocussing the measuring beams. The significance of these effects was calculated and standard operating procedures laid down which ensure reproducibility of results. It is now found that differences in the molecular scattering intensities calculated from separate scans of the same plate, traced days apart, are an order of magnitude less than differences between the intensities derived from other plates of the same compound. This implies that the accuracy of measurement is now greater than the actual definition of the photographic plates.

1.6 Computing

Calculations on the optical densities obtained are performed on the Edinburgh Regional Computing Centre I.C.L. 2972 mainframe computer. The established data reduction[38] and least squares refinement[39] programs used at Edinburgh were edited to cope with the new format of the data arriving from Daresbury. The new programs are included in Appendix I.

The analysis of the data can be conveniently summarised by a flow chart (Figure 1.4). The data arriving from Daresbury is in the form of optical densities. Corrections are made for the flatness of the plates and the saturation of the photographic emulsion (blackness correction), and the sector function is added back to give the uphill curve, which contains contributions from atomic, molecular and extraneous scattering. The relevant atomic numbers for the compound under study are inserted, and using tabulated scattering factors the theoretical atomic scattering is calculated and subtracted, leaving the molecular and extraneous components. Initial estimated values for the independent molecular parameters are inserted along with their associated amplitudes of vibration and anharmonicities. A model program is written to calculate the normal co-ordinates of the atoms from these parameters, and a theoretical molecular scattering curve is calculated. Assuming that the model is correct, the main difference between theoretical and experimental scattering curves is attributable to extraneous scattering (see Chapter 1.7), which can be approximated by a smooth hand-drawn background.

Figure 1.4 Flow Diagram Representing the E.D. Refinement Process

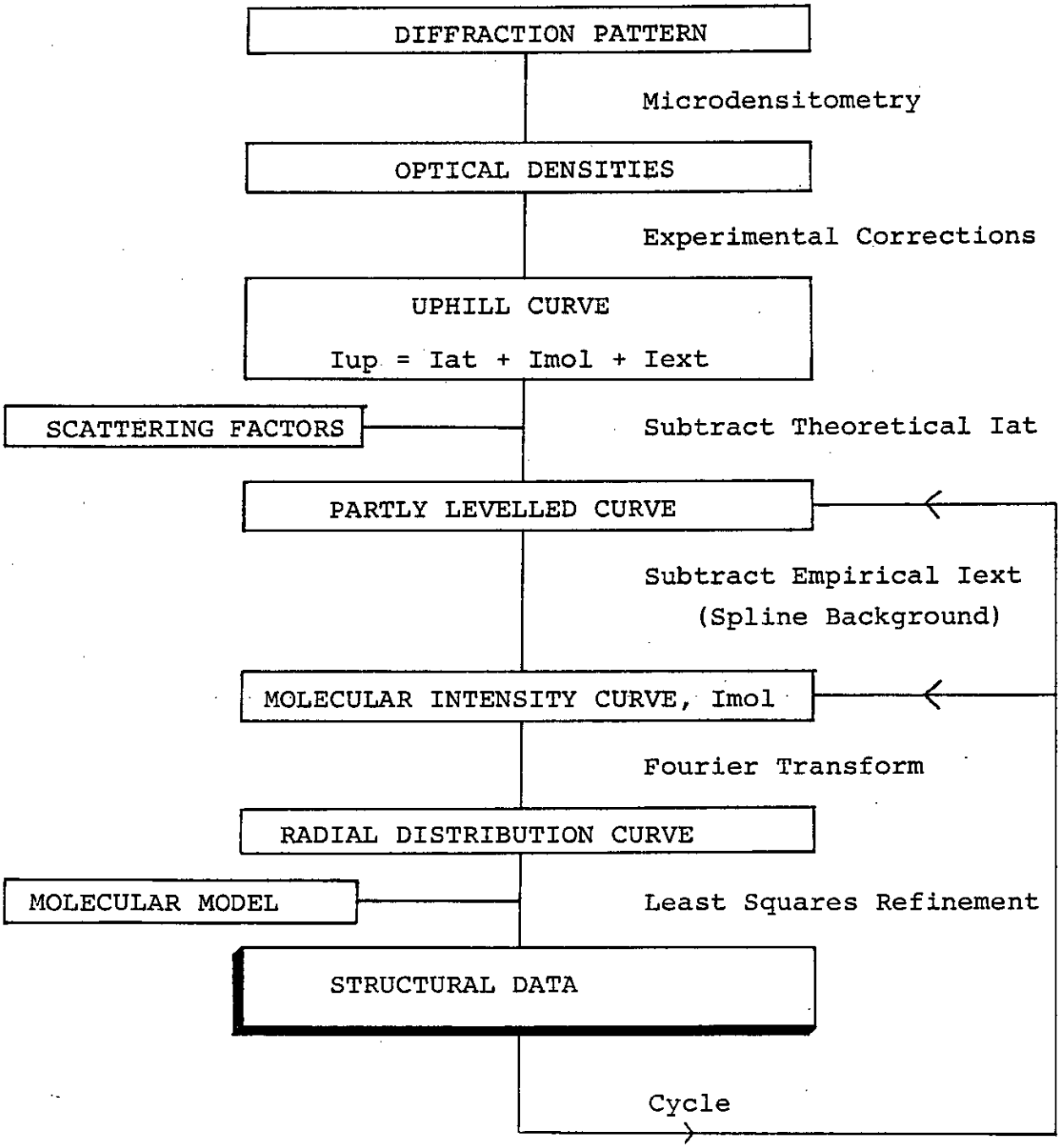

It was decided to devise an automatic background deducting routine using a cubic Spline function algorithm[40]. This technique fits to the data a set of cubic polynomial arcs joined with continuity of first and second derivatives at specified knots. By bringing the knots closer together, increasingly tighter curves can be accommodated until, with two coincident knots, a second derivative discontinuity, or with three, a first derivative discontinuity can be achieved (for program see Appendix I).

The Spline function is useful in E.D. work since the data have more significant and so more steeply varying backgrounds at the extremities of the plates. By concentrating the knots accordingly a suitable fit can be accomplished. Care has to be taken that the period of the background subtracted is such that the corresponding Fourier transform represents distances smaller than interatomic separations.

The independent parameters are now refined using the least squares method, which minimises the R gen factor. This is derived from the R diag factor, which is defined as the sum of the squares of the differences between the points on the theoretical and experimental curves, divided by the sum of the squares of the points on the experimental curve.

$$R_{diag} = \frac{\Sigma (I_{expt} - I_{theory})^2}{\Sigma I_{expt}^2} = \frac{\Sigma D^2}{\Sigma I^2} \qquad (1.16)$$

This can be represented in matrix form as:

$$R_{diag} = \frac{D^1WD}{I^1WI} \qquad (1.17)$$

where W is a diagonal weight matrix, the terms of which represent a trapezoidal weighting function with central values of unity, the upper and lower limits of which are set prior to refinement (see Table 1.1).

Since the standard deviation derived using the least squares method is approximately proportional to the inverse of the square root of the number of observations then, using a purely diagonal weighting matrix, by increasing the number of observations the standard deviation can be made infinitely small. This does not allow for the fact that as the interval between measurements decreases, the correlation between adjacent points increases. The R gen factor allows for this by introducing off-diagonal terms to the weighting matrix[41], the values of which are calculated from the residuals of the least squares fit and which are numerically equal to negative the correlation factor (when the diagonal terms are unity). Using this scheme, as the observation interval is decreased, the correlation increases to a maximum of one half and the standard deviation does not approach zero. Totally random observations have zero correlation, and a negative correlation is possible if there is substantial noise in the background.

1.7 Errors and Limitations

An exhaustive review of the possible errors arising in an E.D. experiment has been produced by Kuchitsu[42].

The introduction of the new microdensitometry service at Daresbury has already been shown to minimise the errors associated with plate tracing, the large number of readings being taken for several photographic plates reducing random errors substantially.

In the data reduction program, standard corrections[43] are applied to allow for the flatness of the plates and saturation of the photographic emulsion.

The possible reduction in the precision of the data at small and large S-values is allowed for by the use of the weighting matrix, lending such points less significance than those in the central region. This effect on definition at small S-values can arise from dirt in the sector gap, or poor calibration of its shape. In order to avoid this, the sector, which has been accurately calibrated using Argon as a standard structure, is kept scrupulously clean.

At large S-values, the effect on definition may be explained by extraneous scattering arising from unwanted radiation, electrons scattered from surfaces within the apparatus (events which may also create X-rays), scattering from residual gas, and double collisions. In Edinburgh these possibilities are minimised as follows:

the aperture allowing the electron beam into the main chamber is opened briefly to spot the centre of the plate and then only during data accumulation to minimise stray electrons; careful alignment of the electron beam plus a zig-zag chamber wall reduces the chance of reflections towards the camera; the use of aluminium components within the chamber reduces the chance of secondary emission of X-rays, which is more likely with heavier metals; finally, efficient pumping and low pressures limit the extent of scattering from residual gas and double collision events.

Systematic errors are reduced by using a benzene calibration every run, which gives accurately determined electron wavelength and camera lengths. The benzene refinements also serve to monitor errors in the amplitudes of vibration. These are caused by point source approximations in the scattering calculations which do not allow for the finite cross-sectional area of the sample and electron beams, or the non-monochromicity of the latter. The small sample and electron beam widths attained at Edinburgh help alleviate this problem, as can be seen by comparing the experimental average benzene amplitudes with those measured spectroscopically (Table 1.2).

Table 1.2 Benzene Amplitudes

	E.D. Experimental Average/pm	Spectroscopy[33] /pm
u(C.C)	44.7 (15)	46.1
u(C.H)	78.5 (40)	77.1
$u(C...C)_m$	57.0 (20)	53.9
$u(C...C)_p$	59.0 (30)	57.0
$u(C...H)_o$	97.4 (40)	99.4
$u(C...H)_m$	117.5 (70)	96.0
$u(C...H)_p$	91.6 (110)	92.0

From Table 1.2 it can be seen that the average experimental amplitudes for bonded distances agree well with the values determined spectroscopically, however, non-bonded amplitudes are less accurate. To allow for these systematic errors, the estimated standard deviations calculated in the least squares refinement are increased by around fifty percent in the case of angles and amplitudes, while point one percent of each distance is added to its uncertainty.

Having allowed for random and systematic errors, there are still four major problematic areas in arriving at the correct structure from electron diffraction data; heavy atoms, light atoms, shrinkage, and overlapping peaks in the radial distribution curve.

The inadequacies of early theories of the electron scattering process led to some anomalous results when heavy atoms were involved. For instance, the structure of

uranium hexafluoride[44] showed two peaks corresponding to the U-F bond length in the radial distribution curve, leading to the conclusion that this molecule surprisingly had an asymmetric structure. It was later found, however, that electron scattering factors were complex in nature[19], leading to this prominent phase shift effect when considering nuclei with increasingly different atomic numbers. Tables of complex scattering factors and phase shifts[27] have now appreciably overcome this problem.

The presence of comparatively light atoms in a molecule causes an altogether different and more intractable problem. The areas of the peaks in the radial distribution curve are proportional to the product of the atomic numbers involved. Peaks involving protons in particular are often vanishingly small[45] and usually it proves necessary to fix proton parameters at "reasonable" values taken from spectroscopy.

The comparison in Figure 1.5 of the radial distribution curves of SPF_2H and SPF_2Br shows this effect distinctly. The bromine associated peaks are all clearly visible, whereas in SPF_2H the proton associated peaks are indiscernible.

Another problem associated with the radial distribution curve occurs if the separation of a pair of interatomic distances is small, say less than 10 pm for a bonded atom pair. The corresponding peaks may then overlap in the radial distribution curve[46,47] and it may be necessary to fix some of the parameters concerned at reasonable values, measured spectroscopically, or simply guessed based on experience.

Figure 1.5 Radial Distribution Curves showing the Light Atom Effect

(a) SPF_2H

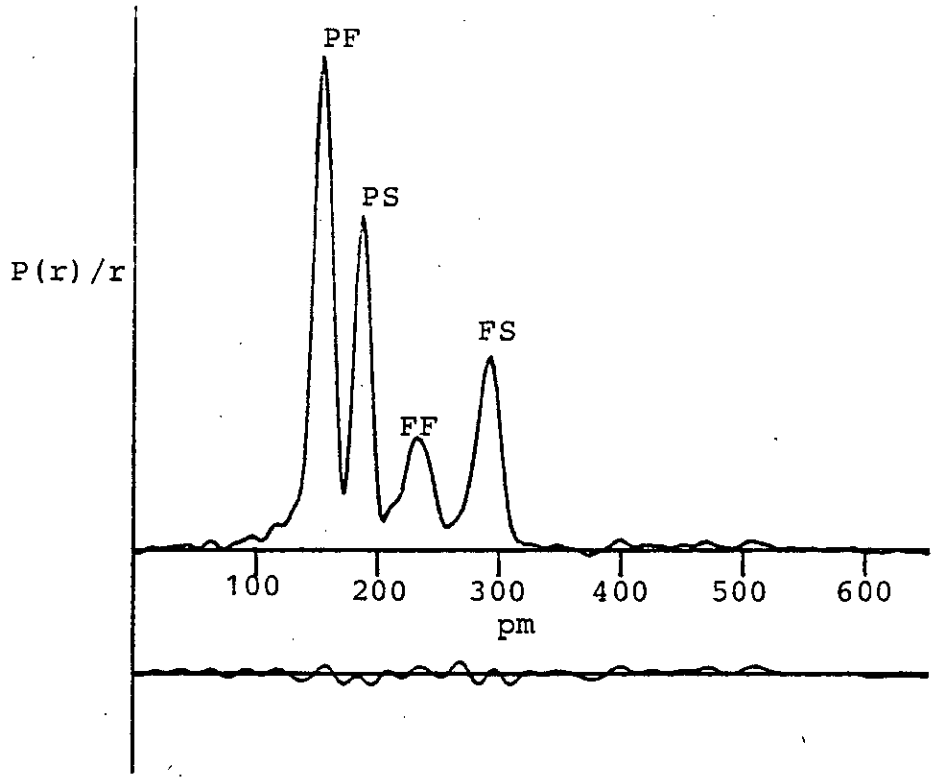

(b) SPF_2Br

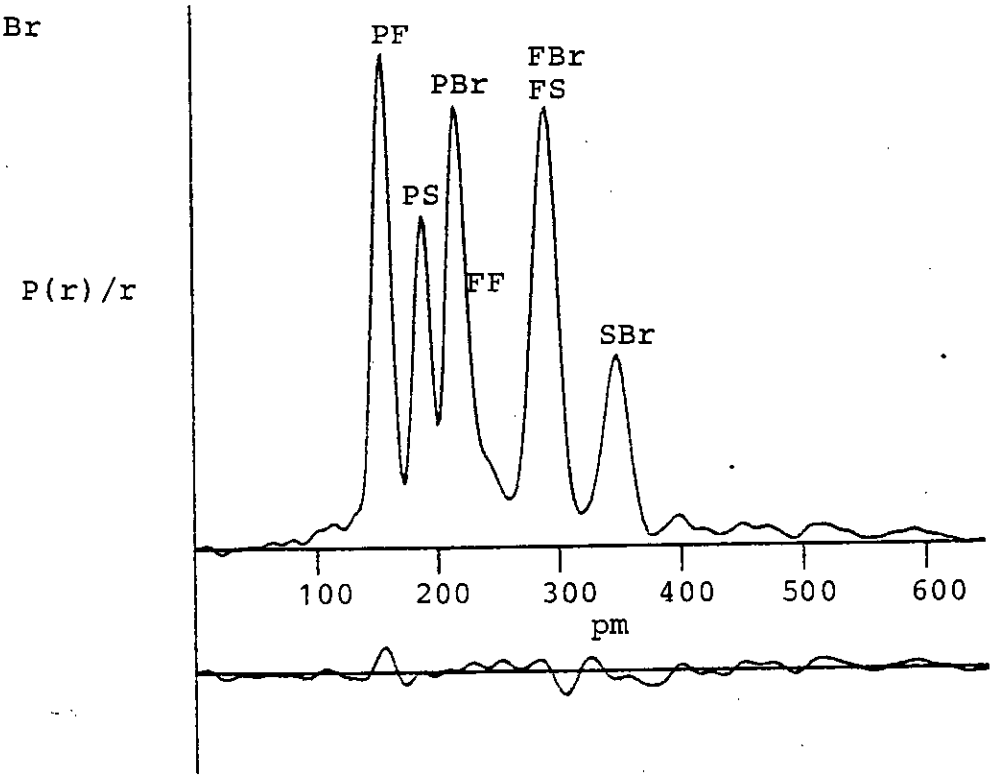

Figure 1.6 Radial Distribution Curves Showing the Overlapping Peaks Effect

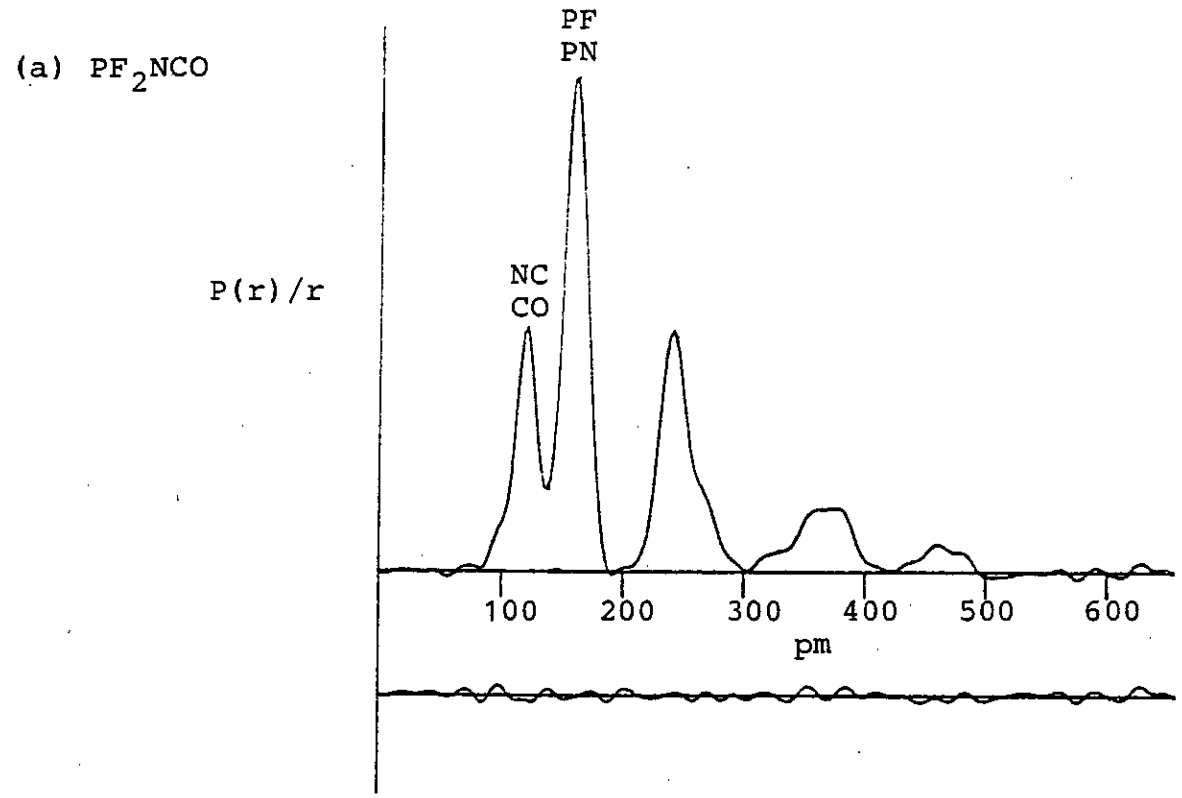

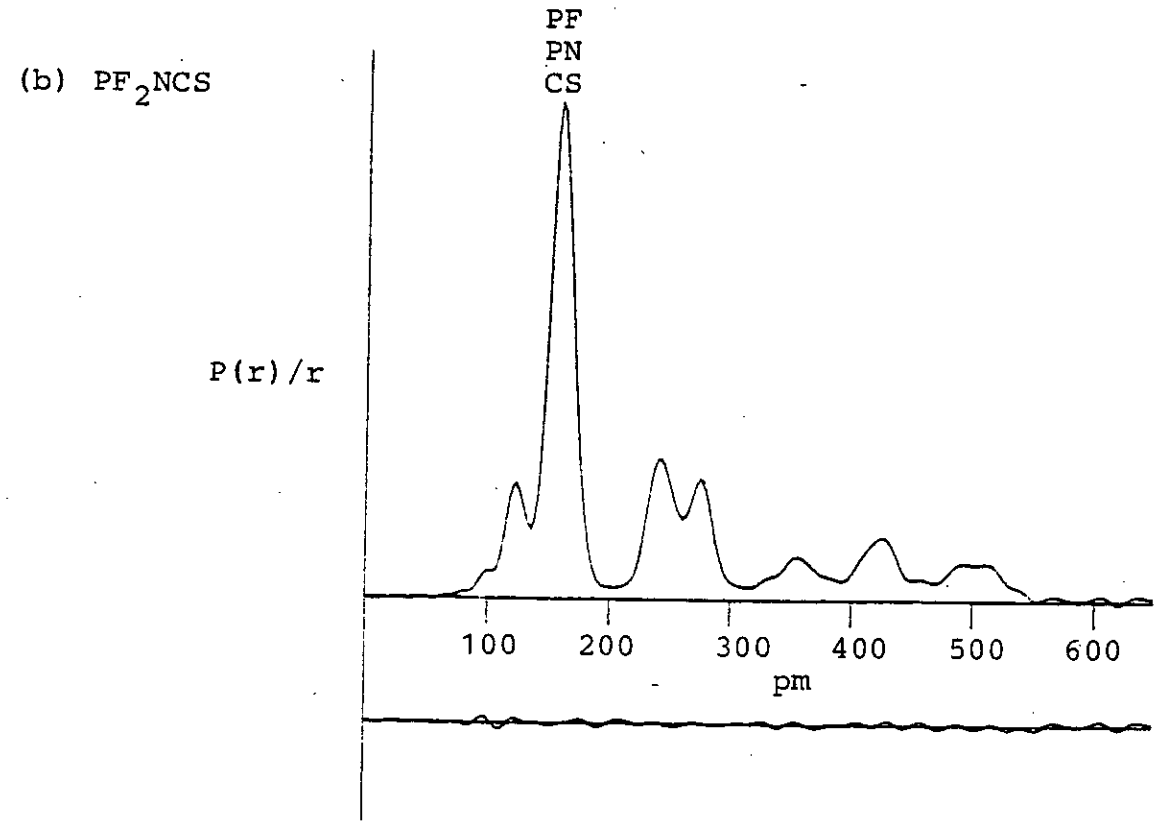

This problem is clearly seen in Figure 1.6 in the case of the fluorophosphine pseudohalides, particularly PF_2NCS, which has three distances covered by one peak in the radial distribution curve. A previous analysis of these structures[48] required the estimation of several of these parameters which were then fixed during refinement.

The other main problem, shrinkage[49], arises from the fact that a molecule is not a rigid structure, but is in constant vibrational motion. The period of interaction of the electron with the molecule is much less than the vibrational period, and so the electron diffraction pattern depends upon the expectation values of the instantaneous atomic separations over the vibrations. If a linear triatomic system is considered (Figure 1.7) then it can be seen that the distance AC is never greater than the sum of AB plus BC, and is often less.

Figure 1.7 The Shrinkage Effect

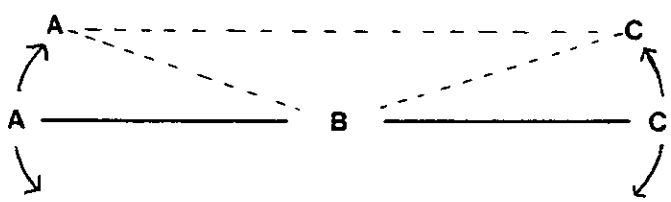

Therefore, averaging over vibrations gives:

$$\langle AC \rangle \quad < \quad \langle AB \rangle \quad + \quad \langle BC \rangle$$

and so the molecule appears to be bent. In order to allow for this effect, a detailed study of the vibrations involved must be carried out (see Chapter 3). Floppy molecules[50], that is those with low frequency, high amplitude modes, are particularly troublesome in this respect.

The many problems associated with a structural analysis by Electron Diffraction have been to a certain extent alleviated by the inclusion of data from spectroscopic sources, and by combined analysis with microwave data[51-56]. The theories linking the distances obtained from various sources are considered in Chapter 3 and are generally well established[57]. However, in certain cases, further information is still required for complete structural determination and one possible extra source is from Liquid Crystal Nuclear Magnetic Resonance Spectroscopy.

CHAPTER TWO

LIQUID CRYSTAL NUCLEAR MAGNETIC RESONANCE SPECTROSCOPY

2.1 Introduction

In 1888 the Austrian botanist, Friedrich Reinitzer, on synthesising cholesteryl benzoate noticed a novel phenomenon[58]; the solid melted at 145°C giving a turbid liquid, which abruptly cleared at 179°C, a process that was reversible. The turbid liquid was found to be birefringent[59], therefore anisotropic, and this mesophase, lying between the solid and liquid phases, became known as liquid-crystalline.

Three classes of this mesophase were categorised[60]; nematic, cholesteric and smectic (which has now been further split into the classes smectic A, B and C). These differ in the amount of internal ordering and are represented diagramatically in Figure 2.1.

In structural work, the nematic mesophase, being the least ordered and therefore most fluid, has proved to be the most useful. The nematic mesophase consists of elongated 'sausage-shaped' molecules, with their long axes statistically parallel, but without any regular overall ordering of the molecular centres of gravity. This local ordering along the major axis of the molecule is often defined by a unit vector known as the director.

There are two theories of ordering in the nematic mesophase. The swarm theory[61] postulates the existence of short-lived clusters of parallel molecules, whereas the continuum theory[62] predicts a gradual change of director orientation as a function of position. Both theories, however, become equivalent on the application of an external constraint such as an electric or magnetic field[63].

Figure 2.4 Schematic representation of packing in liquid crystal types.

(a) nematic

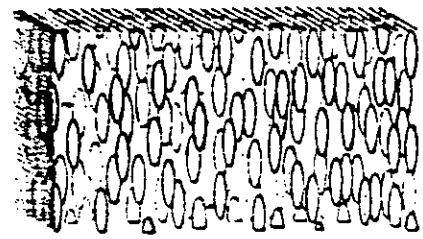

(b) smectic a

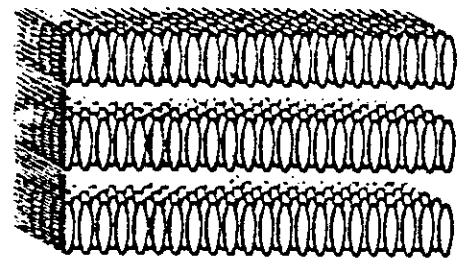

(c) smectic b

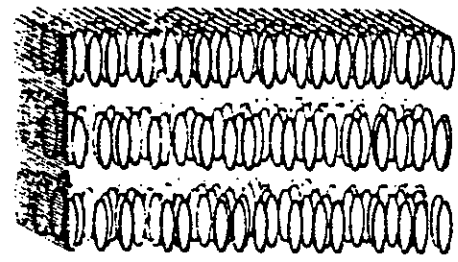

(d) cholesteric

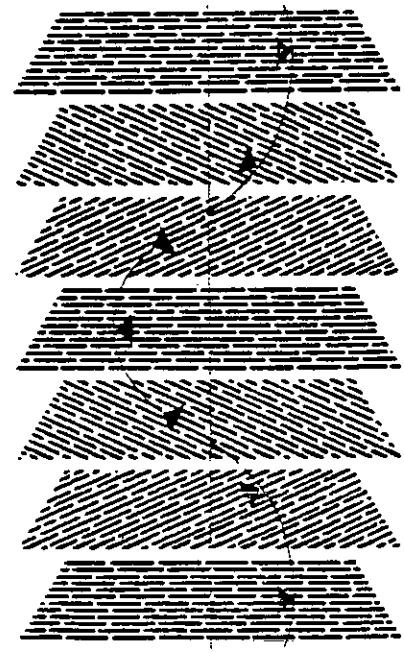

If a magnetic field is applied to the liquid crystal, then each molecule experiences a torque tending to align the direction of least diamagnetic susceptibility, usually the major axis, parallel to the field[64]. Total alignment is achieved at relatively modest field strengths because of the co-operative effect of the strong angular correlation of the directors. It must be noted that although the directors become aligned to the field, the molecules are still in fluid thermal motion[65]. This alignment of the liquid crystal changes its transmission and reflection characteristics for light, a property exploited in the displays of watches and calculators[66].

In a normal Nuclear Magnetic Resonance (N.M.R.) experiment, because of the rapid rotation of molecules in an isotropic liquid, certain information is lost. In particular the direct dipole-dipole magnetic interaction, dependent on molecular geometry, becomes rotationally averaged to zero. Although this information is not lost in the solid state, the many intermolecular couplings observed complicate the issue. In order to obtain useful structural information from direct couplings it would be necessary to constrain individual molecules to align themselves in the field of the N.M.R. Spectrometer. Initial attempts to achieve this, which met with limited success, included the application of electric fields[67] and the embedding of molecules in a polymer matrix or even zeolite channels[68]. It was not until 1963, when Saupe and Englert[69,70] first experimented with liquid crystals as orienting solvents that the direct couplings from N.M.R. became a viable source of structural information.

Much research has previously been carried out at Edinburgh[71] to determine which liquid crystals are viable solvents for this sort of experiment. Several criteria were established: the liquid crystal should become isotropic at a temperature where the compounds under study are not liable to thermal decomposition, they should have low viscosity to allow the sample to dissolve and they should be inert to the solute.

Few liquid crystals were found to satisfy those requirements. Most pure stable liquid crystals possess a nematic range at too high a temperature, while many of the commercial mixtures, such as Merck Phase V, contain azoxy compounds, which have proved reactive with the inorganic solutes studied here[72].

The most suitable solvents found so far at Edinburgh have proved to be a range of eutectic mixtures of cyano biphenyls and terphenyls produced by British Drug Houses and numbered from E1 upwards[73]. These can be represented by the general formula:

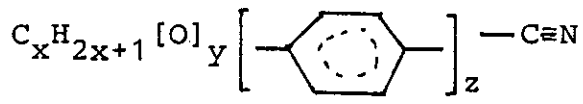

$x = 2, 12 \quad y = 0, 1 \quad z = 2, 3$

Initially E8 was mainly used because of the high orientation parameters obtained, but in this work E5 is preferred for its lower viscosity and lower nematic-isotropic transition temperature.

One trouble with this class of liquid crystals is that they contain a cyanide group. This may in some cases interact with the solute molecule and distort the structure. An associative effect such as this may be instrumental in producing the high orientation parameters observed in E8.

Other groups have noted that the apparent structure of solute molecules may vary depending upon the choice of solvent[74-82]. One group of solvents that are gaining popularity are the Merck AG ZLI liquid crystals[83,84], especially ZLI 1167 which orients perpendicular to the applied field and so can be spun in a conventional spectrometer magnet, reducing field inhomogeneities and improving spectral sharpness. It has now been shown, however, that even these solvents are not totally inert[85].

Combining data from several liquid crystal solvents has been shown to increase the precision of structural determination[86], therefore the more suitable liquid crystals the better - the search continues.

2.2 Theory[16]

Proton N.M.R. spectra of small molecules dissolved in the nematic mesophase of liquid crystals show a series of sharp lines superimposed on broad unresolved humps arising from the solvent itself. This background can be explained by the generally large number of inequivalent protons in a typical liquid crystal molecule and the fact that intermolecular couplings do not average to zero because of the relative immobility of the molecules with respect to their immediate neighbours. The solute molecules, however, can diffuse as rapidly as in normal isotropic solution, and retain sufficient mobility to average to zero the intermolecular interactions they experience.

Although the solute molecule is mobile, dispersion forces[87,88] tend to orient it relative to the director and so to the magnetic field. In an isotropic solution the period of rotation is of the order of 10^{-12} s, but the molecule in a nematic mesophase experiences an anisotropic environment over the N.M.R. experiment timescale of around 10^{-5} s.

This results in the observation of the direct dipole-dipole coupling, D, which is normally averaged to zero by rotation, in addition to the normally observed indirect spin-spin coupling, J, which is, to a first approximation, independent of orientation.

Direct couplings contain information on molecular geometry and the coupling Dij between atoms i and j can be derived from the nuclear spin Hamiltonian to give[89,90];

$$Dij = -\frac{h\,\gamma i\,\gamma j}{8\pi^2}\left\langle\frac{3\cos^2\theta ij - 1}{rij^3}\right\rangle \qquad (2.1)$$

where θij is the angle between the applied magnetic field and the interatomic vector, the interatomic distance is denoted by rij, γ is the magnetogyric ratio, and the angle brackets denote averaging over vibrational and molecular motions.

This can be written as:

$$Dij = -\frac{h\gamma i\gamma j}{4\Pi^2 rij^3} \cdot Sij \qquad (2.2)$$

where Sij is the degree of orientation of the interatomic vector and is given by:

$$Sij = \tfrac{1}{2} < 3\cos^2\theta\ ij - 1 > \qquad (2.3)$$

Sij represents a statistical degree of order[91], taking values from -0.5 to +1.0 corresponding to total alignment from perpendicular to parallel to the applied field, with zero representing a random configuration.

The average orientation of the entire molecule can be defined[92] in terms of a 3 x 3 traceless symmetric matrix, S,:

$$S = \begin{bmatrix} Saa & Sab & Sac \\ Sab & Sbb & Sbc \\ Sac & Sbc & Scc \end{bmatrix} \qquad (2.4)$$

Table 2.1: Non-zero, independent elements of the ordering matrix $S_{\alpha\beta}$ for groups of interacting nuclei according to point group symmetry

Point Group	$S_{\alpha\beta}$
C_1, C_i	S_{zz}, $(S_{xx}-S_{yy})$, S_{xy}, S_{xz}, S_{yz}
C_2, C_{2h}, C_s	S_{zz}, $(S_{xx}-S_{yy})$, S_{xy}
C_{2v}, D_2, D_{2h}	S_{zz}, $S_{xx} - S_{yy}$
C_3, C_{3h}, C_{3v}	S_{zz}
C_4, C_{4h}, C_{4v}	S_{zz}
C_5, C_{5h}, C_{5v}	S_{zz}
C_6, C_{6h}, C_{6v}	S_{zz}
$C_{\infty h}$	S_{zz}
D_{2d}	S_{zz}
D_3, D_{3d}, D_{3h}	S_{zz}
D_4, D_{4d}, D_{4h}	S_{zz}
D_5, D_{5d}, D_{5h}	S_{zz}
D_6, D_{6h}	S_{zz}
$D_{\infty h}$	S_{zz}
S_4, S_6	S_{zz}
K_h, O, O_h, T, T_d	all $S_{\alpha\beta}$ zero

This has a maximum of five independent variables (S_{cc}, $S_{aa}-S_{bb}$, S_{ab}, S_{ac} and S_{bc}), which may be further reduced by choosing a Cartesian co-ordinate system to define the atomic positions such that the maximum number of interatomic vectors lie along the high order molecular symmetry axes (see Table 2.1).

The values of the S matrix elements are given by:

$$S_{\alpha\beta} = \tfrac{1}{2} < 3\cos\theta\alpha \cos\theta\beta - \delta\alpha\beta > \qquad (2.5)$$

$\alpha, \beta = a, b, c$

where $\delta_{\alpha\beta}$ is the Kronecker delta ($\alpha = \beta$, $\delta = 1$; otherwise $\delta = 0$).

The orientation of any particular internuclear vector can be determined from the total orientation matrix, S, using the general relationship between the zz-component of a second rank tensor, A, and its components $A_{\alpha\beta}$ in another axis system:

$$A_{zz} = \sum_{\alpha\beta} \cos\theta_{\alpha z} \cos\theta_{\beta z} \cdot A_{\alpha\beta} \qquad (2.6)$$

$\alpha,\beta = a, b, c$

where the angle $\theta_{\alpha z}$ is that between the z and the α axes.

There are now two alternative approaches to the problem.

Emsley[93] and Lindon use the following approach.

Let $l_{\alpha}^2 = \cos^2\theta_{\alpha z}$, $l_{\alpha\beta} = \cos\theta_{\alpha z}\cos\theta_{\beta z}$ etc., then expanding (2.6) gives:

$$A_{zz} = A_{aa}\, l_a^2 + A_{bb} l_b^2 + A_{cc} l_c^2 + 2A_{ab}\, l_{ab} + 2A_{ac} l_{ac} + 2A_{bc} l_{bc} \qquad (2.7)$$

Now add and subtract the expression:

$$A_o = \frac{1}{3}(A_{aa} + A_{bb} + A_{cc}) \qquad (2.8)$$

giving:

$$A_{zz} = A_o + A_{aa}(l_a^2 - \tfrac{1}{3}) + A_{bb}(l_b^2 - \tfrac{1}{3}) + Acc(l_c^2 - \tfrac{1}{3}) + 2A_{ab} l_{ab} + \ldots \qquad (2.9)$$

from equation (2.5) it can be seen that:

$$l_a^2 - \frac{1}{3} = \frac{2}{3}\cdot\frac{1}{2}(3l_a^2 - 1) = \frac{2}{3} S_{aa} \qquad (2.10)$$

Similarly it can be shown that:

$$l_{ab} = \frac{2}{3} S_{ab} \qquad (2.11)$$

Combining (2.10) and (2.11) with (2.9) gives:

$$A_{zz} = A_o + \frac{2}{3}(A_{aa}S_{aa} + A_{bb}S_{bb} + A_{cc}S_{cc} + 2A_{ab}S_{ab} + 2A_{ac}S_{ac} + 2A_{bc}S_{bc}) \qquad (2.12)$$

Since the S matrix has a zero trace,

$$S_{bb} = - S_{cc} - S_{aa}$$

therefore the term $A_{bb}S_{bb}$ can be written as:

$$A_{bb}S_{bb} = \tfrac{1}{2}A_{bb}S_{bb} + \tfrac{1}{2}A_{bb}(-S_{cc}-S_{aa}) \qquad (2.13)$$

Therefore the sum can be expanded to give:

$$A_{aa}S_{aa} + A_{bb}S_{bb} + A_{cc}S_{cc} = \tfrac{1}{2}A_{aa}S_{aa} + \tfrac{1}{2}A_{aa}(-S_{bb} - S_{cc}) + \tfrac{1}{2}A_{bb}S_{bb} + \tfrac{1}{2}A_{bb}(-S_{aa}-S_{cc}) + A_{cc}S_{cc}$$

$$= \tfrac{1}{2}(S_{aa}-S_{bb})(A_{aa}-A_{bb}) + S_{cc}(A_{cc} - \tfrac{1}{2}A_{aa} - \tfrac{1}{2}A_{bb})$$

$$= \tfrac{1}{2}(S_{aa}-S_{bb})(A_{aa}-A_{bb}) + \tfrac{3}{2}S_{cc}A_{cc} \qquad (2.14)$$

Combining (2.14) and (2.12) gives:

$$A_{zz} = A_o + \tfrac{2}{3}(\tfrac{1}{2}(S_{aa}-S_{bb})(A_{aa}-A_{bb}) + \tfrac{3}{2}S_{cc}A_{cc} + 2A_{ab}S_{ab} + 2A_{ac}S_{ac} + 2A_{bc}S_{bc}) \qquad (2.15)$$

In the case of dipolar couplings the tensor A is traceless, therefore $A_o = 0$, with the values of its elements given by equation (2.2):

$$A_{\alpha\beta} = \frac{-h\gamma_i\gamma_j}{8\pi^2 r_{ij}^3} < 3l_{ij\alpha}^2 - \delta\alpha\beta > \qquad (2.16)$$

Therefore the final expression for the dipolar coupling is:

$$D_{ijzz} = \frac{-h\gamma_i\gamma_j}{8\pi^2 r_{ij}^3} [S_{cc} <3l_c^2 - 1 > + \tfrac{1}{3}(S_{aa} - S_{bb}) <3l_a^2 - 1 - 3l^2_b + 1 > + \tfrac{4}{3}S_{ab} <3l_{ab}> + ...$$

$$D_{ijzz} = \frac{-h\gamma_i\gamma_j}{8\pi^2 r_{ij}^3}\left[S_{cc}\langle 3l_c^2 - 1\rangle + (S_{aa}-S_{bb})\langle l_a^2 - l_b^2\rangle\right.$$

$$\left. + 4S_{ab}\langle l_{ab}\rangle + 4S_{ac}\langle l_{ac}\rangle + 4S_{bc}\langle l_{bc}\rangle\right] \qquad (2.17)$$

It must be noted that the off-diagonal terms in this expansion are a factor of two greater than previously reported[94]. The advantage of using such an expansion is to remove a redundant variable to leave five unknown parameters; S_{cc}, $S_{aa}-S_{bb}$, S_{ab}, S_{ac} and S_{bc}.

The equation for direct couplings now used at Edinburgh is much simpler and has been derived by Diehl[95].

Expanding (2.6) directly leads to:

$$D_{ij} = \frac{-h\gamma_i\gamma_j}{4\pi^2 r_{ij}^3}\left[S_{aa}l^2_a + S_{bb}l^2_b + S_{cc}l^2_c + 2S_{ab}l_{ab} + 2S_{ac}l_{ac}\right.$$

$$\left. + 2S_{bc}l_{bc}\right] \qquad (2.18)$$

Although this expression has six unknowns it can be simply solved simultaneously with

$$S_{aa} = -S_{bb} - S_{cc}$$

to reduce the independent variables to five.

The amount of structural information obtainable from a liquid crystal N.M.R. study is dependent upon the number of couplings observed and the symmetry of the molecule under study. For instance if a molecule of high symmetry,

say C_{3v}, was studied then from Table 2.1 there is only one unknown orientation parameter and therefore the observation of two or more couplings will provide structural information. In this case the orientation matrix is easily established, and using either expression (2.17) or (2.18), any coupling can be determined if a structure has been assumed. The structure may then be refined using a least squares method to fit the observed and calculated couplings. It has been shown that both expression (2.17) and (2.18) lead to equivalent structures[72].

2.3 Sample Preparation

Great care has to be taken when preparing sample tubes to exclude atmospheric moisture which would react with the unstable inorganic molecules under study. The solvent (~0.4 ml) is introduced via a syringe to a 5 mm N.M.R. tube in a dry train under a nitrogen atmosphere. The tube is then transferred to a vacuum line and the solvent degassed by pumping while repeatedly freezing to liquid N_2 temperature until no further gas is evolved on melting.

A 0.3 mmol portion of sample, whose purity has previously been checked by infra-red spectroscopy, is introduced to the line and frozen down into the tube which is then sealed off and removed using a glass-blowing torch. The tube is heated to above the isotropic phase for the liquid crystal and vigorously shaken to ensure complete dissolution. The tube is then ready for study on one of the various N.M.R. spectrometers available in the Department of Chemistry.

2.4 The N.M.R. Spectrometers

A departmental N.M.R. service is available on Bruker WP200 and WH360 spectrometers. These instruments have superconducting magnets, which produce a field parallel to the long axis of the N.M.R. tube, allowing spinning of the sample during data accumulation. This reduces line-widths in the spectra caused by magnetic field inhomogeneities.

The 200 MHz instrument was used to obtain silicon-29, carbon-13 and proton spectra and several proton decoupling experiments were also performed. The 360 MHz instrument was used for observing normal and proton decoupled nitrogen-15 spectra.

The majority of the spectra were run on the veteran Varian Associates XL100 spectrometer which had the advantage that, being user-operated, it was instantly accessible. This machine possesses a conventional magnet therefore the tube remains static during data accumulation in the nematic mesophase, as spinning would disturb the orientation of the sample.

Despite its age this spectrometer still produced good spectra and proved particularly useful on account of its extremely stable low temperature control, a feature found lacking in the more modern machines. The normal liquid N_2 reservoir for cooling the stream of nitrogen which controls the sample temperature was replaced by an acetone/CO_2 slush bath, as extremely low temperatures were not required.

Fluorine, phosphorus and carbon-13 spectra were observed on this instrument, and decoupling experiments involving these nuclei, plus proton, were possible (another feature lacking in the 200 MHz instrument). All samples were run using the built-in external deuterium lock. It has, however, now been found that a sealed capillary of deuteriated solvent added to the liquid crystal solution[96] does not significantly alter the observed parameters, and any line broadening resulting from increased inhomogeneity within the sample tube is amply balanced by the increased resolution obtained by the possibility of shimming up on the observed signal[97]. The Bruker instruments, having inherently stable magnets, do not require a lock.

When performing decoupling experiments on the XL100 Spectrometer, difficulty was sometimes experienced finding the exact position of the peaks to irradiate. This was mainly because the external lock reference frequency drifted from day to day. The expected position of the peak was calculated and the decoupling frequency applied at high power. If no effect was observed then the decoupling frequency was varied in steps of 100 Hz to either side of the initial irradiation until an effect was observed. The decoupling power was then decreased and the peak was "homed-in" upon. By moving the irradiation frequency by the previously measured couplings it was possible to determine which peak had been discovered, and a full set of decoupled spectra could be run.

2.5 Experimental Procedures

If the indirect spin-spin coupling, J, is normally seen, then in a nematic mesophase the coupling observed will be of magnitude J + 2D, where D is the direct dipole-dipole coupling. However, nuclei that are equivalent in an isotropic phase may couple in an anisotropic liquid crystal solution. Extra terms in the coupling Hamiltonian[98] destroy the equivalence and n equivalent nuclei give rise to a multiplet of n lines with couplings of 3D[99].

In order to determine the value of D, it is first necessary to measure J (if it is observed). The preferred method is to take measurements in the isotropic phase of the chosen liquid crystal solvent, as significant differences in coupling with change of solvent have been observed[100]. Usually these couplings are assumed to be constant over the thermal range of the experiment, however, if the couplings are measured in an isotropic deuteriated solvent, such as $CDCl_3$, at the same temperatures as in the liquid crystal solvent, then any variation can be taken into account.

As direct couplings are highly temperature dependent, great care has to be taken when running nematic spectra. Compatible spectra are obtained by ensuring that, when any two nuclei are observed, the common coupling is of the same magnitude in each case. In practice this is difficult to achieve and generally spectra are run over a small temperature range and the couplings linearly interpolated to coincide with previous measurements.

To obtain structural information, the signs of the couplings are required. This is achieved by performing a series of double resonance experiments[101], in which a radio frequency field is applied, perpendicular to the static field, perturbing the spectrum. If a nucleus A is being observed while transitions associated with a nucleus X are irradiated, then the experiment is denoted by A-{X}.

To understand the double resonance experiment, the spin-spin sublevels within the molecule must be considered.

Figure 2.2

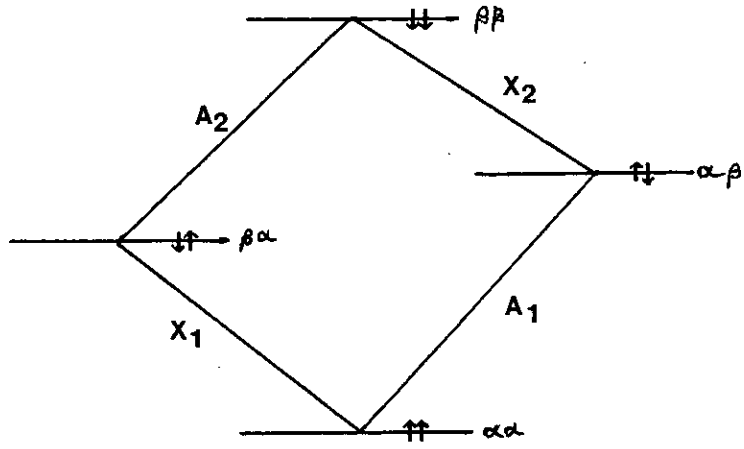

Irradiating at very low powers causes population effects of the spin levels connected by the irradiation frequency, which change the intensities of the observed lines. This is known as the Overhauser effect. If, for example, the transition X_1 is irradiated, then the populations of the two levels connected by this transition will be equalised. As the intensities of lines A_1 and A_2 are dependent on the population difference between their upper and lower levels, that of A_1 will be reduced while that of A_2 will be increased.

At slightly higher irradiating powers, a tickling effect is observed, which, in addition to the population effects, splits the relevant resonance lines into two peaks, caused by quantum mechanical mixing of the sublevels involved. In this case if the X_1 transition is irradiated then both the A_1 and A_2 resonances will be split.

Figure 2.3

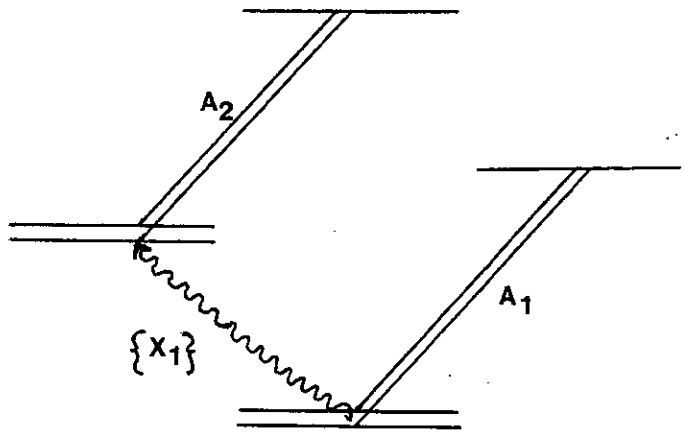

In Figure 2.2 the transitions A_1 and A_2 do not have the same frequency, they differ by the coupling J_{AX}. If J_{AX} is positive then the two middle states, $\alpha\beta$ and $\beta\alpha$, of opposite spin, will have a lower average energy than in the uncoupled case. This means that the A_2 transition will be of higher frequency than the A_1 transition and similarly X_2 will be higher than X_1. For a negative J_{AX} the reverse is true. In the simple AX spectra, there is no visible distinction between these two cases and only the magnitude of the coupling, not its sign, can be determined. However, for a spin system with three or more sets of spins coupled together, the relative signs can be determined.

Figure 2.4

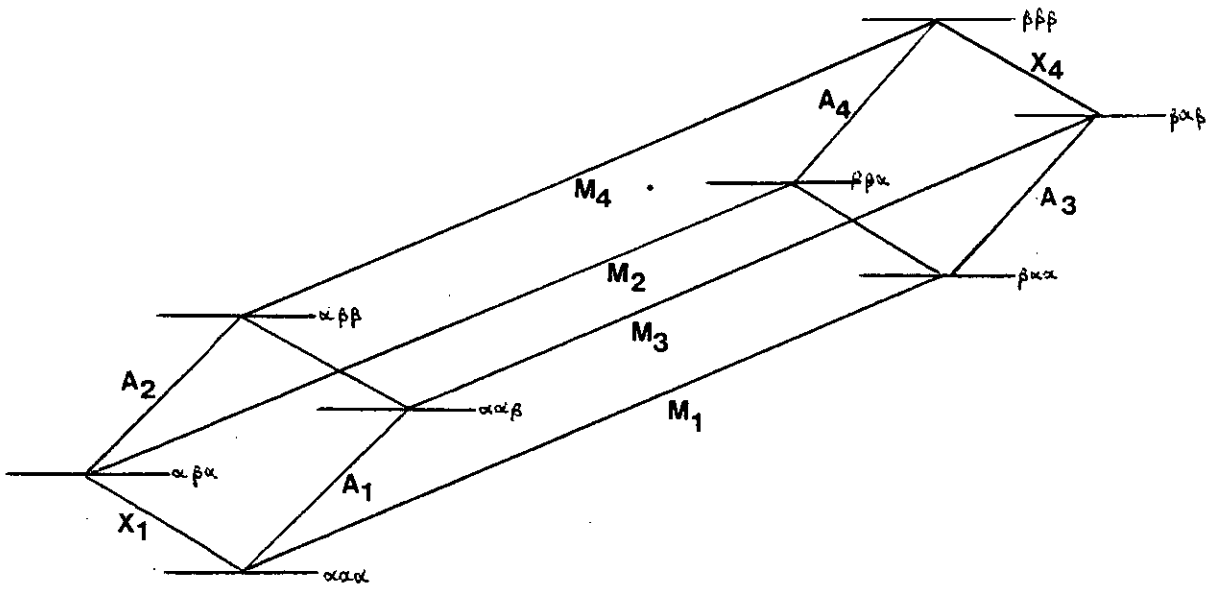

Figure 2.4 represents a simple three spin system, MAX. This will give the following observed A and X spectra:

Figure 2.5

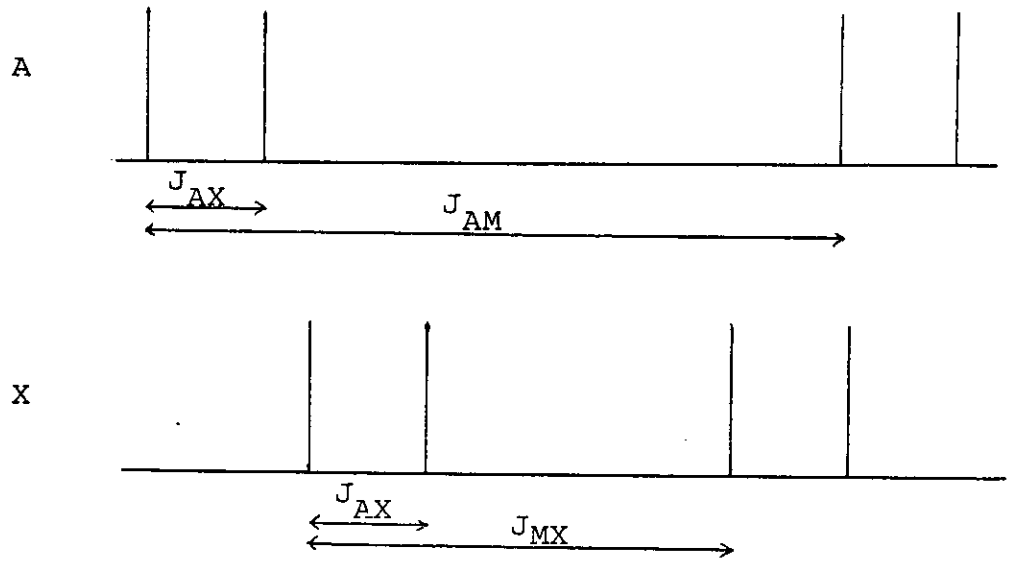

If J_{AM} is positive then, as before, the M(α)A(β) and M(β)A(α) spin states will have a lower average energy than in an uncoupled case. This means that transitions A_3 and A_4 will have a higher frequency than A_1 and A_2. The opposite is true if J_{AM} is negative. The same argument applies for the effect of the sign of J_{MX}.

Now consider an A{X} experiment. If the X spectrum is irradiated at the high frequency pair of transitions then two possible effects are observed in the A spectrum.

Figure 2.6

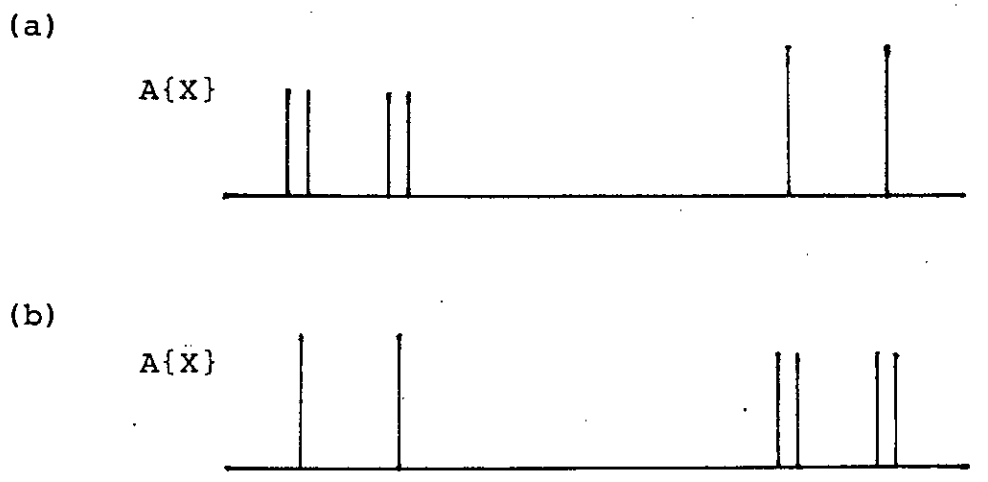

In the case of Figure 2.6(a), the irradiation of the high frequency transitions of the X spectrum have caused an effect on the high frequency transitions of the A spectrum. If J_{MX} is negative, then X_1 and X_2 transitions have been irradiated, affecting the A_1 and A_2 transitions and showing J_{AX} to be negative. Similarly if J_{MX} is positive then so must be J_{AX}. In either case for Figure 2.6(a) the signs of J_{AX} and J_{MX} are the same.

In the second possibility, Figure 2.6(b), the same argument shows that the signs of J_{AM} and J_{MX} must be opposite.

In general when considering more complicated spin systems, if the tickling irradiation is moved to a higher frequency transition and the effect also moves to a higher frequency then the couplings involved are of the same sign, while conversely if the effect moves in the opposite direction the couplings involved are of opposite sign.

The couplings related by decoupling experiments are in fact the reduced coupling constants[102], K, where:

$$J_{AX} / K_{AX} = \frac{- h\gamma_A\gamma_X}{4\pi^2} \qquad (2.19)$$

where γ_A is the magnetogyric ratio for nucleus A.
It is convenient to consider the quantity:

$$K_A = \frac{\gamma_A \sqrt{h}}{2\pi} \qquad (2.20)$$

which has been listed for several nuclei in Table 2.2.

EX BIBL. UNIV. EDINBURGH

Table 2.2

Nucleus	$K = \frac{\gamma_A \sqrt{h}}{2\pi}$
^{1}H	346.574
^{13}C	87.140
^{15}N	-35.125
^{19}F	326.054
^{29}Si	-68.849
^{31}P	140.304

It must be noted that in the case of couplings involving ^{15}N or ^{29}Si, which have negative magnetogyric ratios, the signs of the reduced couplings as derived from the double resonance experiment are opposite to the signs required.

The double resonance method can only determine the relative signs of the couplings, not their absolute values. These must be determined by comparison with a coupling of previously known sign; the indirect PF coupling, for example, is known to be always large and negative[103,104] and it can be assumed that the anisotropic coupling, J + 2D, is also negative.

2.6 Errors and Limitations

The errors and limitations of liquid crystal N.M.R. Spectroscopy as a structural technique fall into three broad categories; the initial constraints imposed by the choice of molecule and its compatibility to study by N.M.R. spectroscopy, accuracy of coupling measurement, and solvent-solute effects and interactions.

The N.M.R. technique is mainly limited to observing molecules containing naturally high abundances of spin ½ nuclei. Of the nuclei observed in this work, proton, fluorine and phosphorus can be observed directly, while isotopic enrichment techniques are required to obtain good spectra from carbon-13 and nitrogen-15. Useful silicon-29 spectra proved difficult to obtain because of the long data accumulation times required.

In order to obtain useful structural information from a molecule, it must be possible to observe more couplings than the number of parameters required to define the orientation (see Table 2.1). This limits the number of suitable molecules to those with high symmetry which require fewer orientation parameters, or those with many spin ½ nuclei[105]. In the latter case the spectra will be second order and exceedingly complex, however, there are spectral analysis computer packages[106,107] available which facilitate their interpretation. In order to simplify the line assignment process, extra information may be obtained by studying deuteriated samples[108] or from the natural abundance carbon-13 and nitrogen-15 satellites[109], or by spinning at the magic angle to give first order spectra[110].

The accuracy of determination of the direct couplings depends on several factors. Initially the indirect J coupling must be determined. This can not be directly measured in the anisotropic nematic mesophase and must be estimated from isotropic measurements, preferably in the chosen liquid crystal solvent. However, in proton and carbon-13 isotropic spectra the peaks corresponding to the liquid crystal itself can obscure the solute peaks and couplings measured in other solvents may be required. In general the procedures for minimising errors from this source are detailed in Chapter 2.5 and the accuracy of J determination is estimated at around ±0.5 Hz.

Nematic spectra are expected to be broader than in the isotropic case because in a viscous liquid the spin-spin relaxation time is reduced, increasing the linewidth. The further broadening of lines at the extremities of spectra has been ascribed to temperature[111,112] and concentration inhomogeneities within the sample tube.

The effect may be minimised by running the experiments at room temperature, and so ensuring thermal equilibrium and stability. At low temperatures a thermal gradient is set up by the cooling stream of nitrogen flowing up past the sample tube, and successive spectra of different nuclei may require linear interpolation of the couplings, which do not necessarily vary linearly with temperature. These problems do not arise with room temperature runs, which also allow the long accumulation times needed to observe nuclei like silicon-29.

It has been found that if the sample tube is removed just prior to data accumulation and shaken vigorously, maximising the dissolution of the sample and minimising concentration inhomogeneities, linewidths can be reduced dramatically[72].

Careful experimental procedure allows the observation of couplings to the following accuracies:

Table 2.3 Accuracy of Coupling Determination in the Nematic Mesophase

Nucleus	Estimated Error/Hz
Proton	0.2
Fluorine	0.5
Phosphorus	0.7
Carbon-13	1.0
Nitrogen-15	1.0
Silicon-29	1.5

Vibrational effects are generally greater than the estimated observation uncertainties, and are discussed in detail in Chapter 3.

The other main limitation to structural determination from L.C. N.M.R. are solvent-solute effects in the oriented environment. The liquid crystal may interact with the solute by dispersion forces, dipole moments, steric effects and specific interactions, any of which may, in principle, affect the structure[113]. These effects are minimised

by the choice of an inert liquid crystal as solvent (which has been discussed in Chapter 2.1). Discrepancies between structures derived from L.C. N.M.R. and Electron Diffraction or Microwave Spectroscopy have also been explained by a two-site theory[114]. This proposes that the solute molecule can undergo rapid exchange between at least two sites of opposite ordering, and so result in a misleading average orientation being observed.

The most popular postulated cause for structural discrepancies is, however, anisotropy in the indirect J coupling[115-118]. Theoretical calculations[119,120] and experimental evidence[121-123] suggest that this effect is negligible for proton couplings, but not necessarily so for heavier nuclei. The magnitude of J anisotropies have been estimated from the difference between observed and calculated direct couplings when they are constrained to conform to a known geometry[124]. This approach is far from satisfactory as it has already been shown that the structure may change in the nematic mesophase. Recently the anisotropy of the indirect FF and CF couplings have been measured in meta-difluorobenzene[125]. This structure can be completely determined from the proton spectrum and therefore differences between the observed and calculated fluorine spectrum are directly attributable to anisotropy of the indirect couplings. The magnitude of this effect was seen to be around 2-3 per cent for the FF coupling, and even greater for the CF coupling. This is therefore equally as important a consideration as vibrational effects.

CHAPTER THREE

VIBRATIONAL CORRECTIONS

3.1 Introduction

The limitations of Electron Diffraction as a structural technique have been discussed in Chapter One, where it was noted that data from other sources could add to the precision of refined structures. In this work additional data from Liquid Crystal N.M.R. Spectroscopy and Microwave Spectroscopy have been used to complement those from Electron Diffraction alone. The problem with such combined analyses is one of compatibility; the operational definition of bondlength being different for each structural technique. It is therefore necessary to understand the physical significance of the experimentally observed parameters in each case.

In each technique the effects of molecular vibrations are averaged differently during data accumulation and these have to be quantified before combined analysis is possible. In general complete vibrational correction to give the equilibrium structure is difficult owing to the lack of precision in evaluating the anharmonic contributions. However, using a set of simple relationships, harmonic corrections can lead to self-consistent structures which are compatible for various techniques.

3.2 The Equilibrium Structure

The most fundamental definition of interatomic distance parameters is the equilibrium r_e structure, in which all the intramolecular modes are assumed frozen at the minima of their respective potential energy curves.

The equilibrium structure is that obtained from ab initio wave function calculations[126]. It is, however, physically a purely hypothetical structure because even at a temperature of absolute zero molecules will still undergo zero-point vibrations. Its main use is as a constant standard structure to which internuclear parameters measured by any of the host of available structural techniques may be compared and related by allowing for vibrational effects.

The definition of the equilibrium structure is dependent on the concept of an intramolecular potential energy surface, which arises from consideration of the Born-Oppenheimer approximation[127]. This assumes that, since the kinetic energy of the electrons in a bond is several orders of magnitude greater than that of the nuclei involved, then their respective contributions to the total energy of the system may be independently considered. The vibrations of the nuclei can therefore be shown to occur within the constraints of an isotopically invariant electronic potential surface.

It has been found that although the vibrational energy levels are dependent on nuclear mass, the effect on internuclear separations is negligible[128] and the equilibrium structure can be considered isotopically invariant. The validity of the Born-Oppenheimer approximation is therefore assumed in most structural work.

3.3 Electron Diffraction

The Electron Diffraction experiment leads to a set of distance parameters known as the r_a structure. This is derived from the centre of gravity of the peaks in the radial distribution curve (see Chapter 1.2) given by $P(r)/r$. If vibrational averaging is denoted by angle brackets then:

$$r_a = \langle r_{ij}^{-1} \rangle^{-1} \qquad (3.1)$$

where r_{ij} is the instantaneous separation of atoms i and j.

Interatomic stretching vibrations are usually considered as classical Morse oscillations, since the Morse function (3.2) has been shown to be a reasonable approximation to interatomic potential energy curves[129,130].

$$V(r_{ij}) = D\{1 - \exp[-a(r_{ij} - r_e)]\}^2 \qquad (3.2)$$

If the vibration has a mean square parallel amplitude of u^2, then the probability distribution for the bond-length can be derived from the groundstate wave function to give:

$$P(r) = \left(\frac{1}{2\pi u^2}\right)^{\frac{1}{2}} \{1 + ax + \frac{ax^3}{6u^2}\} \exp\frac{-x^2}{2u^2} \qquad (3.3)$$

where $x = r - r_e$.

Suitable averaging of this expression[24,131] leads to:

$$r_a = r_e + \frac{3au^2}{2} - \frac{u^2}{r_e} \qquad (3.4)$$

In practice the Morse anharmonicity constant, a, is assumed to be 200 pm^{-1} for bonded, and zero for non-bonded distances, and the experimentally measured r_a is used as the denominator instead of r_e in the third term, as a good approximation.

A simple conversion is often made to give the r_g structure where:

$$r_g = r_a + \frac{u^2}{r_a} \qquad (3.5)$$

The r_g structure now differs from the equilibrium structure by only one term:

$$r_g = r_e + \frac{3au^2}{2} \qquad (3.6)$$

The r_g structure represents the instantaneous separation of a pair of atoms averaged over a Boltzmann distribution of the available molecular vibration energy levels, that is $r_g = \langle r \rangle$, therefore:

$$r_g^2 = \langle \Delta x^2 \rangle + \langle \Delta y^2 \rangle + (r_e + \langle \Delta z \rangle)^2 \qquad (3.7)$$

where the angle brackets represent vibrational averaging. Expanding (3.7) as a binomial series gives:

$$r_g = r_e + \langle \Delta z \rangle + \frac{(\langle \Delta x^2 \rangle + \langle \Delta y^2 \rangle)}{2r_e} + \delta r$$

where δr is a negligible term associated with centrifugal stretching[132].

Therefore to a good approximation r_g can be expressed as:

$$r_g = r_e + \langle \Delta z \rangle + K \qquad (3.8)$$

where $K = \frac{(\langle\Delta x^2\rangle + \langle\Delta y^2\rangle)}{2r_e}$

The r_a and r_g structures exhibit an effect known as shrinkage (see Chapter 1.7). If a linear triatomic XYZ is considered then the shrinkage effect, δ_g, may be calculated from equation 3.8, giving:

$$\delta_g = r_g(XY) + r_g(YZ) - r_g(XZ)$$

In this case the $\langle\Delta z\rangle$ terms will cancel to give[133]:

$$\delta_g = K(XY) + K(YZ) - K(XZ) \qquad (3.9)$$

This approach can be extended for non-linear polyatomics, and shows that only harmonic perpendicular amplitude corrections are required to allow for the shrinkage effect and for conversion to a self-consistent structure such as the r_α structure[134] which is given by:

$$r_\alpha = r_g - K \qquad (3.10)$$

Therefore:

$$r_\alpha = r_e + \langle\Delta z\rangle \qquad (3.11)$$

The r_α structure represents the average projection of the instantaneous internuclear separation onto the equilibrium axis. Although it only differs from the equilibrium structure by one term this depends on anharmonic contributions to the vibrational corrections which are difficult to evaluate with much precision[22]. Although there have been recent attempts to attain the equilibrium structure[135-138], the r_α structure which depends only on harmonic vibrational corrections[139]

is still most useful for combined analysis work.

Problems still arise, however, with floppy molecules. The structural effects of low frequency, high amplitude bending modes are only poorly approximated by a harmonic rectilinear co-ordinate analysis. The consideration of these modes in curvilinear co-ordinates[140] is more realistic, however, the theory and calculations are extremely complex and so far have only been extended to study triatomic systems.

3.4 Liquid Crystal N.M.R.

Nuclear Magnetic Resonance spectra of molecules oriented in the nematic phase of a liquid crystal solvent lead to the observation of the direct dipole-dipole couplings. These couplings are inversely proportional to the cube of the internuclear separation and therefore:

$$r_d = \left\langle \frac{1}{r_{ij}^3} \right\rangle^{-1/3} \qquad (3.12)$$

Expanding as a binomial series as before (see equation 3.7) gives:

$$r_d = r_e + \langle \Delta z \rangle + \frac{\langle \Delta x^2 \rangle + \langle \Delta y^2 \rangle - 4\langle \Delta z^2 \rangle}{2r_e^2} \qquad (3.13)$$

The application of vibrational corrections is however not as simple as this, as the D couplings are affected by the anisotropic molecular motion as well as by vibrational nuclear motion[141,142].

The co-operative nature of vibrational and rotational motion leads Burnell and de Lange[143,144] to suggest that they must be considered inter-dependent, but then corrections become increasingly complicated. The differences between the correlation times for molecular reorientation motion of around 10^{-9} s and for vibrational motion of around 10^{-13} s indicate that they can be treated as practically independent motions[145].

It was shown in Chapter 2.3 that the orientation of the molecule could be described by an orientation matrix, S, the elements of which are given by:

$$S_{\alpha\beta} = \tfrac{1}{2} (3 \cos_{\alpha}\theta \cos_{\beta}\theta - \delta_{\alpha\beta}) \qquad (3.14)$$

The direct D couplings are then defined as:

$$D_{ij} = \frac{-K_{ij}}{r^3} \sum_{\alpha\beta} \cos_{\alpha}\theta \cos_{\beta}\theta S_{\alpha\beta} \qquad (3.15)$$

where α,β = X, Y, Z.

It is a general rule that the sum of the products of the elements of two matrices A and B is equivalent to the trace of the matrix product AB^1. In this case the S orientation matrix is symmetric therefore $S = S^1$ and equation (3.15) can be rewritten as:

$$D_{ij} = -K_{ij} \, Tr(S\Phi^{ij}) \qquad (3.16)$$

where

$$\Phi^{ij}_{\alpha\beta} = \left\langle \frac{r_{\alpha}^{ij} \, r_{\beta}^{ij}}{r_{ij}^{5}} \right\rangle_{v}$$

where the angle brackets represent averaging over vibrational motion.

If the interatomic separation r is considered as

$$r = R + \Delta \tag{3.17}$$

where Δ is the instantaneous excursion of r from the equilibrium value R, then expanding Φ in powers of the components of Δ leads to[146]:

$$\Phi = \Phi_e + \Phi_{harm} + \Phi_{anharm} + \text{higher terms} \tag{3.18}$$

where

$$\Phi_e = \frac{R_\alpha R_\beta}{R^5} = \frac{\cos_\alpha\theta \cos_\beta\theta}{R^3} \tag{3.19}$$

and

$$\Phi_{harm} = [C_{\alpha\beta} - 5 \sum_\gamma \cos_\gamma\theta (C_{\alpha\gamma}\cos_\beta\theta + C_{\beta\gamma}\cos_\alpha\theta) + \frac{5}{2}\cos_\alpha\theta\cos_\beta\theta \sum_{\gamma\delta} C_{\gamma\delta}(7\cos_\gamma\theta\cos_\delta\theta - \delta_{\gamma\delta})]/R^5 \tag{3.20}$$

where $\alpha,\beta,\gamma,\delta$ = X, Y, Z and $\delta_{\gamma\delta}$ is the Kronecker delta. The covariance matrices, C, are defined as:

$$C_{\alpha\beta} = \langle\Delta_\alpha\Delta_\beta\rangle_v \tag{3.21}$$

Similarly to the Electron Diffraction case, because of the difficulties involved in the evaluation of anharmonic effects, only the harmonic contribution will be considered. Correcting for harmonic vibrations leads to the r_α structure[147] which is equivalent to that obtained from Electron Diffraction if the temperatures of the experiments are the same.

3.5 Microwave Spectroscopy

The microwave experiment leads to a structure derived from the rotational constant[148]:

$$B = \frac{h}{8\pi^2 \mu r^2} \tag{3.22}$$

If a simple diatomic molecule is considered then the rotational constant for the ground vibrational state, B_o, will yield a bond length

$$r_o = \langle r^{-2} \rangle^{-\frac{1}{2}} \tag{3.23}$$

However in polyatomics the situation is not as simple because of Coriolis couplings[149] between the normal modes, and this simple relationship is destroyed.

Vibrational corrections to attain the r_e equilibrium structure from the B_e equilibrium rotational constant may be represented as a sum of the rotation-vibration interaction constants, α_i, over the 3N-6 normal modes, i, of degeneracy d_i:

$$B_e = B_o + \tfrac{1}{2} \sum_{i}^{3N-6} d_i \alpha_i \tag{3.24}$$

For very simple molecules it is possible to measure α_i directly from the spectra. However for most polyatomics these constants are not easily obtained. The α_i constants can be separated into harmonic plus anharmonic contributions.

$$\alpha_i = \alpha_i(\text{harm}) + \alpha_i(\text{anharm}) \tag{3.25}$$

As before the anharmonic effects are difficult to evaluate, but the harmonic contributions can be derived from a normal co-ordinate analysis[150]. Applying harmonic corrections gives the r_z structure from:

$$B_z = B_o + \tfrac{1}{2} \sum_{i}^{3N-6} d_i \alpha_i(\text{harm}) \qquad (3.26)$$

This represents the mean positions of the nuclei in the ground vibrational state

$$r_z^2 = \langle \Delta x \rangle_o^2 + \langle \Delta y \rangle_o^2 + (r_e + \langle \Delta z \rangle_o)^2 \qquad (3.27)$$

$$r_z = r_e \left[1 + \frac{2\langle \Delta z \rangle_o}{r_e} + \frac{\langle \Delta x \rangle_o^2 + \langle \Delta y \rangle_o^2 + \langle \Delta z \rangle_o^2}{r_e^2}\right]^{\frac{1}{2}}$$

Expanding as a power series gives:

$$r_z = r_e + \langle \Delta z \rangle_o + \frac{\langle \Delta x \rangle_o^2 + \langle \Delta y \rangle_o^2}{2r_e} + \ldots\ldots \qquad (3.28)$$

The third and higher terms are negligible leaving

$$r_z = r_e + \langle \Delta z \rangle_o \qquad (3.29)$$

Equation (3.28) should be compared with the expression, (3.8), for r_g from Electron Diffraction. The linear averages $\langle \Delta x \rangle$, $\langle \Delta y \rangle$ and $\langle \Delta z \rangle$ are of the order of magnitude $\langle \Delta r^2 \rangle / r_e$ [57] which is around 1.0 pm. If the ratio of the square of the linear averages to the quadratic average is considered then, from above:

$$\frac{\langle \Delta r \rangle^2}{\langle \Delta r^2 \rangle} \cong \frac{\langle \Delta r^2 \rangle}{r_e^2} \qquad (3.30)$$

This shows why the third term is important in (3.8) but negligible in (3.28).

3.6 Combined Analysis

The previous sections have described the physical significance of the structures measured by Electron Diffraction, Liquid Crystal N.M.R. Spectroscopy and Microwave Spectroscopy and discussed the effects of vibrational averaging in each case. The difficulties involved in evaluating the effect of anharmonicity in the vibrational corrections have been pointed out and therefore in combined analysis only harmonic corrections are considered. These lead to the following structural definitions.

Electron Diffraction	$r_\alpha = r_e + \langle\Delta z\rangle$
Liquid Crystal N.M.R.	$r_\alpha = r_e + \langle\Delta z\rangle$
Microwave	$r_z = r_e + \langle\Delta z\rangle_o$

In the case of the r_α structures the $\langle\Delta z\rangle$ term represents a thermal average over a Boltzmann distribution of the available vibrational states, while in the r_z structure the $\langle\Delta z\rangle_o$ term is an average in the ground vibrational state. In general, differences between r_α and r_z structures are small, but it is possible to extrapolate the r_α structure to absolute zero[151] at which point it becomes equivalent to the r_z structure.

$$r_\alpha^o = \lim_{T \to 0K} r_\alpha$$

The simplest way to carry this out is to extrapolate to r_g^o and then interconvert[152,153]. Previously it has been shown (equation 3.8) that:

$$r_g = r_e + \langle\Delta z\rangle_T + K_T \qquad (3.31)$$

If the bond is considered to vibrate independently from the rest of the molecule, that is assuming a diatomic approximation, then:

$$\langle \Delta z \rangle_T \cong \frac{3}{2} a \langle \Delta z^2 \rangle_T \qquad (3.32)$$

Thus from equation (3.31):

$$r_g^o = r_g - \frac{3a}{2} (\langle \Delta z^2 \rangle_T - \langle \Delta z^2 \rangle_o) - (K_T - K_o) \qquad (3.33)$$

From equation (3.10):

$$r_\alpha^o = r_g^o - K_o \qquad (3.34)$$

Therefore:

$$r_\alpha^o = r_g - \frac{3a}{2} (\langle \Delta z^2 \rangle_T - \langle \Delta z^2 \rangle_o) - K_T \qquad (3.35)$$

where $K_T = \dfrac{(\langle \Delta x^2 \rangle_T + \langle \Delta y^2 \rangle_T)}{2r_e}$

Note that, in this expression, K has been measured at the temperature of the experiment and not at absolute zero as previously reported[22,57].

In order to evaluate the vibrational corrections, a harmonic force field for the molecule under study has to be constructed. An established program[154], GAMP, is used, which is based on Schachtschneider's GMAT routines[155]. The input includes the molecular geometry and the fundamental vibrational modes with their assigned frequencies, observed from infra-red and Raman spectroscopy.

Initial trial estimates for the force constants are refined until the observed frequencies are reproduced. This can be achieved by changing individual force constants, or by a least squares refinement or by a "direct fit" method. Consideration of the potential energy distribution matrix ensures that the modes have been correctly fitted to their assigned frequencies. The output now includes the relevant vibrational corrections (both parallel and perpendicular) for the temperature of the experiment and at absolute zero.

The Electron Diffraction parameters are corrected for vibrations according to equation (3.35). Previously the experimental mean square parallel amplitudes were used to convert to the r_g structure, but now spectroscopic values are used for all terms in the vibrational corrections.

The microwave spectroscopy parameters were corrected to give the B_z rotational constants from equation (3.26) using a program obtained from Oslo, originally written by Hilderbrandt[156]. The liquid crystal N.M.R. parameters were corrected according to equation (3.20) using Diehl's[146] program, VIBR.

These programs both require the setting up of an input file containing the molecular geometry, the atomic masses, the normal vibrational modes and their associated force constants (from GAMP), and in the case of VIBR, the orientation parameters. The output from the Oslo program includes the calculated values for B_o (which should agree

with those observed experimentally), and the corrections to give B_z for each isotopic species. The VIBR program outputs the calculated vibrational frequencies and the direct D couplings with their harmonic corrections. This program may be cycled two or three times until the observed and calculated couplings agree.

The established Electron Diffraction refinement program (see Chapter 1.6) allows for the inclusion of data from other sources. The weighting matrix (equation (1.17)) is extended diagonally, with the extra data being weighted according to the inverse of the square of the uncertainty of the observation. In the case of the vibrationally corrected parameters, an additional uncertainty of ten percent of the vibrational correction was included. Model programs are written to extract the structural information from the extra data, typical examples of which may be found in Appendix I.

It is therefore possible, using harmonic vibrational corrections, to combine data obtained from Electron Diffraction, Liquid Crystal N.M.R. and microwave spectroscopy. This has been shown previously[51-56,124] to increase the precision of structural determination from any single technique. This result is verified by the detailed structural and vibrational analysis of several compounds in this thesis.

CHAPTER FOUR

THE MOLECULAR STRUCTURE OF DIFLUOROPHOSPHINE CYANIDE, DETERMINED BY USING A COMBINATION OF DATA FROM ELECTRON DIFFRACTION AND LIQUID CRYSTAL N.M.R. SPECTROSCOPY

4.1 Introduction

It has been shown in the preceeding chapters that Liquid Crystal N.M.R. Spectroscopy (L.C.N.M.R.) can be a possible source of structural information. It has been suggested that, by applying suitable vibrational averaging corrections, this information can be made compatible with that obtained from gas phase Electron Diffraction (E.D.) experiments[71]. However, it has been pointed out that, in addition to being in a different phase, the molecule dissolved in a liquid crystal may experience dispersion forces, steric effects and specific interactions, any of which could, in theory, affect the structure. In order to investigate the validity of a structural analysis combining data from both Electron Diffraction and Liquid Crystal N.M.R. Spectroscopy a series of difluorophosphine pseudohalides has been studied.

These compounds are suitable for study by L.C.N.M.R. as, by suitable isotopic enrichment, up to seven couplings can be observed. Only three parameters are required to define the orientation (Cs symmetry, Table 2.1), therefore the problem is over-determined and useful structural information can be obtained.

Although these compounds have been studied previously by E.D. alone[48,157], the refinements suffered from the problem of overlapping peaks in the radial distribution curve (see Chapter 1.7), and several parameters had to be

held fixed at reasonable estimated values. The inclusion of extra data from L.C.N.M.R. should enable these parameters to be freed and refined.

The first member of the series to be studied was difluorophosphine cyanide, the results for which are discussed in this chapter. Trends and observations for the entire series of compounds are discussed in Chapter 6.

4.2 Experimental

A sample of PF_2CN was prepared by a standard method[159,160] by the reaction between difluorophosphine bromide and silver cyanide. The difluorophosphine bromide was prepared from the reaction between difluorophosphinedimethylamine[161] and hydrogen bromide[162]:

$$(CH_3)_2NPF_2 + 2HBr \rightarrow PF_2Br + [(CH_3)_2NH_2]Br$$

The silver salt was prepared from silver nitrate and potassium cyanide solutions. The precipitate was washed with alcohol then dry ether and pumped on overnight in an ampoule. For Liquid Crystal N.M.R. experiments a small sample was produced from doubly labelled potassium cyanide.

An excess of the PF_2Br was condensed onto the silver salt in the ampoule in the dark and allowed to warm to room temperature for five minutes. The product was purified by fractionation and its purity checked by infrared spectroscopy.

4.3 Data Collection

4.3.1 Electron Diffraction

A sample of PF_2CN was prepared and its purity checked by infrared spectroscopy. However, at the end of the Electron Diffraction run, during which the sample was kept at 273 K in an ice bath, the ampoule was seen to contain a white solid and on development the plates contained a substantial percentage (>30%) of PF_3. The same problem repeated itself at a second attempt. It was assumed that an auto-catalysed reaction was taking place.

$$3PF_2CN \rightarrow 2PF_3 + P(CN)_3$$

In the end, plates that had been run previously were retraced by the new microdensitometry service at Daresbury. The relevant experimental details are listed in Table 1.1.

4.3.2 Liquid Crystal N.M.R. Spectroscopy

Samples were prepared containing 0.3 mmol of the doubly-labelled $PF_2{}^{13}C{}^{15}N$ in 0.5 ml of 'E5' liquid crystal as solvent in 5 mm N.M.R. tubes. These solutions were found to become isotropic at a temperature of around 300 K.

Phosphorus, fluorine and carbon-13 spectra were obtained on the Varian XL100 Spectrometer (see Chapter 2.4) in the pulsed Fourier transform mode. During the low temperature runs, the normal liquid nitrogen cooling system was replaced by an acetone/dry ice slush bath to increase thermal stability.

Nitrogen-15 spectra were obtained from the departmental service on the Bruker WH360 spectrometer.

The indirect J couplings (Table 4.2) were measured in the liquid crystal solutions heated until they became isotropic. The signs of these couplings had been previously established by Reid[163].

The direct D couplings (Table 4.2) were calculated from measurements in the nematic mesophase at 253 K and 283 K. The relative signs of the couplings were established by a series of double resonance experiments (Table 4.1) and their absolute values determined by comparison with the PF coupling which is always large and negative[104,164].

Examples of the spectra obtained, and the double resonance experiments carried out, are shown in Figure 4.1.

4.4 Structural Refinements

4.4.1 Electron Diffraction

In all structural refinements it was assumed that PF_2CN possesses Cs symmetry. A model program was written with six independent parameters, the PF, PC and CN directly bonded distances, and the <FPF, <FPC and <PCN angles.

Initially the r_a structure was refined (Table 4.3). It proved possible to refine all the parameters and amplitudes of vibration. The <PCN angle was first fixed at 180°, but when freed it refined to 181.5° with a large uncertainty. This apparent non-linearity was assumed to be caused by the shrinkage effect (see Chapter 1.7).

A normal co-ordinate analysis using the program GAMP (see Chapter 3.6) was carried out to determine the spectroscopic amplitudes of vibration. A harmonic force field was refined which exactly fitted the observed vibrational frequencies[159,165] which are listed in Table 4.4 with their assignments. The harmonic vibrational corrections were calculated as outlined in Chapter 3 and are listed in Table 4.5(a).

The r_z^o structure was refined, initially fixing the <PCN angle at 180°. When this angle was subsequently freed (Table 4.6, Refinement A) it refined to a value nearer linearity than in the r_a structure, and the R_{gen} factor was unaffected at 8.1%, although the uncertainties associated with the other angles increased slightly. This angle is therefore essentially linear, which is at odds with the microwave result[166] which calculates an angle of 171°.

The molecular scattering and radial distribution curves for the E.D. data are shown in Figures 4.2 and 4.3 respectively.

4.4.2 Electron Diffraction plus Liquid Crystal N.M.R. Spectroscopy

A new model program was written to extract the structural information from the Liquid Crystal N.M.R. data. Three refinable parameters were added to define the orientation (Cs symmetry, Table 2.1), calculated according to equation 2.18. The direct couplings were added to the E.D. refinement program with weights inversely proportional to the square of their uncertainties.

Initially the orientation parameters were allowed to refine, with the structure held fixed at the E.D. only result. It was found that the observed D couplings could not be closely reproduced, and structural parameters refined to unreasonable values when freed.

It was decided to perform a differences method refinement to check whether the values and signs of the indirect J couplings had been properly assigned. The coupling observed in the nematic mesophase, Δ, is of magnitude J + 2D (except for the FF coupling where Δ = 3D). If measurements are made at two different temperatures then only the D component of the coupling will vary, and subtraction will cancel out the J dependence. This method creates a new set of pseudo-couplings and a differences orientation matrix.

$$\Delta_1 - \Delta_2 = J_1 + 2D_1 - J_2 + 2D_2 \qquad 4.1$$

But $J_1 = J_2$, therefore:

$$\frac{\Delta_1 - \Delta_2}{2} = D_1 - D_2 \qquad 4.2$$

The direct D coupling is given by (equation 2.2):

$$D_{ij} = \frac{-h\gamma_i\gamma_j}{4\pi^2 r_{ij}^3} \cdot S_{ij} \qquad 4.3$$

It can be assumed that the structure is invariant for small changes in temperature, therefore:

$$\frac{\Delta_1 - \Delta_2}{2} = \frac{-h\gamma^2}{4\pi^2 r^3} [S_1 - S_2] \qquad 4.4$$

(for the FF couplings the difference should be divided by three rather than two).

The effects of vibration on the differences orientation matrix and pseudocouplings have not yet been fully worked out, therefore, so far this method is more useful as a check on J coupling signs rather than a source of structural information. The structure derived by this method is, however, listed in Table 4.6 as Refinement B, and most parameters are seen to agree with the E.D. only r_α^o values, within the combined E.S.D.'s.

The observed and calculated differences were found to agree fairly well, except that for the PC couplings. When this difference was weighted out (Refinement C, Table 4.6) the structure and R_{gen} factor improved and the other observed and calculated differences agreed within 0.5 Hz.

Using this evidence for an anomalous PC coupling, it was given a correspondingly low weight in all future refinements. The structures refined using a combination of data from E.D. and L.C.N.M.R. are listed in Table 4.6.

Vibrational corrections were calculated using the program VIBR[146] (Table 4.5(b)) as explained in Chapter 3.4. In general the corrected and calculated couplings agree within the uncertainty involved, except for the PC coupling.

4.5 Discussion

The structure of difluorophosphine cyanide in the liquid crystal solvent is compatible with that observed in the gas-phase E.D. experiment. Including the direct D couplings in a combined structural analysis has had little effect on the overall fit of the E.D. data as measured by the R gen factor, and the molecular parameters remain within the combined E.S.D.s. The structure is seen to be essentially the same at both temperatures considered in the liquid crystal solution.

The observed couplings have been reproduced to within their E.S.D.s, except for the PC coupling. If the structure is allowed to refine to accommodate this coupling, the <FPF and <FPC angles distort significantly to unreasonable values.

There are several possible explanations for the failure to fit the PC coupling. The fact that the effect is seen to increase with the magnitude of the coupling indicates that anharmonicity of the indirect component could be a significant factor. Alternatively, anharmonicities in other couplings might cumulatively produce this effect. It was attempted to find evidence for this by changing the weights for each coupling in turn, but this met with no success. The geometry may become distorted from the Cs symmetry, and extra orientation parameters were included in the refinement to allow for this, but could not account for the PC coupling in a satisfactory manner.

The <PCN angle is seen to be essentially 180° in the E.D. structure, but 171° in the microwave structure[166]. The liquid crystal data did not fit the microwave angle and gave further support for the E.D. result, by reducing the uncertainty in this parameter dramatically in the combined analysis (Table 4.6).

There is further discussion of the results for the entire series of difluorophosphine pseudohalides in Chapter 6.

Table 4.1 Double Resonance Experiments for PF_2CN

(a) Isotropic Couplings[163]

Experiment	Couplings Related	Relative Signs	
		K	J
$^{31}P\{^{15}N\}$	PC and CN	opposite	equal
$^{19}F\{^{15}N\}$	PF and PN	equal	opposite
	FC and CN	equal	opposite
$^{19}F\{^{13}C\}$	PF and PC	equal	equal

(b) Nematic Couplings (253 K)

Experiment	Couplings Related	Relative Signs	
		K	Δ*
$^{19}F\{^{31}P\}$	PN and NF	equal	equal
	PC and CF	equal	equal
	PF and FF	opposite	opposite
$^{31}P\{^{15}N\}$	CN and CP	equal	opposite
	FN and FP	equal	opposite
$^{31}P\{^{13}C\}$	PN and CN	equal	equal
	PF and CF	equal	equal
$^{19}F\{^{13}C\}$	CN and FN	equal	equal
	CP and PF	equal	equal
	CF and FF	opposite	opposite

* $\Delta = J + 2D$ (except for FF coupling, $\Delta = 3D$)

Table 4.2 Couplings/Hz for PF_2CN

Nuclei	J	Δ^*_{253K}	D_{253K}	Δ^*_{283K}	D_{283K}
CF	+22.0(5)	-261.9(5)	-142.0(7)	-195.9(2)	-109.0(6)
CN	-10.0(5)	+191.4(4)	+100.7(7)	+155.0(3)	+82.5(6)
CP	-137.2(5)	-273.5(4)	-68.2(7)	-251.1(3)	-57.0(6)
PF	-1258.0(15)	-1115.3(3)	+71.4(15)	-1145.0(2)	+56.5(15)
PN	+11.1(5)	+28.0(3)	+8.5(6)	+25.0(2)	+6.95(6)
FN	0.0(5)	+42.7(2)	+21.4(6)	+33.4(2)	+16.7(6)
FF	-	+135.6(3)	+45.2(3)	-20.9(2)	-7.0(2)

* $\Delta = J + 2D$ (except for FF coupling, $\Delta = 3D$)

Table 4.3 Molecular Parameters for PF_2CN (E.D. only, r_a structure)

Independent Distances	Distance/pm	Amplitude/pm
P-F	157.3(1)	5.3(2)
P-C	180.8(5)	8.2(5)
C≡N	115.0(5)	6.3(7)
Dependent Distances		
F...F	236.2(4)	6.0(6)
F...C	254.5(4)	7.5(5)
P...N	295.8(4)	8.7(5)
F...N	351.6(12)	22.2(9)
Independent Angles/°		
<FPF	97.3(3)	
<FPC	97.4(4)	
<PCN	181.5(25)	

Table 4.4 Vibrational Frequencies and Assignments for PF_2CN

Species	Frequency/cm^{-1}	Approximate Description
A'	2194.0	C≡N stretch
	869.0	P-F stretch (symm.)
	629.0	P-C stretch
	549.0	<PCN deformation (in-plane)
	347.0	<FPF deformation
	185.0	PF_2 wag
A''	867.0	P-F stretch (asymm.)
	460.0	<PCN deformation (out-of-plane)
	145.0	PF_2 rock

Table 4.5 Vibrational Corrections for PF_2CN

(a) Electron Diffraction

Distance	u_T/pm	$K_T + \frac{3a}{2}\Delta u^2$	r_α^o correction/pm $(K_T + \frac{3a}{2}\Delta u^2 - \frac{u_T^2}{r})$
PF	4.15	0.62	0.51
PC	4.73	0.28	0.16
CN	3.51	0.73	0.62
FF	7.56	0.52	0.28
FC	11.64	0.20	-0.33
PN	5.07	0.30	0.21
FN	14.10	0.11	-0.46

(b) Liquid Crystal N.M.R. Spectroscopy

283 K

	D_{obs}	Correction	D_α^o *	D_{calc} **
FF	-7.0(2)	1.9	-5.1(3)	-5.1
FP	56.5(15)	2.4	58.9(15)	58.6
FC	-109.0(6)	-0.8	-108.2(6)	-107.6
PC	-57.0(6)	-0.3	-57.3(6)	-76.2
FN	16.7(6)	-0.1	16.6(6)	16.9
PN	6.95(6)	0.05	7.0(6)	7.4
CN	82.5(6)	2.5	85.0(7)	85.0
253 K				***
FF	45.2(3)	2.8	48.0(4)	48.0
FP	71.4(15)	3.0	74.4(16)	74.2
FC	-142.0(7)	-1.1	-140.9(8)	-140.2
PC	-68.2(7)	-0.5	-68.7(7)	-97.8
FN	21.4(6)	-0.2	21.2(6)	21.9
PN	8.5(6)	0.1	8.6(6)	9.3
CN	100.7(7)	3.2	103.9(10)	103.8

*An uncertainty of 10% was assumed for vibrational corrections

**Calculated from Refinement E

***Calculated from Refinement G

Table 4.6 Structural Refinements for PF_2CN

Independent Distances/pm	A/ E.D. only (r_α^o)	B/Diffs	C/ Diffs (except PC)	D/ 283 K	E/ 283 K + vibn. corrections	F/ 253 K	G/ 253 K + vibn. corrections
P-F	156.8(1)	156.9(1)	156.8(1)	156.9(1)	156.9(1)	156.9(1)	156.9(1)
P-C	181.3(6)	182.8(6)	181.3(5)	182.3(5)	182.3(5)	181.9(5)	182.0(5)
C≡N	114.3(5)	113.3(6)	114.4(5)	113.7(5)	113.7(5)	114.0(5)	113.9(5)
Independent Angles/°							
<FPF	97.4(4)	97.3(5)	97.4(4)	97.2(4)	97.1(4)	97.3(4)	97.2(4)
<FPC	97.3(4)	96.2(4)	97.4(4)	96.7(4)	96.6(3)	96.9(4)	96.8(4)
<PCN	180.6(25)	179.0(10)	181.6(10)	179.2(6)	178.7(6)	179.7(6)	179.4(6)
R_{gen} factor	8.1%	9.2%	8.2%	8.2%	8.2%	8.0%	7.9%

Figure 4.1 Selected L.C.N.M.R. Spectra for PF_2CN

(a) ^{19}F isotropic

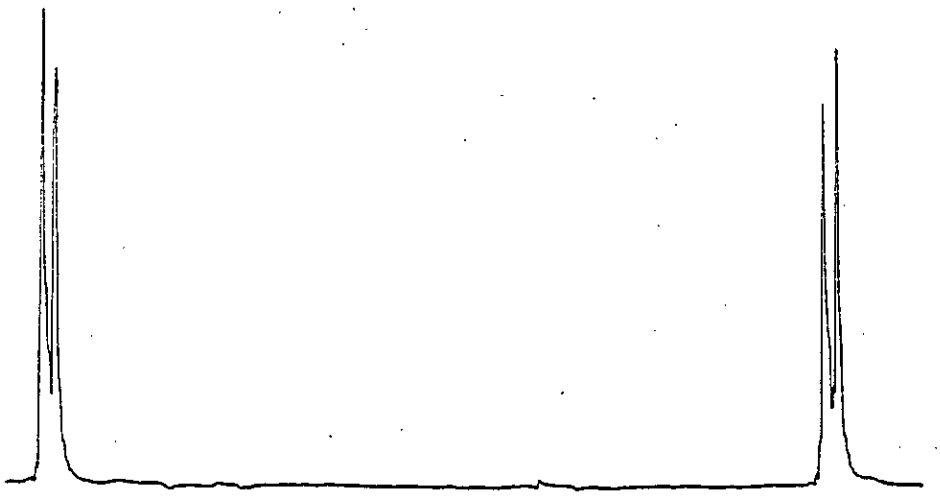

(b) ^{31}P isotropic

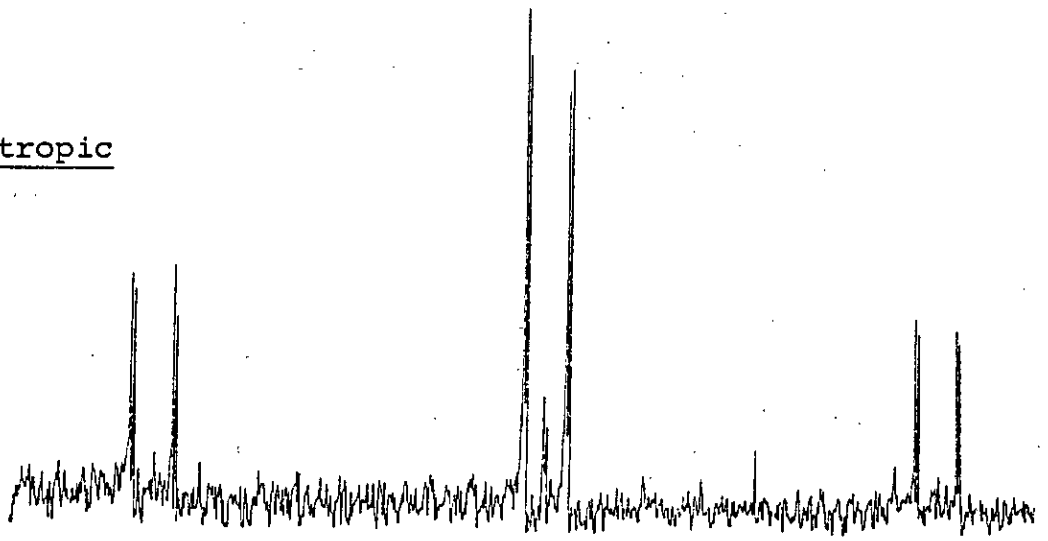

(c) ^{13}C isotropic (showing L.C. solvent peaks)

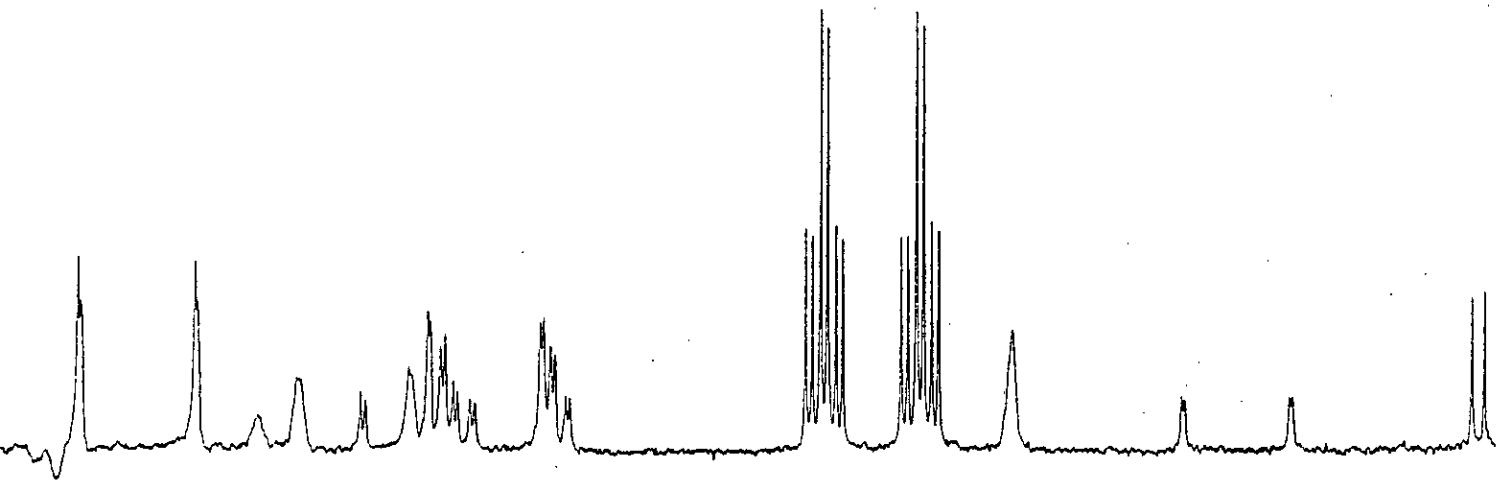

Figure 4.1 (contd.)

(d) ^{19}F (253 K)

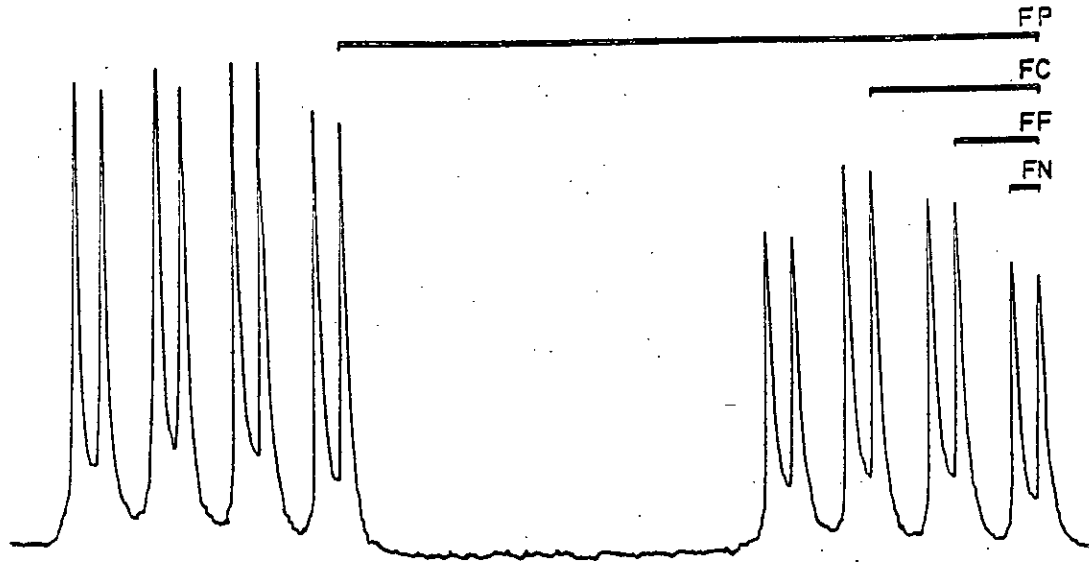

(e) ^{31}P (253 K)

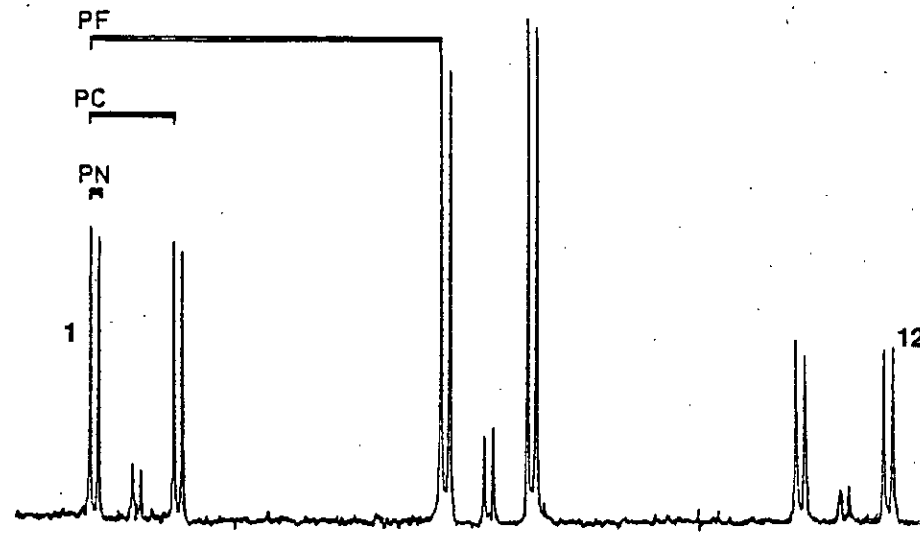

(f) ^{13}C (253 K)

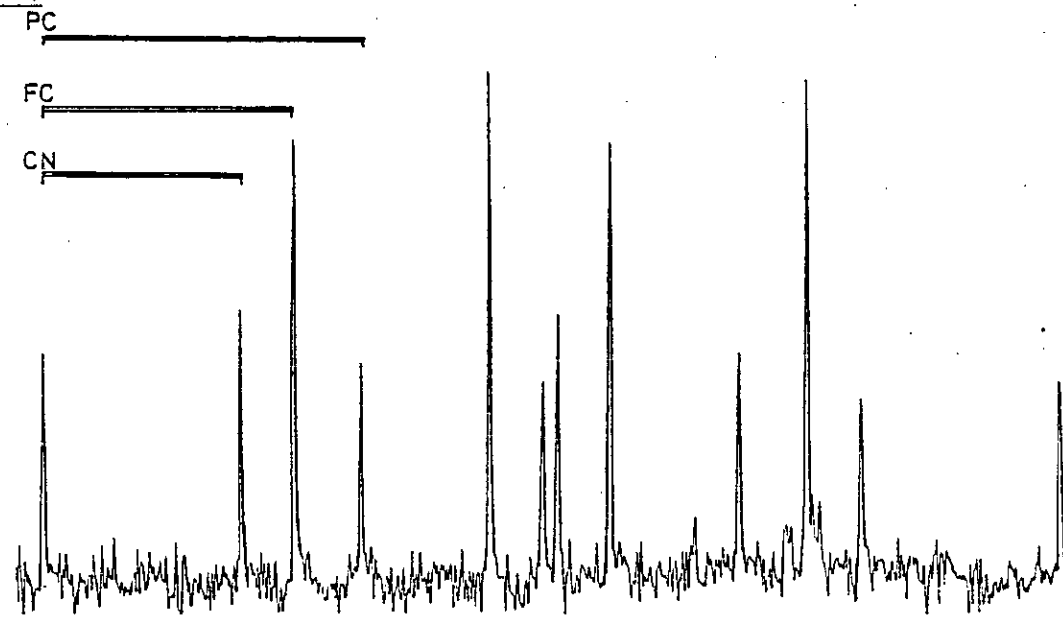

Table 4.1 (contd.): $^{19}F\{^{31}P\}$ Double Resonance Experiment (253 K)

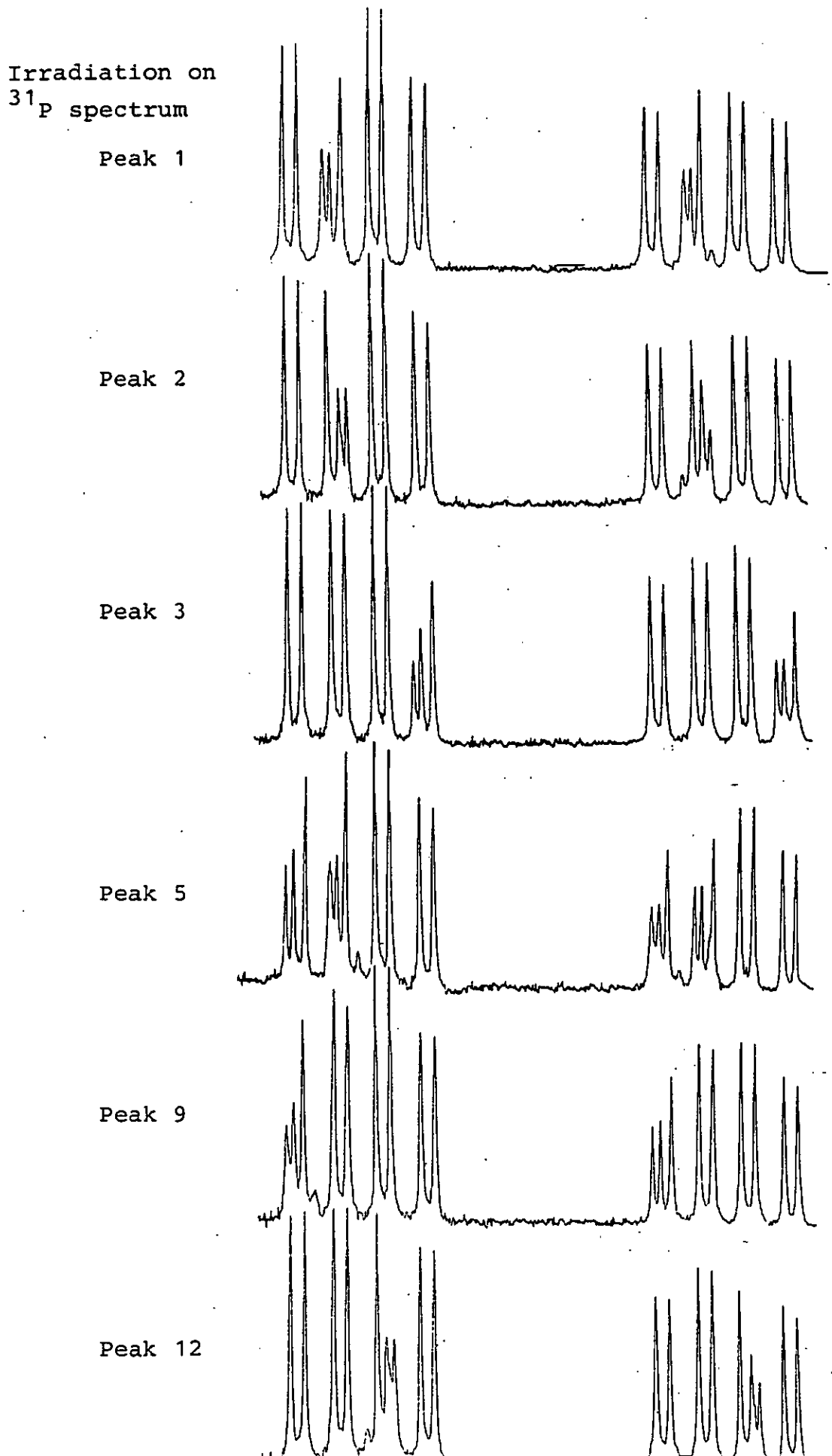

Figure 4.2 Observed and Final Weighted Difference Molecular Scattering Intensities for PF_2CN

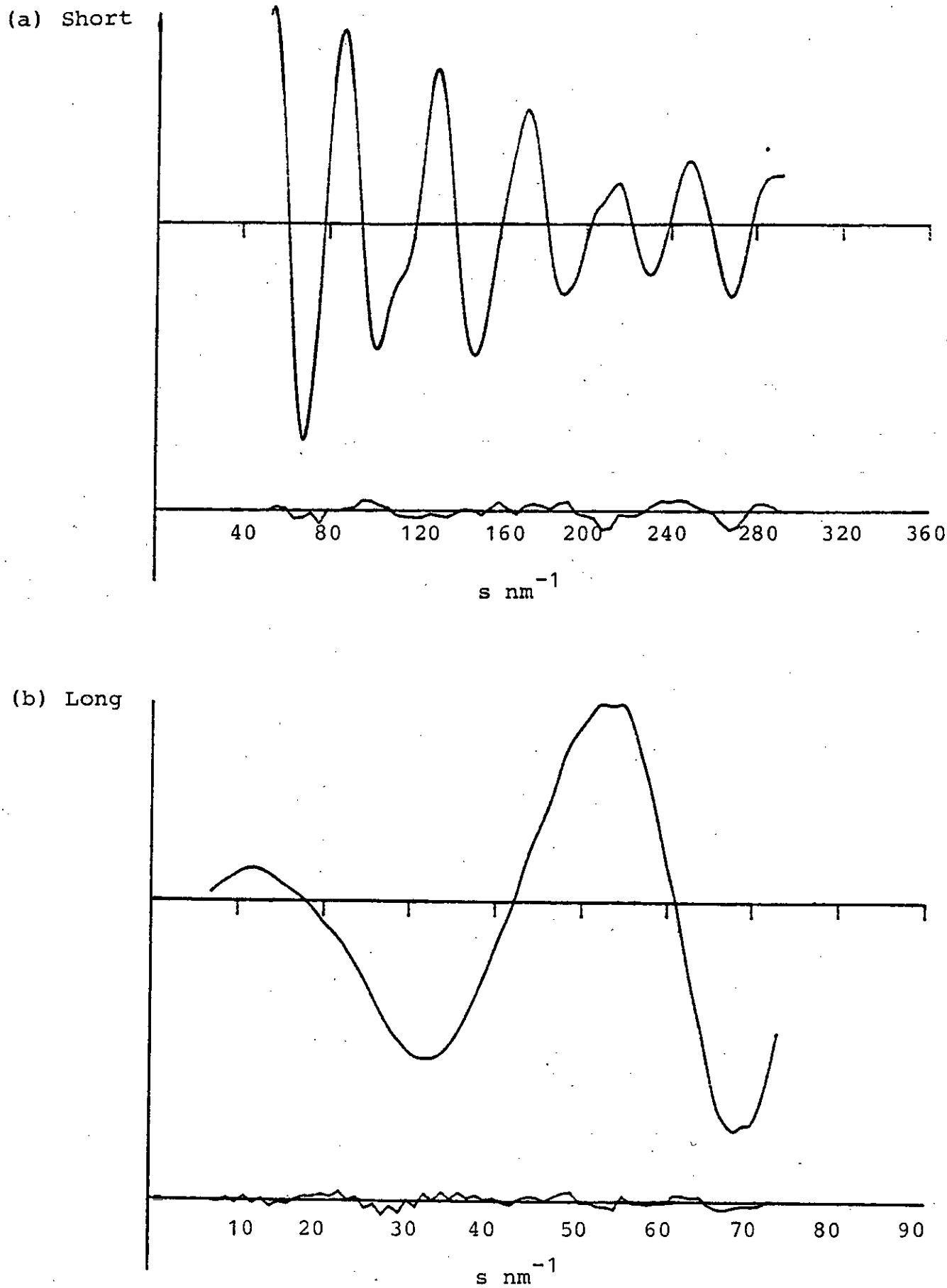

Figure 4.3 Observed and Difference Radial Distribution Curve for PF_2CN

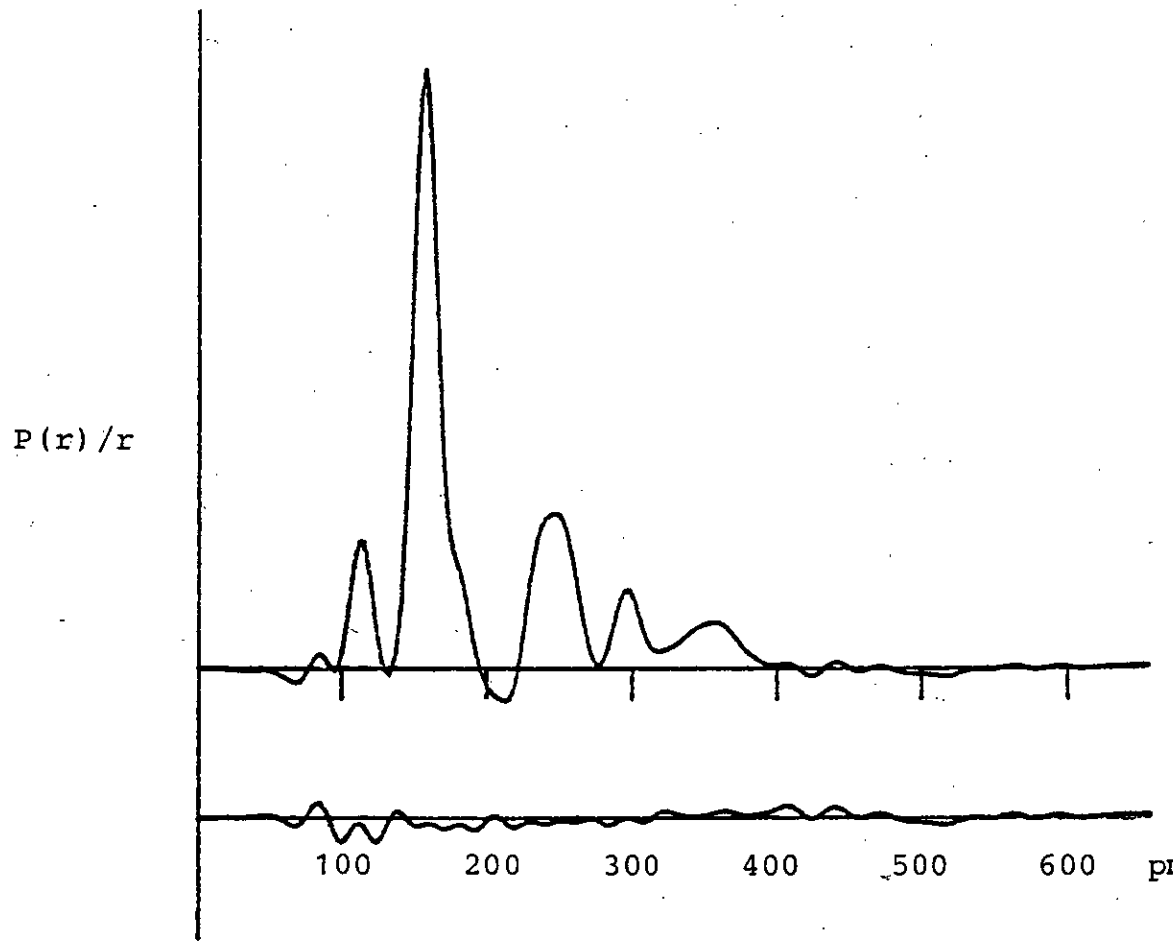

CHAPTER FIVE

THE MOLECULAR STRUCTURE OF DIFLUOROPHOSPHINE ISOTHIOCYANATE, DETERMINED USING A COMBINATION OF DATA FROM ELECTRON DIFFRACTION AND LIQUID CRYSTAL N.M.R. SPECTROSCOPY

5.1 Introduction

The second member of the series of difluorophosphine pseudohalides to be studied was the isothiocyanate. In a previous structural study[48] by Electron Diffraction (E.D.) alone, the problem of overlapping peaks in the radial distribution curve (see Chapter 1.7) necessitated the fixing of certain parameters at reasonable estimated values. It is hoped that the inclusion of data from Liquid Crystal Nuclear Magnetic Resonance Spectroscopy (L.C.N.M.R.) will allow the refinement of these parameters.

The success of this combination of data is critically discussed in this chapter, and the difluorophosphine pseudohalides are discussed as a series in Chapter 6.

5.2 Experimental

A sample of difluorophosphine isothiocyanate was prepared by the reaction between difluorophosphine bromide and silver isothiocyanate[167]. The difluorophosphine bromide was prepared as before (see Chapter 4.2). The isothiocyanate salt was prepared by a standard sulfonation[168] of potassium cyanide, followed by the reaction with silver nitrate solution to give the silver isothiocyanate precipitate, which was washed with alcohol and dry ether, and pumped dry overnight in a tap ampoule. For liquid crystal N.M.R. experiments, a small sample was prepared from doubly labelled potassium cyanide. A yield of 80% was recorded.

An excess of PF_2Br was condensed onto the silver salt in the dark and allowed to warm to room temperature for five minutes. The product was purified by fractionation and its purity checked by infrared spectroscopy.

5.3 Data Collection

5.3.1 Electron Diffraction

A sample of PF_2NCS was prepared and run on the University of Edinburgh Electron Diffraction Apparatus. The plates obtained were sent to Daresbury to be traced by the new microdensitometry service there. The relevant experimental details are listed in Table 1.1.

5.3.2 Liquid Crystal N.M.R. Spectroscopy

A sample was prepared containing 0.3 mmol of the doubly-labelled $PF_2{}^{15}N{}^{13}CS$ in 0.5 ml of "E5" liquid crystal as solvent in a 5 mm N.M.R. tube.

Phosphorus, fluorine and carbon-13 spectra were obtained on the Varian XL100 Spectrometer (see Chapter 2.4), while nitrogen-15 spectra were obtained from the departmental service on the Bruker WH360 Spectrometer.

The indirect J couplings (Table 5.2) were measured in the isotropic liquid crystal solution, heated to around 313 K. The signs of these couplings have been previously established by Reid[163].

The direct D couplings (Table 5.2) were calculated from the observed couplings in the nematic mesophase at 253 K and 283 K. The relative signs of the couplings were established by a series of double resonance experiments (Table 5.1) and their absolute values determined by comparison with the PF coupling, which is always large and negative[104].

Examples of the spectra obtained and double resonance experiments carried out are shown in Figure 5.1.

5.4 Structural Refinements

5.4.1 Electron Diffraction

A model program was written for refining the structure of PF_2NCS with nine independent parameters, the four directly bonded distances, the four angles <FPF, <FPN, <PNC and <NCS, and the torsional rotation around the PN bond. This latter parameter was defined as zero when the <FPF bisector lay trans to the NCS chain.

Initially the r_a structure was refined assuming Cs symmetry, with a linear NCS chain and zero torsion. The radial distribution curve (Figure 5.3) shows that the peaks corresponding to the PF, PN and CS distances are coincident, and it proved impossible to refine all three concurrently, therefore the CS distance was fixed at a reasonable estimated value. The linear <NCS angle was freed and refined to a value close to 180° but with a large uncertainty. The deviation from linearity is assumed to be a shrinkage effect. The least squares correlation

matrix (Table 5.4) shows this angle to be highly correlated with the <PNC angle. The torsion angle was stepped from 0° to 20°, and a shallow minimum was found at 4°.

The amplitudes of vibration of distances of similar magnitude were tied together at the ratios of their spectroscopic values. The final r_a structure is listed in Table 5.3 and the corresponding R_{gen} factor was 5.4%.

Compared to a previous structural analysis[48], the R_{gen} factor has been halved. This could be largely because of the improved microdensitometry and better background corrections. Small differences in the structures could be explained by the refinement of the <NCS angle and the different fixed torsional angle. In this refinement the variation in the R_{gen} factor with torsional angle shows a broad minimum around zero, with the local minimum at 4° statistically insignificant even at the 75% confidence level[169]. It has been predicted[165] that the torsional angle represents a mean deviation from the Cs symmetry species, rather than a true distortion of the ground state structure.

In order to allow for the vibrational and shrinkage effects the r_α^o structure was refined. A normal co-ordinate analysis was carried out using the GAMP routine (see Chapter 3.6). A harmonic force field was developed which fitted the observed vibrational frequencies[165] exactly. The spectroscopic amplitudes of vibration were used to calculate the harmonic vibrational corrections (Table 5.5) as outlined in Chapter 3.

The r_{α}^{o} structure was now refined (Table 5.6, Refinement A), fixing the <NCS angle at 180° and the torsion at zero. The R_{gen} factor was found to increase slightly to 5.7%, an effect expected with fewer refining parameters.

The main effects of the vibrational corrections have been to reduce the independent interatomic distances slightly (as predicted by theory in Chapter 3), and to widen the <PNC angle, which is affected by shrinkage in the r_a structure.

The molecular scattering and the radial distribution curves for the E.D. data are shown in Figures 5.2 and 5.3 respectively.

5.4.2 Electron Diffraction plus Liquid Crystal N.M.R. Spectroscopy

A new model program was written to extract the structural information from the Liquid Crystal N.M.R. data. Three refinable parameters were added to define the molecular orientation (Cs symmetry, Table 2.1), calculated according to equation 2.18. The direct couplings were added to the E.D. refinement program with weights inversely proportional to the squares of their uncertainties.

Initially the orientation parameters were allowed to refine with the structure held fixed at the E.D. only result. It was found that the observed D couplings could not all be closely reproduced. It was decided to initially ignore the couplings involving carbon-13, concentrating on the more rigid F_2PN moiety.

Vibrational corrections were applied using the program VIBR[146] (see Chapter 3.4) and are listed in Table 5.5b. The final structures using combined data from E.D. and L.C.N.M.R. (ignoring couplings to carbon) at 283 K and 253 K are listed in Table 5.6 as Refinements B and C respectively. The structures obtained before vibrational corrections were applied to the L.C.N.M.R. data were essentially the same, and have therefore not been listed.

In order to ascertain that the indirect J couplings had been correctly assigned, a "differences method" refinement was carried out (see Chapter 4.4.2). The observed and calculated differences are listed in Table 5.7 and the

resulting structure is given as Refinement D in Table 5.6.

The R_{gen} factor for Refinement D is high, and from Table 5.7 it can be seen that several of the difference pseudo-couplings have not been accurately fitted. By considering each in turn, it was found that ignoring the difference pertaining to the CN couplings, although not fitting perfectly the remaining pseudocouplings, had the most beneficial effect on the R_{gen} factor (Table 5.6, Refinement E).

Using this evidence for an anomalous CN coupling, it was decided to ignore this coupling in Refinement F (Table 5.6). The remaining couplings measured at 283 K were corrected for vibrations as before, and the agreement between observed and calculated couplings is shown in Table 5.5b.

5.5 Discussion

The structure of difluorophosphine isothiocyanate in the combined analyses, B and C, is slightly different from that obtained from E.D. data alone. However, the structural skeleton has remained essentially unaltered, with each interatomic distance agreeing to within the combined estimated standard deviations (esd's).

The major skeletal effect is an apparent lengthening of the P-N distance in the combined refinements. In the E.D. only case, this parameter is correlated with the P-F distance, because of the overlapping peaks effect (see chapter 1.7). The inclusion of the Liquid Crystal N.M.R. data effectively removes this correlation (see Table 5.8) and so may result in the more realistic value for this parameter.

More significant changes between the refinements are noticed in the angles. A strong correlation between the <FPF and <FPN angles has been reduced by the inclusion of the L.C.N.M.R. data (see Table 5.8), and this is reflected in a reduced uncertainty for each of these parameters. Small discrepancies in the angles could be explained by solvent-solute effects (see Chapter 2.6) and by changes in going from the gas to the liquid phase, which, in the case of a "floppy" molecule such as PF_2NCS, may be significant.

There is exact agreement between Refinements B and C, showing that the structure of PF_2NCS dissolved in the liquid crystal does not change with temperature.

The "differences method" refinements D and E showed some evidence for an anomalous CN coupling. However, even ignoring this coupling, Refinement F did not manage to fit the remaining couplings satisfactorily. An attempt to allow for a possible distortion from Cs symmetry, by increasing the number of refinable orientation parameters, showed little improvement.

In the case of PF_2NCS the best structure has been obtained by ignoring the couplings to the carbon atom, which are affected by low frequency, high amplitude vibrations. The remaining couplings (in Refinements B and C) show excellent agreement between calculated and observed values (Table 5.5b), while the least squares correlation matrices (Table 5.8) show that correlations arising from overlapping peaks have been reduced.

The orientation parameters refined to the following values:

	253 K	283 K
S_{zz}	-0.030	-0.018
S_{xx-yy}	0.050	0.052
S_{xy}	0.122	0.085

These show the expected increase in orientation at the lower temperature. The z-axis, along the F...F distance, is seen to orient perpendicular to the field, giving a negative S_{zz} value. The x-axis has been defined as lying along the P-N bond, however, the linear N=C=S chain, lying in the xy plane, has the most significant orientational effect, aligning itself preferentially parallel to the field.

Table 5.1 Double Resonance Experiments for PF_2NCS

(a) Isotropic Couplings

Experiment	Couplings Related	Relative Signs	
		K	J
$^{19}F\{^{13}C\}$	FN and CN	equal	equal
$^{19}F\{^{15}N\}$	FC and NC	equal	opposite
	FP and PN	equal	opposite
$^{31}P\{^{15}N\}$	FN and PF	opposite	equal

(b) Nematic Couplings (253 K)

Experiment	Couplings Related	Relative Signs	
		K	Δ*
$^{31}P\{^{13}C\}$	PN and CN	equal	equal
	PF and CF	equal	equal
$^{31}P\{^{15}N\}$	PC and NC	equal	opposite
	PF and NF	equal	opposite
$^{19}F\{^{15}N\}$	FP and NP	equal	opposite
	FC and NC	equal	opposite
	FF and NF	opposite	equal
$^{19}F\{^{13}C\}$	FP and CP	equal	equal
	FN and CN	equal	equal
	FF and CF	opposite	opposite

* $\Delta = J + 2D$ (except for FF coupling, $\Delta = 3D$)

Table 5.2 Couplings/Hz for PF_2NCS

Nuclei	J	Δ^*_{253K}	D_{253K}	Δ^*_{283K}	D_{283K}
PF	-1322.5(5)	-1272.4(2)	+25.0(7)	-1244.0(25)	+39.0(2
PC	0.0(5)	-128.6(10)	-64.3(12)	-97.6(4)	-48.8(5
FC	+5.1(5)	-158.9(5)	-82.0(8)	-115.0(10)	-60.0(1
CN	-30.5(2)	+545.0(15)	+287.8(15)	+379.0(20)	+205.0(2
PN	+94.4(3)	+175.4(15)	+40.5(15)	+164.0(10)	+35.0(1
FN	-11.3(3)	+129.1(4)	+70.2(5)	+91.0(5)	+51.1(5
FF	-	+635.1(5)	+211.7(5)	+363.0(20)	+121.0(2

* $\Delta = J + 2D$ (except for FF coupling, $\Delta = 3D$)

Table 5.3 Molecular Parameters for PF_2NCS

(E.D. only r_a structure)

Independent Distances	Distance/pm	Amplitude/pm
P-F	157.3(1)	5.0(2)
P-N	167.4(4)	5.0(tied to u(PF))
C=N	121.5(3)	3.5(fixed)
C=S	155.3(fixed)	5.0(tied to u(PF))
Dependent Distances		
F...F	238.6(9)	7.1(3)
F...N	245.0(7)	10.1(tied to u(FF))
F...C	353.3(8)	16.3(9)
F...C	356.8(7)	16.3(9)
F...S	501.0(8)	22.1(9)
F...S	506.4(8)	22.1(9)
P...C	273.9(10)	11.5(14)
P...S	423.2(6)	12.4(5)
N...S	276.8(2)	5.0(7)
Independent Angles/°		
<FPF	98.6(7)	
<FPN	97.9(5)	
<PNC	142.4(16)	
<NCS	181.9(26)	
Torsion	4.0(fixed)	

Table 5.4 Least Squares Correlation Matrix (x100) for PF_2NCS (E.D. only r_a structure)

PN	<FPN	<PNC	<NCS	u(PF)	u(FF)	u(NS)	
-46							PF
		-40		-68			PN
		-68	57				NC
	-74				64		<FPF
					-56		<FPN
			-90				<PNC
						-70	u(PC)

Note: Only elements with |absolute value| ≥ 40 included

Table 5.5 Vibrational Corrections for PF_2NCS

(a) Electron Diffraction

Distance	u_T/pm	$(\frac{3a}{2}\Delta u^2 + K_T)$	r_α^o correction/pm $(\frac{3a}{2}\Delta u^2 + K_T - \frac{u_T^2}{r})$
PF	4.23	1.76	1.65
PN	5.81	1.91	1.71
NC	3.89	1.50	1.38
CS	3.66	2.31	2.22
FF	6.76	2.10	1.91
FN	7.42	3.04	2.82
FC	12.88	0.81	0.34
FS	18.48	0.03	-0.65
PC	9.96	0.29	-0.07
PS	13.27	0.40	-0.02
NS	4.11	3.13	3.07

(b) Liquid Crystal N.M.R. Spectroscopy

283 K	D_{obs}	Correction*	D°_{α}	D_{calc}**
PF	39.0(29)	13.7	52.7(30)	52.4
PC	-48.8(5)	-0.2	-49.0(5)	-46.7
FC	-60.0(12)	-0.5	-60.5(12)	-58.5
CN	205.0(20)	10.9	215.9(25)	181.2
PN	35.0(11)	2.4	37.4(13)	39.0
FN	51.1(5)	3.4	54.5(7)	58.0
FF	121.0(20)	18.3	139.3(30)	139.2
253 K				***
PF	25.0(7)	14.8	39.8(16)	39.9
PN	40.5(15)	2.6	43.1(15)	43.0
FN	70.2(5)	4.3	74.5(7)	74.5
FF	211.7(5)	24.2	235.9(25)	235.8

* An uncertainty of 10% was assumed for vibrational corrections

** Calculated from Refinement F

*** Calculated from Refinement C

Table 5.6 Structural Refinements for PF_2NCS

Independent Distances/pm	A E.D. only (r_α^o structure)	B 283 K (excluding C couplings) (+ vibn. corrections)	C 253 K (excluding C couplin (+ vibn. corrections)
P-F	155.0(2)	155.0(2)	155.0(2)
P-N	165.4(5)	166.5(5)	166.5(5)
N=C	120.5(3)	120.8(4)	120.8(4)
C=S	155.3(fixed)	155.3(fixed)	155.3(fixed)
Independent Angles/^{o}			
<FPF	98.3(7)	100.8(6)	100.9(6)
<FPN	99.3(5)	96.8(3)	96.8(2)
<PNC	146.4(10)	145.5(11)	145.5(11)
R_{gen}	5.7%	8.0%	7.9%

Table 5.6 (contd.)

Independent Distances/pm	D Differences Method	E Differences (excluding CN Coupling)	F 283 K (excluding CN couplin (+ vibn. correction)
P-F	154.9(3)	155.0(2)	155.0(2)
P-N	168.2(7)	166.5(4)	166.9(5)
N=C	119.4(6)	120.9(4)	120.7(5)
C=S	155.3(fixed)	155.3(fixed)	155.3(fixed)
Independent Angles/°			
<FPF	101.8(9)	100.6(5)	101.0(7)
<FPN	96.5(3)	97.3(3)	96.7(3)
<PNC	144.5(14)	144.8(10)	144.2(11)
R_{gen}	13.2%	7.7%	8.4%

Table 5.7 Differences Method for PF_2NCS

Nuclei	Δ* 253 K	Δ* 283 K	Diff/2**	Calc. (Refinement D)	Calc. (Refinement E)
PF	-1272.4	-1244.0	-14.2	-14.4	-14.3
PC	-128.6	-97.6	-15.5	-15.5	-14.5
FC	-158.9	-115.0	-22.0	-23.8	-21.4
CN	545.0	379.0	83.0	81.4	70.7
PN	175.4	164.0	5.7	5.9	6.7
FN	129.1	91.0	19.1	22.0	20.0
FF	635.1	363.0	90.7	90.9	90.8

* $\Delta = J + 2D$ (except for FF coupling, $\Delta = 3D$)

** Except for FF coupling, Diff/3

Table 5.8 Least Squares Correlation Matrices (x100) for the r_α^o structures of PF_2NCS

(a) E.D. only (refinement A)

PN	<FPN	<PNC	u(PF)	u(FF)	u(NS)	
-54			48			PF
	-42	-57	-71			PN
		-50				CN
	-73			89		<FPF
				-74		<FPN
			43			<PNC
					-61	u(PC)

(b) E.D. + L.C.N.M.R. (Refinement C)

<PNC	S_{zz}	S_{xx-yy}	S_{xy}	u(PF)	u(FF)	u(NS)	
-51				-51			PN
-56							CN
	-71	-49	53		75		<FPF
		76	-45		-60		<FPN
		48	-43				S_{zz}
						-58	u(PC)

Note: Only elements with |absolute value| ≧40 included

Figure 5.1 Selected L.C.N.M.R. Spectra for PF_2NCS

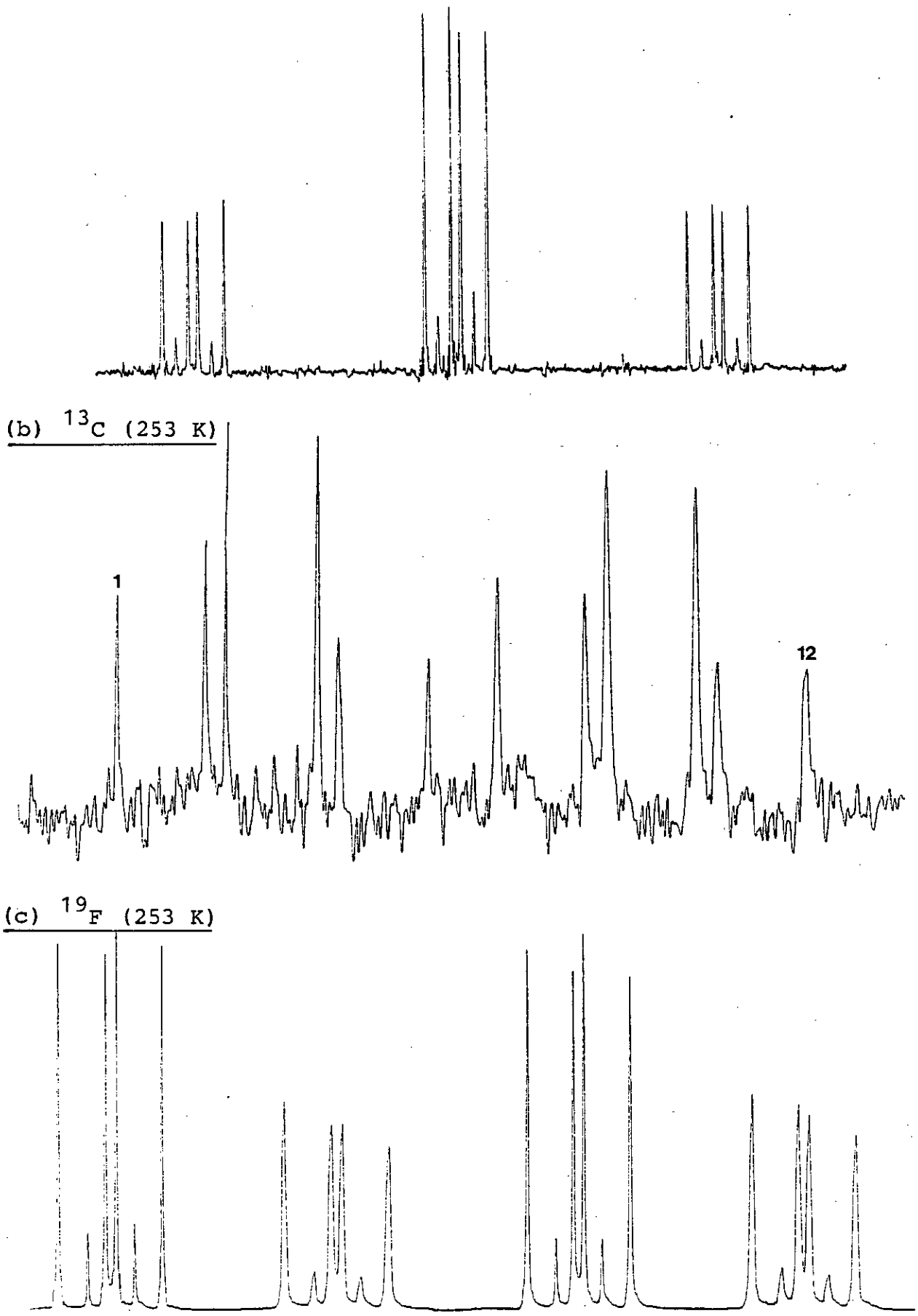

Figure 5.1 (contd.) $^{31}P\{^{13}C\}$ Double Resonance Experiment (253 K)

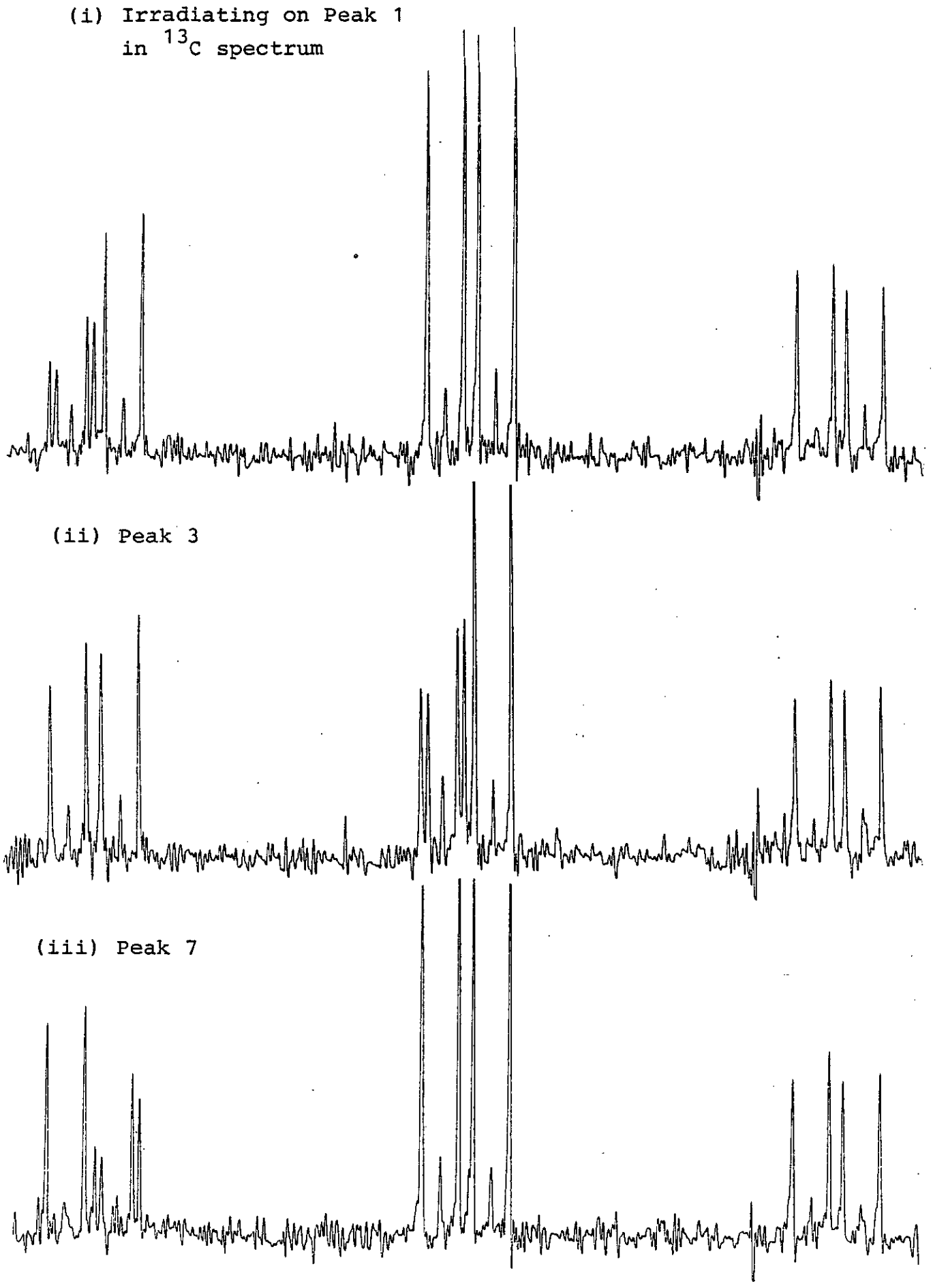

Figure 5.2 Observed and Final Weighted Difference Molecular Scattering Intensities for PF_2NCS

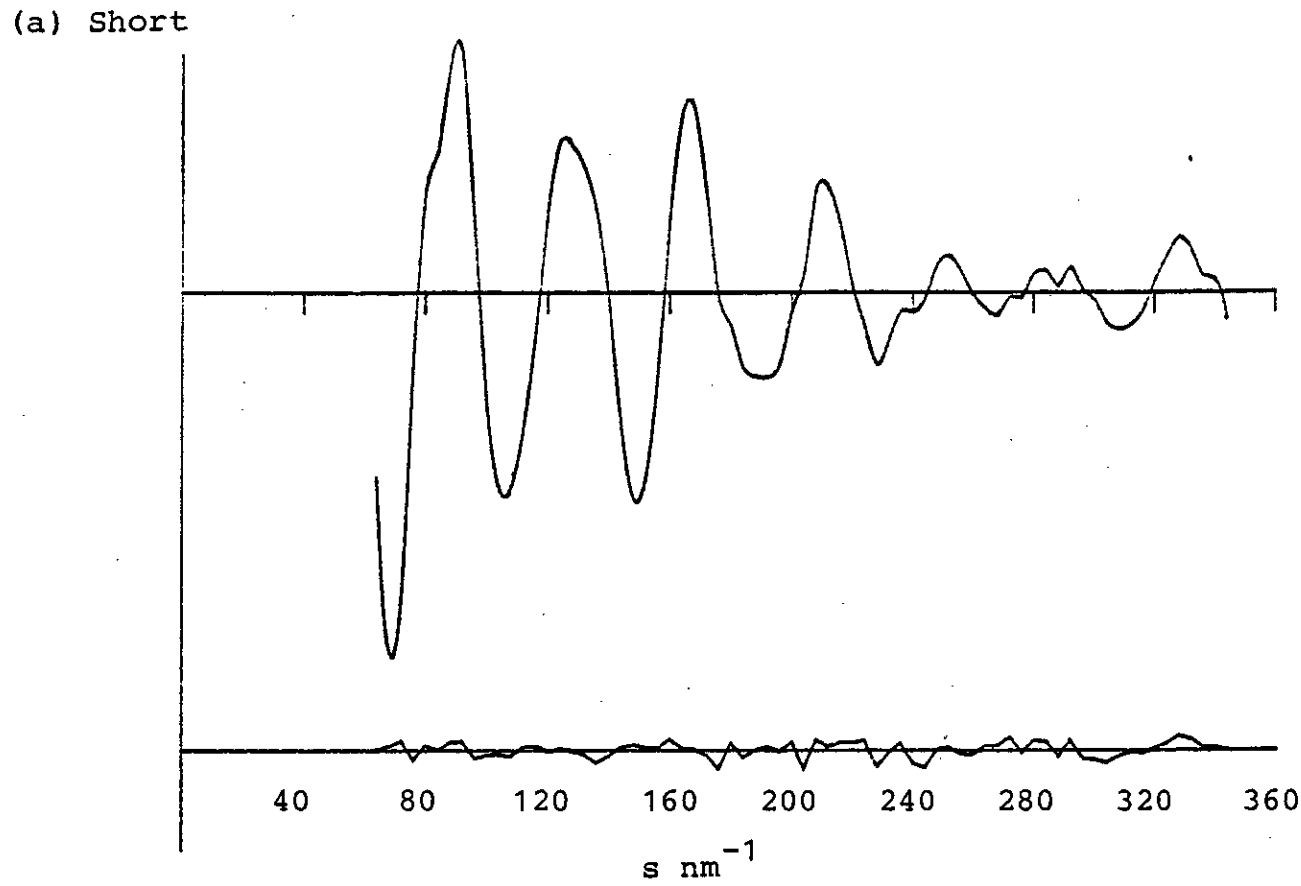

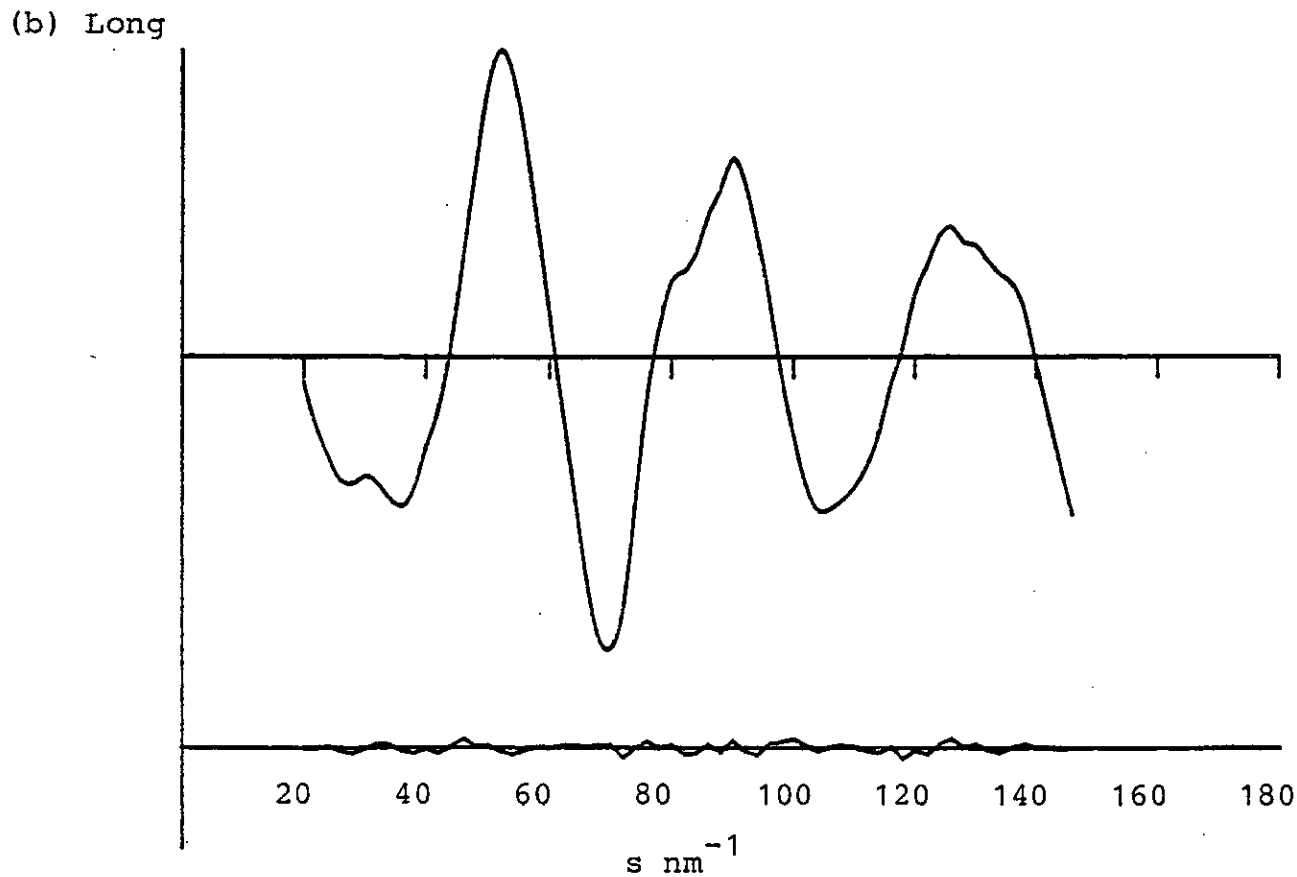

Figure 5.3 Observed and Difference Radial Distribution Curves for PF_2NCS

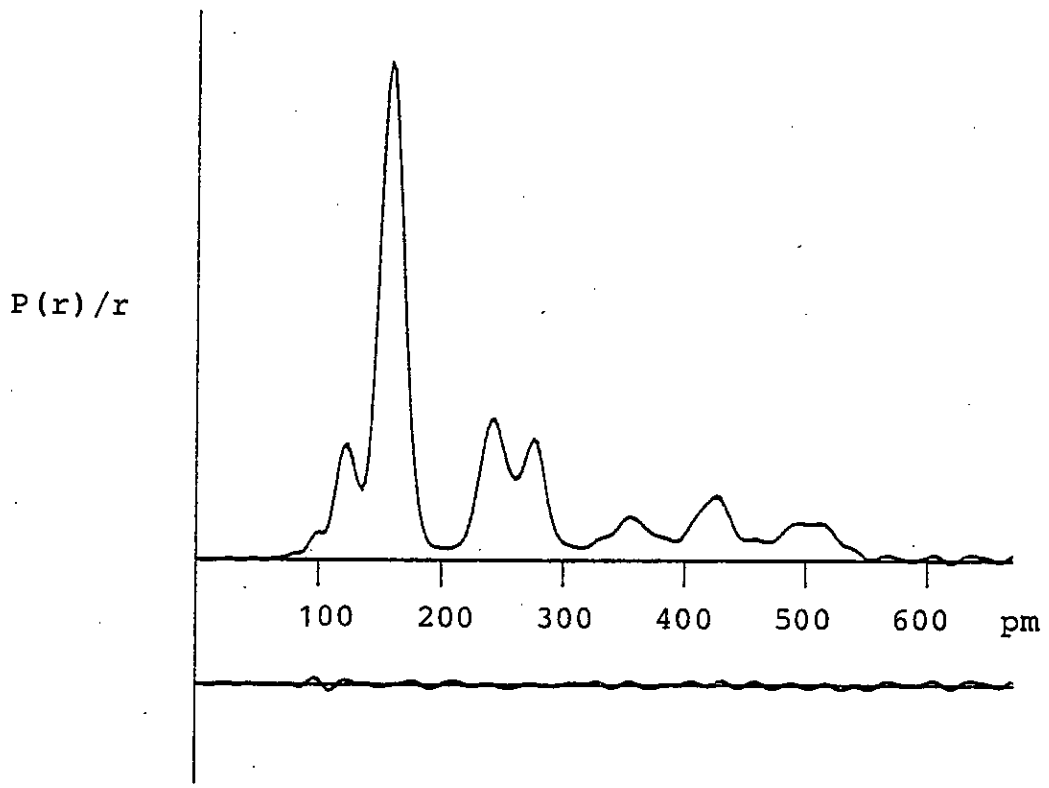

CHAPTER SIX

THE MOLECULAR STRUCTURE OF DIFLUOROPHOSPHINE ISOCYANATE, DETERMINED USING A COMBINATION OF DATA FROM ELECTRON DIFFRACTION AND LIQUID CRYSTAL N.M.R. SPECTROSCOPY

6.1 Introduction

The third and final member of the series of difluorophosphine pseudohalides studied was the isocyanate. In a previous structural study by Electron Diffraction (E.D.) alone, the problem of overlapping peaks in the radial distribution curve (see Chapter 1.7) necessitated the fixing of certain parameters at reasonable estimated values. In introducing extra data from Liquid Crystal N.M.R. Spectroscopy (L.C.N.M.R.) it was hoped to reduce this problem. The extent to which this has been achieved is discussed and a comparison of the results for the entire series of difluorophosphine pseudohalides is made in the final section of this chapter.

6.2 Experimental

A sample of difluorophosphine isocyanate was produced by the reaction between difluorophosphine bromide and silver isocyanate[167]. The difluorophosphine bromide was prepared as before (see Chapter 4.2). The isocyanate salt was prepared by the standard method[170] from potassium cyanide. This was then reacted with silver nitrate solution to give the silver isocyanate which was washed with alcohol then dry ether, and pumped dry overnight in a tap ampoule. For Liquid Crystal N.M.R. experiments, a small sample was prepared from doubly labelled potassium cyanide. A yield of around 80% was recorded.

An excess of PF_2Br was condensed onto the silver salt in the dark and allowed to warm to room temperature for five minutes. The product was purified by fractionation and the purity checked by infrared spectroscopy.

6.3 Data Collection

6.3.1 Electron Diffraction

A sample of PF_2NCO was prepared and its purity checked by infrared spectroscopy. Electron diffraction scattering intensities were recorded photographically on the Edinburgh E.D. Apparatus. The plates obtained were traced by the new microdensitometry service at Daresbury. The relevant experimental details are listed in Table 1.1.

6.3.2 Liquid Crystal N.M.R. Spectroscopy

A sample was prepared containing 0.3 mmol of doubly labelled $PF_2{}^{15}N{}^{13}CO$ in 0.5 ml of "E5" liquid crystal as solvent in a 5 mm N.M.R. tube. This solution became isotropic at a temperature of around 305 K.

Phosphorus, fluorine and carbon-13 spectra were run on the Varian Associates XL-100 Spectrometer while nitrogen-15 spectra were obtained from the departmental service on the Bruker WH-360 spectrometer.

The indirect J coupling constants (Table 6.2) were measured in the isotropic liquid crystal solution, heated to 313 K. Double resonance experiments (Table 6.1) agreed with a previous study[163], and the signs of the couplings

were determined by comparison with the PF coupling which is always large and negative[104].

The direct D coupling constants (Table 6.2) were measured in the liquid crystal solution at temperatures of 253 K and 283 K, and a series of double resonance experiments determined their relative signs, which were again related to the negative PF coupling.

Examples of the spectra obtained and the double resonance experiments carried out are shown in Figure 6.1.

6.4 Structural Refinements

6.4.1 Electron Diffraction

A model program was written for refining the structure of PF_2NCO with nine independent parameters: the four directly bonded distances, the four angles <FPF, <FPN, <PNC and <NCO, and the torsional rotation around the PN bond. This latter parameter was defined as zero when the <FPF bisector lay trans to the NCO chain.

Initially the r_a structure was refined assuming Cs symmetry, with a linear NCO chain and zero torsion. It was possible to refine all the structural parameters except the NC and FN amplitudes of vibration, which were tied to the CO and FF amplitudes of vibration respectively, with ratios taken from the spectroscopic values determined by GAMP. The reason for the choice of the tied amplitudes of vibration is apparent from the radial distribution curve (Figure 6.3), which shows that the peaks corresponding to the NC and CO distances and the FN and FF distances are coincident.

The NCO chain was varied from 170° to 190° in one degree steps. A shallow minimum in the R factor was detected at 174°, at which value the angle was fixed. It is assumed that the deviation from linearity is mainly a shrinkage effect, caused by high amplitude, low frequency bending modes.

The torsional angle around the PN bond was varied similarly and gave a minimum at 4°, this was however statistically insignificant[169]. It has been predicted[165]

that the torsional angle represents a mean deviation from Cs symmetry rather than a true distortion of the ground vibrational state structure.

The final r_a structure is listed in Table 6.3, with a corresponding R_{gen} factor of 9.3%. The improvement in the R_{gen} factor compared to a previous structural analysis[48] could be explained by the improved microdensitometry and better background corrections. Small differences in the structures could be explained by the allowed deviation from linearity of the <NCO angle.

In order to allow for the vibrational and shrinkage effects, the r_α^o structure was refined. A normal co-ordinate analysis was carried out using the GAMP routine (see Chapter 3.6). A harmonic force field was developed which fitted the observed vibrational frequencies[165] exactly (Table 6.4). The spectroscopic amplitudes of vibration were used to calculate the harmonic vibrational corrections (Table 6.5) as outlined in Chapter Three.

The r_α^o structure was now refined (Table 6.6, refinement A), fixing the <NCO angle at 180° and the torsion at zero. The R_{gen} factor was found to increase slightly to 9.6%, an effect expected with fewer refining parameters.

The main effects of the vibrational corrections have been to reduce the independent interatomic distances slightly (as predicted in Chapter 3), and to increase the precision of determination of the parameters associated with the linear N=C=O group, which would be expected to exhibit the greatest shrinkage effects.

The molecular scattering and radial distribution curves for the E.D. data are shown in Figures 6.2 and 6.3 respectively.

6.4.2 Electron Diffraction plus Liquid Crystal N.M.R. Spectroscopy

A new model program was written to extract the structural information from the Liquid Crystal N.M.R. data. Three refinable parameters were added to define the orientation (Cs symmetry, Table 2.1), calculated according to equation 2.18. The observed direct couplings were added to the E.D. refinement program with weights inversely proportional to the squares of their uncertainties.

Initially the orientation parameters were allowed to refine, with the structure held fixed at the E.D. only result. It was found that all the observed D couplings could not be closely reproduced, and structural parameters refined to unreasonable values when freed, with a large associated R_{gen} factor.

It was decided to concentrate on the more rigid part of the molecule and initially ignore the couplings to the carbon nucleus, which could be complicated by the effects of low frequency, high amplitude bending modes.

Vibrational corrections were applied using the program VIBR[146] (see Chapter 3.4) and are listed in Table 6.5(b). The final structures including L.C.N.M.R. data taken at 253 K and 283 K, but ignoring the couplings to carbon, are listed in Table 6.6 as Refinements B and C respectively.

A differences method refinement was carried out (see Chapter 4.4.2) to check that the J couplings had been correctly assigned. The results (Table 6.6, Refinements D and E) show an anomalous CN coupling.

In Refinement F all the couplings have been included except the CN coupling, with the associated vibrational corrections listed in Table 6.5(b).

6.5 Discussion

The structure of difluorophosphine isocyanate in the combined refinements B and C (Table 6.6) is the same as that obtained from Electron Diffraction alone, within the estimated standard deviations (esd's) for each parameter. The refinements are very similar, showing little thermal effect on structure, there is good agreement between the observed and calculated couplings (Table 6.5(b)), and there has been only a small increase in the R_{gen} factor.

In refinements B and C, the four couplings represent four extra pieces of structural information. However, three parameters are required to define the orientation, therefore, from a simplistic viewpoint, there has been a net gain of one piece of structural information. In this case the effect has been to tie down the <FPN angle. This is confirmed in the least squares correlation matrices (Table 6.8), which show that the strong correlation between the <FPF and <FPN angles has been removed.

It proved impossible to fit all seven observed couplings concurrently, even by introducing extra orientation parameters to allow for possible distortion from Cs symmetry in solution.

A "differences method" refinement D was carried out to check the J coupling signs and assignments (see Chapter 4.4.2). This gave a very high R_{gen} factor and unreasonable values for certain parameters. Varying the weight of each difference in turn, it was found that there was an apparent anomaly in the CN difference. When this was ignored in Refinement E a reasonable structure resulted, and the calculated and expected differences agreed to within 1 Hz (Table 6.7).

Consequently, in Refinement F, the CN coupling was ignored and a satisfactory structure was obtained, with the calculated values of the remaining couplings agreeing well with the observed values (Table 6.5(b)).

The inclusion of the extra two couplings to carbon has improved slightly the precision of determination of all the angles, the major effect being, as would be expected, on the <PNC angle. The other parameters agree with those obtained from E.D. alone to within the combined esd's. The <PNC angle is affected by low frequency, high amplitude bending modes, and may well be distorted in solution.

6.6 Discussion: The Difluorophosphine Pseudohalides

One important function of the structural chemist is to produce evidence to substantiate or repudiate current theories of bonding. At the present, one particular area of contention is over the apparent widening of angles and shortening of bondlengths at silicon[171,172], germanium[173] and phosphorus[174] sites, as compared to values predicted by the Schomaker-Stevenson rule[175] (which takes the sum of the Pauling covalent radii[176] and corrects for differences in the electronegativity of the atoms involved). This effect was originally ascribed to (p-d)π bonding[177], although alternative explanations[178,179] have now been proposed, and the truth is probably a combination of several mechanisms.

Although the effect is not as pronounced as in their silicon analogues, the difluorophosphine pseudohalides have been previously shown[48,154] to exhibit wide valence angles at nitrogen and short PN bonds. However, the accuracy of determination of these structures has been hindered by shrinkage and by overlapping peak effects, as the PF and PN bondlengths are of similar magnitude.

It was hoped that the inclusion of data from Liquid Crystal N.M.R. would help to overcome these difficulties. This has been partially achieved, with the extra data resulting in dramatic reductions in the correlations caused by overlapping peaks, particularly in the case of PF_2NCO. The shrinkage effect, however, remains a more intractable problem.

On reflection, despite the many observable couplings, the difluorophosphine pseudohalides have not been a particularly suitable series of compounds for a preliminary feasibility study on the combination of data from Liquid Crystal N.M.R. and Electron Diffraction. They are "floppy" molecules[50], possessing low frequency, high amplitude bending modes which have shallow potential minima. Solvent-solute interactions on solution in the liquid crystal (see Chapter 2.6) could significantly constrain these motions and result in slight changes in structure in going from the gas to the liquid phase.

It has been attempted to observe directly the effect on the vibrational modes of dissolution in a liquid crystal by studying the infra-red spectrum. Observing the simple hydrogen cyanide molecule[180], although most information was masked by the solvent background, certain peaks were seen to be shifted in solution. The significance of this effect on the vibrational corrections merits further study.

The inability to fit all the observed couplings is, however, still not explained, as the vibrational corrections have only a small effect on the molecular parameters. The possibility of distortion from Cs symmetry was considered for each molecule, and although the inclusion of two extra orientation parameters to allow for this did not seem

to improve matters, this remains the most likely explanation. Although it is unsatisfactory to resort to the universal panacea of anisotropy in the couplings (see Chapter 2.6), there seems to be some evidence for this, especially in the CN coupling. There is, as yet, no literature to support this observation.

The study of the more rigid F_2PN moiety, however, gives some indication of the advantages of the combined analysis. The observed couplings are all fitted to within their uncertainties, and the precision of determination of the structural parameters has been increased in comparison to the E.D. only results.

Table 6.1 Double Resonance Experiments for PF_2NCO

(a) Isotropic Couplings

Experiment	Couplings Related	Relative Signs	
		K	J
$^{19}F\{^{15}N\}$	PF and PN	equal	opposite
$^{19}F\{^{13}C\}$	FN and CN	equal	equal

(b) Nematic Couplings (253 K)

Experiment	Couplings Related	Relative Signs	
		K	Δ*
$^{31}P\{^{13}C\}$	PN and CN	equal	equal
	PF and CF	equal	equal
$^{31}P\{^{15}N\}$	PF and NF	equal	opposite
	PC and NC	equal	opposite
$^{19}F\{^{15}N\}$	FP and NP	equal	opposite
	FC and NC	equal	opposite
	FF and NF	equal	opposite
$^{19}F\{^{13}C\}$	PF and CP	equal	equal
	FN and CN	equal	equal
	FF and CF	equal	equal

* $\Delta = J + 2D$ (except for FF coupling, $\Delta = 3D$)

Table 6.2 Couplings/Hz for PF_2NCO

Nuclei	J	Δ^*_{253K}	D_{253K}	Δ^*_{283K}	D_{283K}
PF	-1307.0(7)	-1844.4(5)	-268.7(8)	-1664.3(5)	-178.7(8)
PC	-11.5(8)	-50.6(10)	-19.6(15)	-43.4(4)	-16.0(10)
FC	-8.5(4)	-98.8(4)	-45.15(6)	-75.0(5)	-33.3(7)
CN	-22.7(5)	+443.2(8)	+233.0(9)	+318.5(20)	+170.6(22)
PN	+89.2(8)	+53.0(6)	-18.1(10)	+71.6(4)	-8.8(9)
FN	-13.7(5)	+70.5(4)	+42.1(6)	+52.2(4)	+33.0(6)
FF	-	-184.3(4)	-61.4(4)	-221.3(3)	-73.8(3)

* $\Delta = J + 2D$ (except for FF coupling, $\Delta = 3D$)

Table 6.3 Molecular Parameters for PF_2NCO

(E.D. only r_a structure)

Independent Distances	Distance/pm	Amplitude/pm
P-F	157.2(2)	4.7(3)
P-N	167.9(4)	4.6(8)
N=C	121.8(25)	3.4(tied to u(CO))
C=O	117.6(21)	3.7(15)
Dependent Distances		
F...F	237.2(16)	7.1(6)
F...N	244.0(14)	11.8(tied to u(FF))
F...C	354.4(24)	25.2(40)
F...C	350.4(23)	25.2(40)
F...O	464.5(15)	19.2(15)
F...O	458.1(15)	19.2(15)
P...C	268.6(12)	11.1(16)
P...O	373.4(23)	13.3(12)
N...O	239.0(6)	3.7(12)
Independent Angles/°		
<FPF	98.0(10)	
<FPN	97.2(10)	
<PNC	135.3(20)	
<NCO	174.0(fixed)	
Torsion	4.0(fixed)	

Table 6.4 Vibrational Frequencies and Assignments for PF_2NCO

Species	Frequency/cm^{-1}	Approximate Description
A'	2283	N=C stretch
	1422	C=O stretch
	853	P-F stretch (symm.)
	714	P-N stretch
	604	N=C=O deformation (in-plane)
	451	<FPF deformation
	324	PF_2 wag
	113	<PNC deformation
A''	839	P-F stretch (asymm.)
	630	N=C=O deformation (out-of-plane)
	367	PF_2 rock
	70	Torsion

Table 6.5 Vibrational Corrections for PF_2NCO

(a) Electron Diffraction

Distance	u_T/pm	$(\frac{3}{2}a\ \Delta u^2 + K_T)$	r_α^o correction/pm $(\frac{3}{2}a\ \Delta u^2 + K_T - \frac{u}{r}T^2)$
PF	4.25	1.02	0.91
PN	5.07	1.11	0.96
NC	3.51	1.29	1.19
CO	3.63	1.99	1.88
FF	6.57	1.25	1.06
FN	7.46	1.69	1.46
FC	11.80	0.33	-0.07
FO	16.79	0.14	-0.47
PC	8.99	0.16	-0.14
PO	12.58	0.63	0.21
NO	4.00	2.75	2.68

(b) Liquid Crystal N.M.R. Spectroscopy

283 K	D_{obs}	Correction*	D_α^o	D_{calc} **
PF	-178.7(8)	-2.0	-180.7(8)	-180.8
PN	-8.8(9)	-0.2	-9.0(9)	-9.0
FN	33.0(6)	1.1	34.1(6)	34.0
FF	-73.8(3)	3.5	-70.3(5)	-70.3
253 K				***
PF	-268.7(8)	-4.2	-272.9(10)	-272.9
PC	-19.6(15)	-0.1	-19.7(15)	-21.0
FC	-45.2(6)	0.1	-45.1(6)	-45.7
CN	233.0(9)	12.2	245.2(16)	167.3
PN	-18.1(10)	-0.5	-18.6(10)	-18.8
FN	42.1(6)	1.3	43.4(6)	43.2
FF	-61.4(4)	4.5	-56.9(6)	-57.0

*An uncertainty of 10% was assumed for vibrational corrections

Table 6.6 Structural Refinements for PF_2NCO

Independent Distances/pm	A E.D. only (r_α^o)	B 253 K (excluding C couplings) (+ vibn. corrections)	C 283 K (excluding C couplings) (+ vibn. corrections)
P-F	156.3(2)	156.3(2)	156.3(2)
P-N	167.1(4)	167.3(4)	167.4(4)
N=C	119.8(9)	119.8(9)	119.7(9)
C=O	116.1(8)	116.1(8)	116.2(8)
Independent Angles/^{o}			
<FPF	95.8(9)	96.4(9)	96.3(9)
<FPN	97.7(8)	96.8(2)	96.6(2)
<PNC	137.3(12)	136.7(12)	136.5(12)
R_{gen} factor	9.6%	9.9%	10.0%

Table 6.6 (contd.)

Independent Distances/pm	D Diffs.	E Diffs. (excluding CN Coupling)	F 253 K (excluding CN coupling) (+ vibn. corrections)
P-F	156.7(4)	156.3(2)	156.3(2)
P-N	170.0(9)	167.2(4)	167.3(4)
N=C	108.0(9)	119.0(11)	118.8(10)
C=O	120.6(11)	116.8(10)	116.5(10)
Independent Angles/^{o}			
<FPF	98.7(13)	95.8(5)	96.8(8)
<FPN	95.7(4)	97.5(4)	96.8(2)
<PNC	139.2(20)	137.1(11)	139.8(11)
R_{gen} factor	28.6%	10.3%	11.3%

Table 6.7 Differences Method for PF_2NCO

Nuclei	Δ^*_{253K}	Δ^*_{283K}	Diff/2**	Calc. (Refinement D)	Calc. (Refinement E)
PF	-1844.4	-1664.3	-90.05	-90.3	-90.3
PC	-50.6	-43.4	-3.6	-4.3	-4.4
FC	-98.8	-75.0	-11.9	-13.4	-10.9
CN	443.2	318.5	62.35	61.3	40.3
PN	53.0	71.6	-9.3	-9.4	-8.6
FN	70.5	52.2	9.15	11.1	9.6
FF	-184.3	-221.3	12.3	12.1	12.2

* $\Delta = J + 2D$ (except for FF coupling, $\Delta = 3D$)

** Except for FF coupling, Diff./3

Table 6.8 Least Squares Correlation Matrices (x100) for the r_α^o structures of PF_2NCO

(a) E.D. only (Refinement A)

PN	CO	<FPN	<PNC	u(PF)	u(PN)	u(CO)	u(FF)	u(FC)	
-48				61	77				PF
				-71	-59				PN
	-96		-68			-97		48	NC
			62			96		-48	CO
		-74	50				75		<FPF
							-48		<FPN
						65		-74	<PNC
					85				u(PF)

(b) E.D. + L.C.N.M.R. (Refinement B)

PN	CO	<FPN	S_{zz}	S_{xx-yy}	S_{xy}	u(PF)	u(PN)	u(CO)	u(FF)	u(FC)	
-45		64		-83	47	60	76				PF
		90				-69	-57				PN
	-74							-90			NC
								89			CO
			95		76				45		<FPF
				86	-54	71	67				<FPN
								58		-62	<PNC
					71				50		S_{zz}
						56	45				S_{xx-yy}
							85				u(PF)

Note: Only elements with |absolute values| ≥45 included.

Figure 6.1 Selected Liquid Crystal N.M.R. Spectra for PF_2NCO

(a) ^{13}C (253 K)

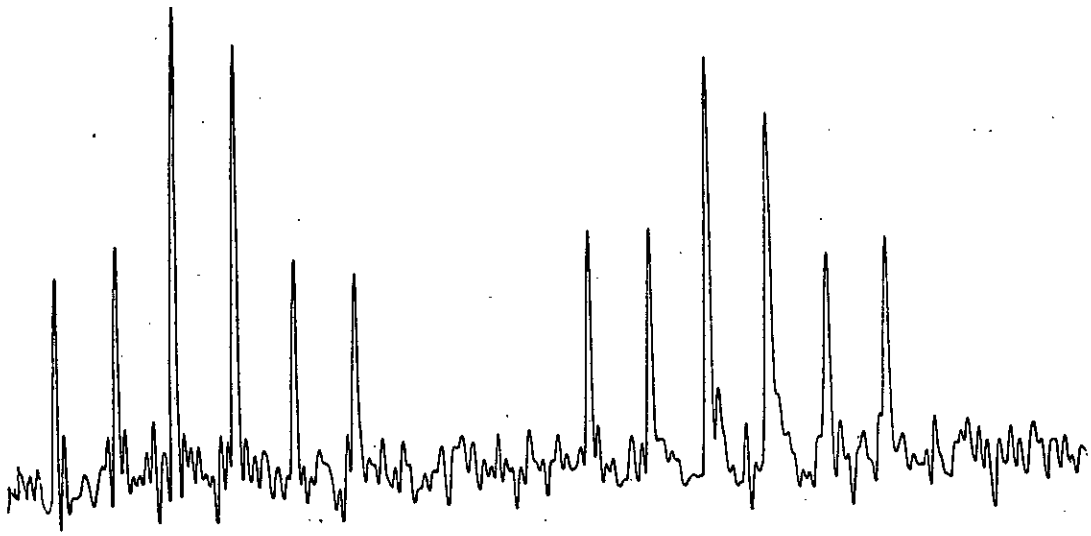

(b) ^{19}F (253 K)

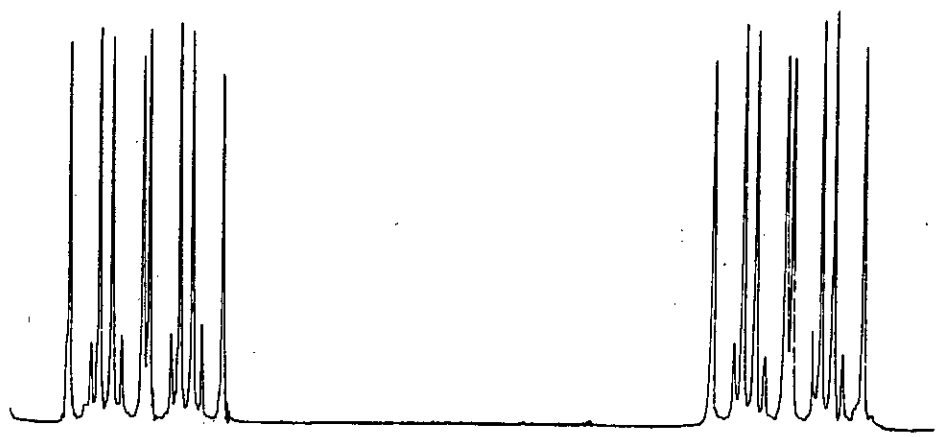

(c) ^{31}P (253 K)

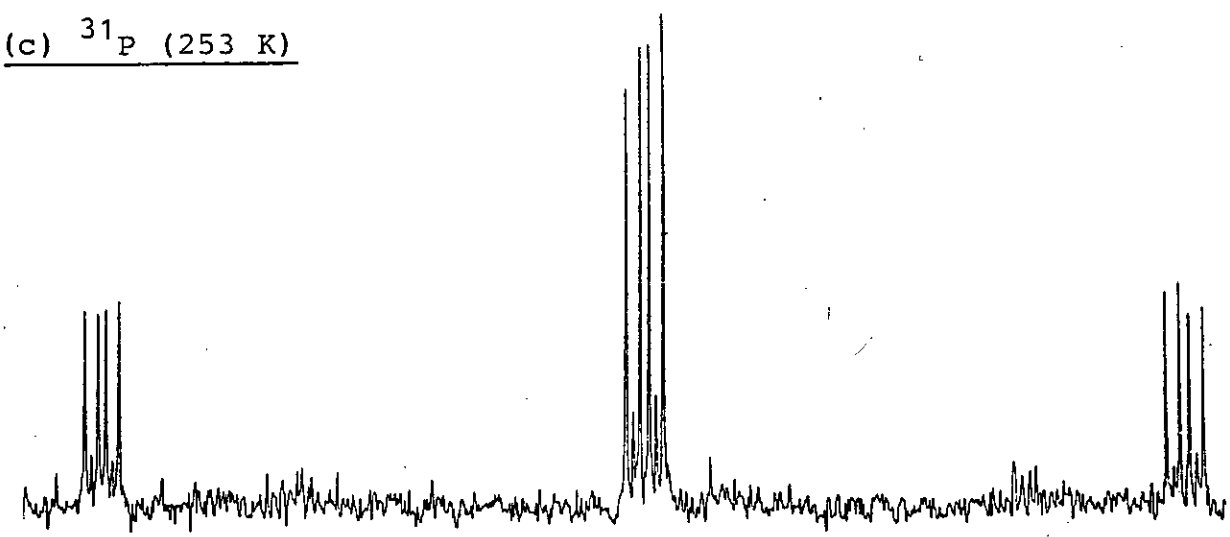

Figure 6.1 (contd.) $^{19}F\{^{15}N\}$ Double Resonance Experiment (253 K)

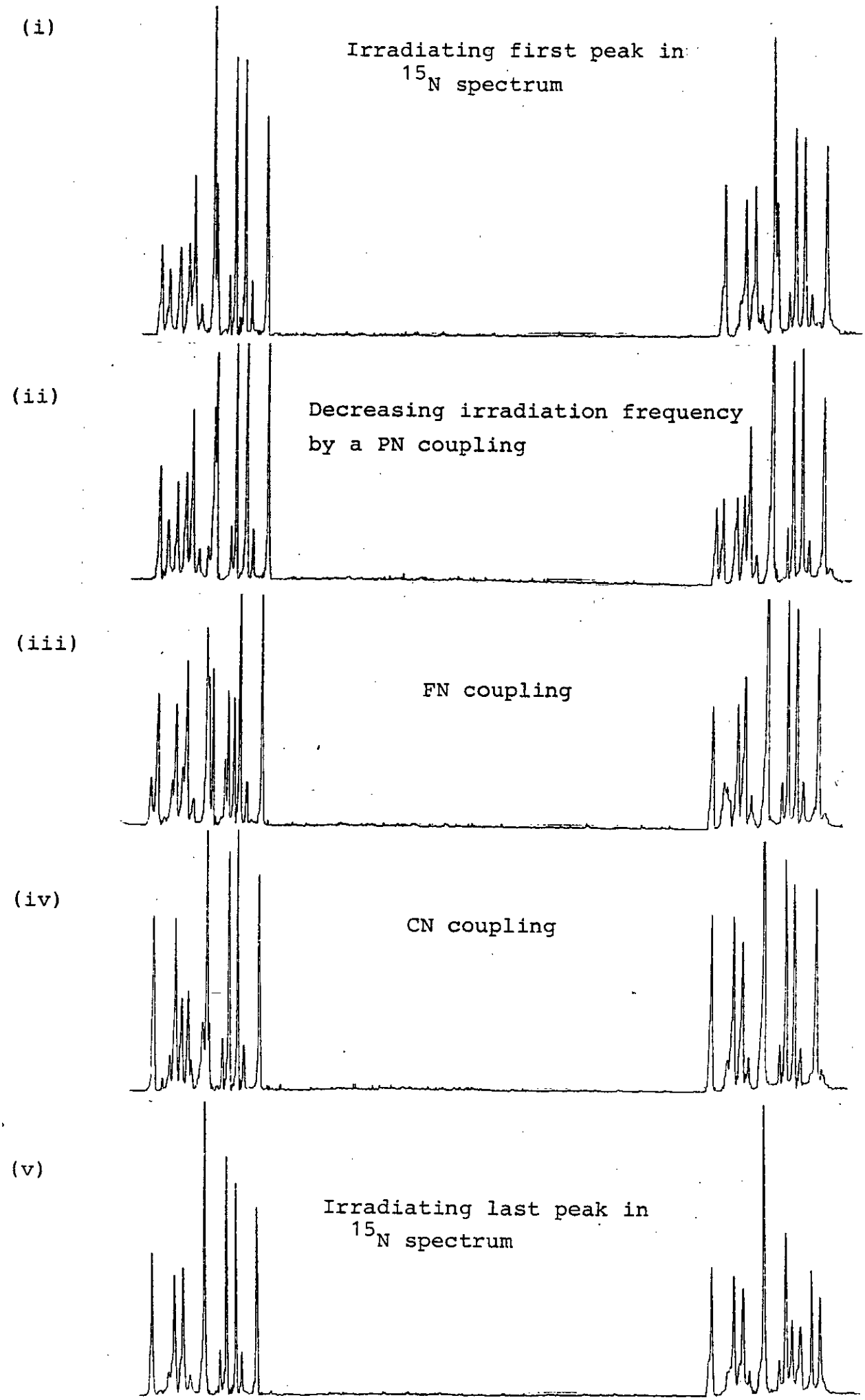

Figure 6.2 Observed and Final Weighted Difference Molecular Scattering Intensities for PF_2NCO

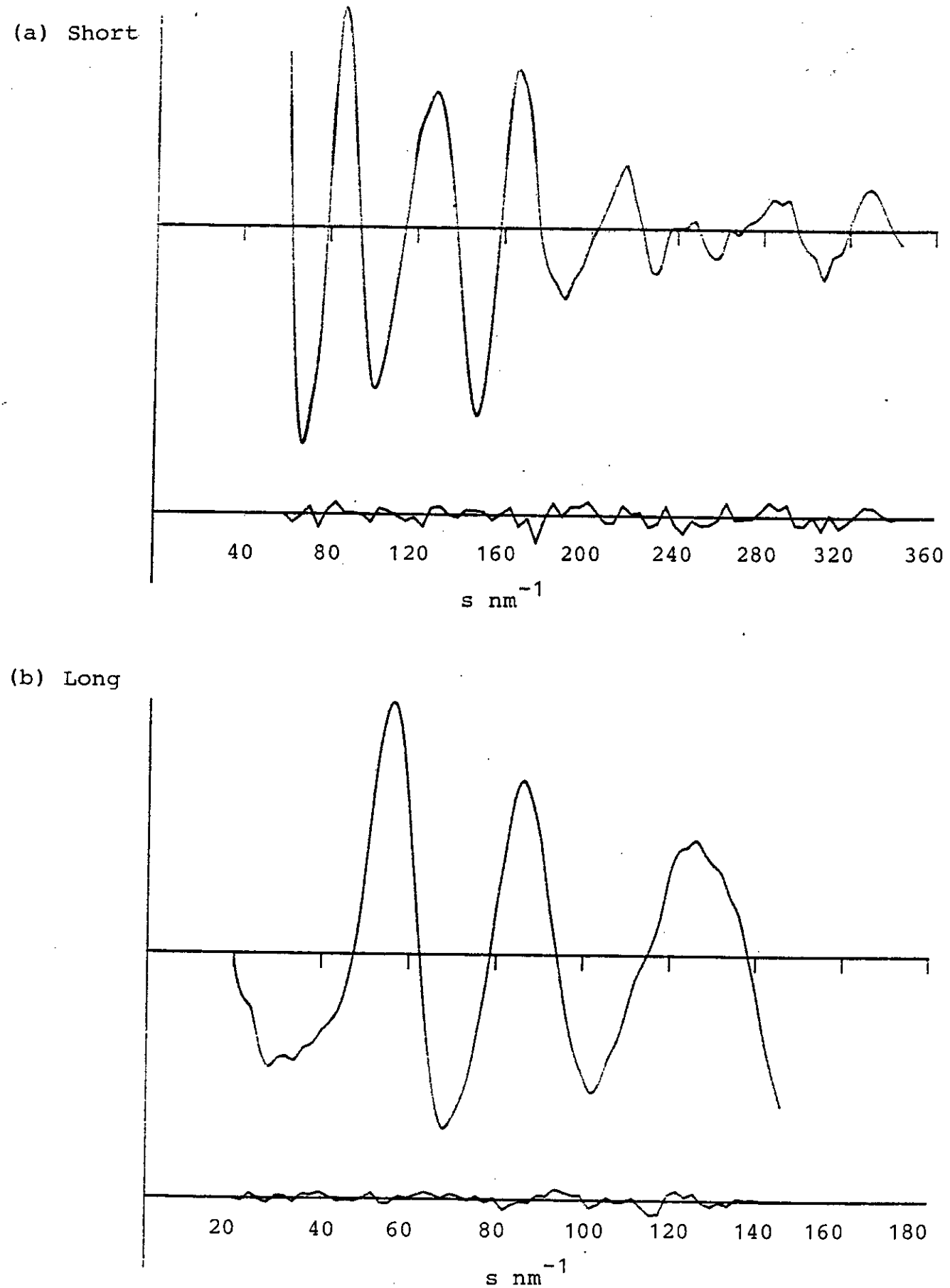

Figure 6.3 Observed and Difference Radial Distribution Curve for PF_2NCO

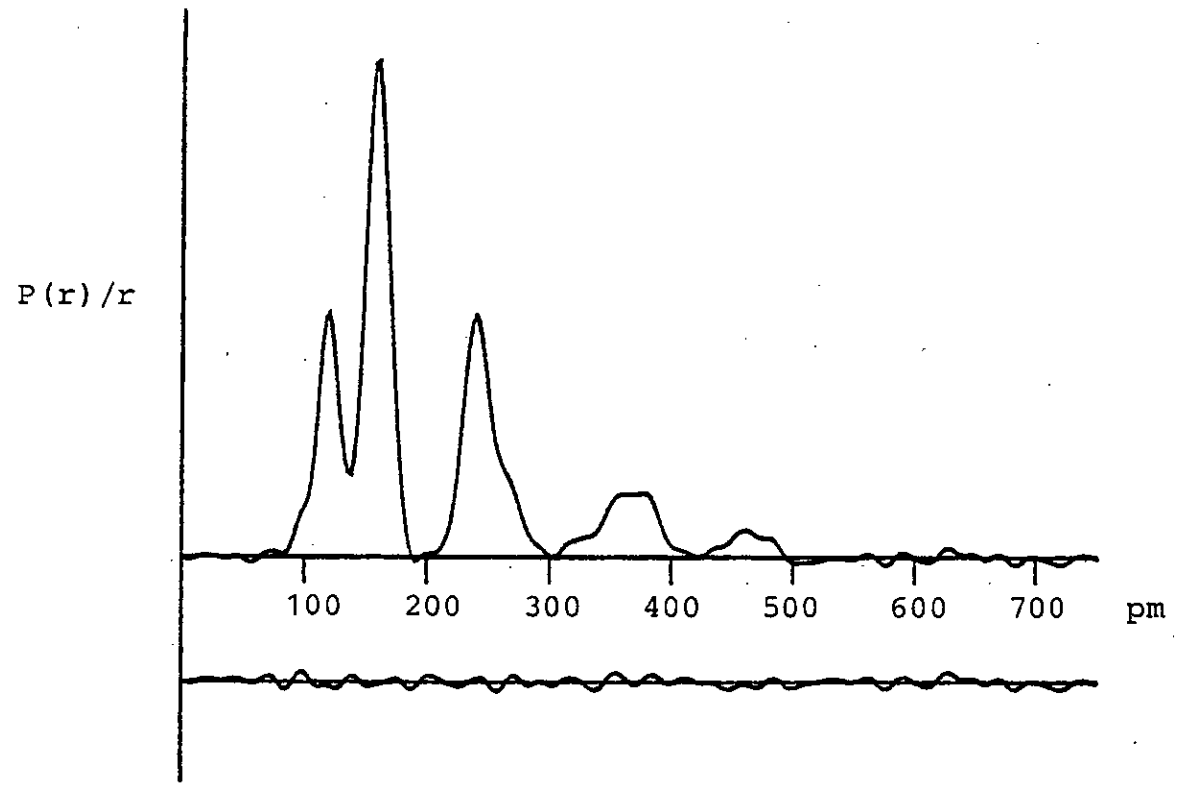

CHAPTER 7

THE MOLECULAR STRUCTURE OF DIFLUOROPHOSPHINE SULPHIDE, DETERMINED BY USING A COMBINATION OF DATA FROM ELECTRON DIFFRACTION, LIQUID CRYSTAL N.M.R. SPECTROSCOPY AND MICROWAVE SPECTROSCOPY

7.1 Introduction

The problems associated with the combination of data from Electron Diffraction (E.D.) and Liquid Crystal N.M.R. Spectroscopy (L.C.N.M.R.) in the previous chapters have partly stemmed from the consideration of molecules possessing low frequency, high amplitude modes of vibration. It is difficult to allow exactly for the effect of these vibrations when converting data from each source to the r_s structure (see chapter 3). It was decided that a more rigid molecule would be a more suitable candidate for a combined structural analysis, and difluorophosphine sulphide was chosen.

The structure of this compound has previously been determined by both Electron Diffraction[45] and Microwave Spectroscopy[181]. However, neither method can claim to locate the proton with great accuracy. In the E.D. analysis, the peaks in the radial distribution curve corresponding to the proton bonded and non-bonded distances are of very low intensity and coincide with more significant peaks, necessitating the fixing of all hydrogen parameters at reasonable values throughout the refinement. The extra information from Liquid Crystal N.M.R. Spectroscopy allows these parameters to be refined.

It is interesting to compare the structure of difluorophosphine sulphide with its selenide analogue. This compound was the first to be studied by a combination of E.D. and L.C.N.M.R. techniques[124].

7.2 Experimental

A sample of PF_2HS was prepared by the reaction between hydrogen sulphide and PF_2Br in the presence of mercury, under reduced pressure, by vigorously shaking a glass bulb containing the reagents[182].

$$PF_2Br + H_2S \xrightarrow{Hg} PF_2HS + HBr$$

The product was purified by fractionation under vacuum and the purity tested by infra-red spectroscopy. A yield of around fifty percent was obtained.

7.3 Data Collection

7.3.1 Electron Diffraction

The data collected previously[45] were used again. The plates had been run on a Balzers KD.G2 Diffraction Apparatus[32] at Manchester and were retraced by the new microdensitometry service at Daresbury. The relevant experimental details are listed in Table 1.1.

7.3.2 Microwave Spectroscopy

The rotational constants of Nave and Sheridan[181] were used (Table 7.1).

7.3.3 Liquid Crystal N.M.R. Spectroscopy

Samples were prepared containing 0.3 mmol of PF_2HS in 0.4 ml of "E5" liquid crystal as solvent in 5 mm N.M.R. tubes. These solutions were found to possess a nematic phase between 235 and 295 K. A sample was also prepared containing 0.3 mmol of PF_2HS in 0.4 ml of $CDCl_3$.

All the N.M.R. experiments were carried out using the Varian Associates XL100 Spectrometer (see Chapter 2.4) in the pulsed Fourier transform mode. This instrument has built-in decoupler coils and a low temperature operation facility.

The indirect J coupling constants (Table 7.3) were measured in the isotropic liquid crystal solution heated to 313 K. Measurements taken in $CDCl_3$ solution at both 293 K and 253 K showed that the couplings varied slightly with temperature. It was assumed that a similar variation would occur in the couplings measured in the liquid crystal solution and so they were scaled accordingly.

The PH coupling in particular was substantially different in each solvent, emphasizing the importance of measuring the couplings in the isotropic phase of the liquid crystal. A series of double resonance experiments was carried out on the $CDCl_3$ solution (Table 7.2(a)) and the absolute signs of the couplings determined by relating them to the PF coupling, which is always large and negative[104]. The isotropic results were similar to those found in a previous study[83].

The direct D coupling constants were measured in the liquid crystal solution over a range of temperatures around 262 K and linearly extrapolated to this temperature (Table 7.4). It has been shown in previous chapters that the molecular structure changes insignificantly with temperature, therefore there is little to be gained by taking measurements at several temperatures. The relative signs of the couplings were determined by a series of double resonance experiments

(Table 7.2(b)) and their absolute values given by comparison once again to the negative PF coupling.

In addition to the double resonance experiments, a two-dimensional spectrum was run on the departmental Bruker WH360 Spectrometer. This method gives a contour plot of the peaks involved, with one axis representing the proton spectrum and the other axis the phosphorus spectrum. From the positions of the peaks in two-dimensions, it can be directly seen that the low-field proton resonances correspond to the high-field phosphorus resonances and vice-versa. It can therefore be simply deduced, from consideration of the spin-levels involved (as outlined in Chapter 2.5), that the PF and FH couplings must be of opposite sign. This elegant method is much simpler than a time consuming series of double-resonance experiments, unfortunately, so far, only the proton/phosphorus combination is available.

Examples of the spectra obtained in the isotropic and nematic phases, including double resonance experiments, are shown in Figure 7.1. The two-dimensional spectrum is shown in Figure 7.2.

7.4 Structural Refinements

7.4.1 Electron Diffraction Only (Refinement A)

In all structural refinements it is assumed that PF_2HS possesses C_s symmetry. A model program was written with six independent parameters, the PH, PF and SF distances and the <FPF, <SPF and <SPH angles, and one dependent parameter, the <FPH angle.

A normal co-ordinate analysis using the GAMP routine (see Chapter 3.6) was carried out to determine the amplitudes of vibration. A harmonic force field was developed which exactly fitted the observed vibrational frequencies[181] which are listed in Table 7.5 with their assignments. One of the fundamental modes has not been observed for PF_2HS, this is the lowest frequency A'' symmetry mode, assigned to the PF_2 rock. In the case of SPF_2Cl[184] this band occurs at 250 cm^{-1}. Varying the frequency around this value had, as expected, the greatest effect on the u(S...F) calculated amplitude, which agreed with that obtained from the electron diffraction refinement when the fundamental mode was fixed at 230 cm^{-1}.

The r_a structure was now refined from the E.D. data alone. All parameters were allowed to refine except those associated with the proton, which were fixed at the values obtained from the normal co-ordinate analysis. When the proton distance and angle were allowed to refine the values dropped to unreasonable levels with huge E.S.D.S.

The final r_a structure (see Table 7.6 and 7.7) is the same as previously reported[45]; however, the Rgen factor has been reduced from 12% to 6%. This may be because of the improved plate tracing or better background substraction.

The r_α^o structure (see Table 7.9) was refined using the vibrational corrections outlined in Chapter 3, with the amplitudes of vibration calculated by the normal co-ordinate analysis. The corrections are listed in Table 7.8(a).

The molecular scattering intensity and the radial distribution curves for PF_2HS are shown in Figures 7.3 and 7.4 respectively.

7.4.2 The Microwave Structure (Refinement B)

The microwave structure was calculated using a program which calculated the moments of inertia from the rotational constants of each isotopic species. An input starting structure was refined by a least squares method and the final structure agreed with that reported previously[181].

Harmonic vibrational corrections were applied (Table 7.8(b)) as described in Chapter 3.5, to convert to the B_z rotational constants from which the r_z structure was calculated, for comparison with the E.D. r_α^o structure (see Table 7.9).

7.4.3 Electron Diffraction Plus Microwave Structure (Refinement C)

A new model program was written to calculate structural information from the B_z rotational constants. These were added as extra data to the E.D. refinement program, with weights proportional to the inverse of the square of their uncertainty. The well defined parameters agreed with the E.D. only structure, but when the proton parameters were freed, the <SPH angle fell to a low value with a very large E.S.D. The fall was not as dramatic as in the E.D. only case, so the inclusion of the microwave data has caused a slight improvement. The R gen factor was in this case 5.6%, which has dropped slightly from the E.D. only case, because of the freeing of the proton parameters. The structure is listed in Table 7.9 for comparison with the other refinements.

7.4.3 E.D. plus L.C.N.M.R. Structure (Refinement D)

A new model program was written to extract the structural information from the Liquid Crystal N.M.R. data. Three refinable parameters were added to define the orientation (C_s symmetry, Table 2.1), calculated according to equation 2.18. The direct couplings were added to the refinement program with weights inversely proportional to the square of their uncertainties.

Initially the orientation parameters were allowed to refine, with the structure held fixed at the E.D. only result. The well defined distances were then freed, with their

amplitudes of vibration, and finally the proton distances were allowed to refine. The amplitudes of vibration associated with the proton bonded and non-bonded distances were held fixed at the spectroscopic values throughout.

Using the program VIBR[146], vibrational corrections were applied to the direct couplings as described in Chapter 3.4 (see Table 7.8(c)).

The combined E.D. plus L.C.N.M.R. r_α^o structure was now refined (Table 7.9), and gave a final R_{gen} factor of 4.8%. The <HPS angle was found to be better defined than for the E.D. plus microwave refinement, but the PH distance was less well defined. The parameters not involving the proton remained within the combined E.S.D.s for each data combination.

7.4.4 E.D. plus L.C.N.M.R. plus Microwave Structure (Refinement E)

For the first time data from three separate sources have been combined, to give a simple r_α^o structure. With the inclusion of additional data, the R_{gen} factor would be expected to rise, and has, but only to 6.5%. The couplings and rotational constants are fitted to within their E.S.D.'s. The uncertainties associated with each parameter have dropped from the previous refinements and all parameters have sensible values.

The parameters from each refinement may be compared in Table 7.9 and the least squares correlation matrix for the combined refinement is presented in Table 7.10.

7.5 Discussion

The structure of SPF_2H is in itself unremarkable. However, the fact that it has been possible to fit all the data from E.D., microwave spectroscopy and L.C.N.M.R. together is encouraging. As expected, by introducing the extra data, the correlations between the geometric parameters in Table 7.10 are seen to increase, but, their uncertainties have nevertheless been reduced. Refinement D, E.D. plus L.C.N.M.R., is strikingly similar to the structure previously derived for $SePF_2H$[124] by a similar combination of data.

The parameters that were well defined by E.D. alone have remained fairly constant throughout each subsequent refinement, showing that the structure has changed little in going from the gas to the liquid phase. Table 7.11 lists for comparison, the P-F and P=S bondlengths and associated angles, and Table 7.12 the P-H bondlengths, for a variety of related compounds. Although direct comparison is hampered by the fact that the parameters listed represent different structures, several important trends may be observed.

Variations in bondlengths are caused by a combination of subtle effects. In the case of the P-F bondlength, the most important effect seems to be the number of other electronegative atoms, particularly fluorine, attached to the phosphorus centre. In considering the series going from PF_3 to PF_2H to PH_3, the P-F and P-H bond lengths increase because the repulsion of the P-H bonding electron pair is larger than that of P-F, because the increased electro-

negativity shifts the electron density towards the fluorine. This highly polar PF bond has been observed to give rise to a large chemical shift to high freq. in phosphorus N.M.R. experiments, and a higher than estimated dipole moment[185].

The P-F bond lengths in four co-ordinate PF_2SH are seen to be shorter than those in PF_3, while in five co-ordinate PF_5 the equatorial P-F distances are shorter still. This shortening with increased co-ordination has been explained in terms of a shrinking central atom as more highly electronegative atoms are attached, and by changes in the bonding electron orbital hybridisation[186]. The magnitude of this effect in going from four to five co-ordinate is not as great as going from three to four co-ordinate, because of an opposing steric effect tending to lengthen bonds with increasing co-ordination number.

The trend with electronegative substituents is seen in the increase in P-F bondlength through the series SPF_3, SPF_2Cl, SPF_2Br, SPF_2I and SPF_2H, and also OPF_2H, SPF_2H and $SePF_2H$. The effect on the P=S bondlength is not so clear cut, with the distance in SPF_2H lying in the middle of the series SPF_3, SPF_2Cl, SPF_2Br and SPF_2I. Perhaps the steric effect of the bulky Br and I groups serves to balance the expected decrease in bondlength from electronegativity considerations.

The FPF angle lies in the range for this angle in SPF_2X compounds. There seems to be a distinct series, increasing from $SePF_2H$ to SPF_2H to OPF_2H. This could be caused by the increasing electronegativity of the

substituent group delocalising the bonding electrons away from the phosphorus centre and so reducing the repulsion and increasing the angle. Also, according to Bartell's "hard-sphere" theory[187], the non-bonded F..F distance remains fairly constant, therefore as the P-F bond lengths have been seen to shorten, so the FPF angle will increase.

The P-H distances shown in Table 7.12 once again represent different structures. In general the parameters vary as $r_\alpha^o < r_o < r_a$. Electronegativity effects are noticed in the reduction of the P-H distance in going from PH_3 to PF_2H, an effect also found in the series $SePF_2H$, SPF_2H and OPF_2H. A decrease in the P-H distance in going from three to four co-ordinate phosphorus is noticed. This could be explained in terms of increased s character in the hybridised bonding electron orbitals in the four co-ordinate system.

Table 7.1 Rotational Constants for the PF_2HS Isotopic Species

	$PF_2H^{32}S$	$PF_2D^{32}S$	$PF_2H^{34}S$
A(MHz)	8336.572(6)	7976.61(3)	8333.40(3)
B(MHz)	3725.667(3)	3641.52(3)	3596.86(3)
C(MHz)	2805.302(2)	2798.88(3)	2731.91(3)

Table 7.2 Double Resonance Experiments for PF_2HS

(a) Isotropic Couplings

Experiment	J Couplings Related	Relative Signs
$^{31}P-\{^{19}F\}$	PH and FH	equal
$^{19}F-\{^{1}H\}$	PF and PH	opposite
$^{19}F-\{^{31}P\}$	FH and PH	equal

(b) Nematic Couplings

Experiment	Δ* Couplings Related	Relative Signs
$^{19}F-\{^{1}H\}$	PF and PH	opposite
	FF and FH	equal
$^{31}P-\{^{1}H\}$	PF and FH	opposite

* $\Delta = J + 2D$ (except for FF coupling, $\Delta = 3D$)

Table 7.3 Isotropic Couplings for PF_2HS

Nuclei	$CDCl_3$ (298K)	$CDCl_3$ (253K)	E5 (313K)	E5 (scaled to 262 K)
PF	-1157.3(5)	-1158.3(4)	-1156.8(5)	-1157.8(8)
PH	+737.5(1)	+740.9(5)	+758.0(5)	+761.0(8)
FH	+97.8(1)	+97.8(2)	+98.0(5)	+98.0(5)

Table 7.4 Direct Couplings for PF_2HS

Nuclei	J	Δ* (262K)	D
PF	-1157.8(8)	-1015.8(5)	+ 71.0(8)
PH	+761.0(8)	+2025.0(10)	+632.5(12)
FH	+98.0(5)	+973.6(5)	+437.8(7)
FF	-	+789.4(5)	+263.1(5)

* $\Delta = J + 2D$ (except for FF coupling, $\Delta = 3D$)

Table 7.5 Vibrational Frequencies and Assignments for PF_2HS

Species	Frequency/cm^{-1}	Approximate Description
A'	2458	P-H stretch
	1019	P-H deformation (in-plane)
	923	$P-F_2$ stretch (symm)
	710	P=S stretch
	419	PF_2 wag (in-plane)
	344	FPF deformation
A''	963	P-H wag (out-of-plane)
	901	PF_2 stretch (asymm)
	230*	PF_2 rock

* Estimated from E.D. amplitudes of vibration

Table 7.6 Distances and Amplitudes of Vibration for the E.D. only r_a Structure of PF_2HS

		Distances/pm	Amplitudes/pm
d1	(P-H)	140.0 (fixed)	8.4 (fixed)
d2	(P-F)	154.9 (1)	3.4 (5)
d3	(P=S)	187.7 (2)	3.5 (5)
d4	(F...F)	235.6 (7)	7.5 (9)
d5	(S...F)	291.0 (5)	7.8 (3)
d6	(S...H)	280.5 (fixed)	11.0 (fixed)
d7	(F...H)	231.3 (fixed)	12.0 (fixed)

Table 7.7 Least Squares Correlation Matrix x100 for the E.D. only r_a Structure of PF_2HS

PS	<FPS	u(PF)	u(PS)	u(SF)	K_1	K_2	K_3	
100	-62						40	PS
	100							<FPS
		100	57	43	80	50		u(PF)
			100		71	46		u(PS)
				100	53			u(SF)
					100	62		K_1

Note: Only |elements| > 40 are included

Table 7.8 Vibrational Corrections for PF_2HS

(a) E.D.

Distance	u_T/pm	$(\frac{3a}{2}\Delta u^2 + K_T)$	r_α^o correction/pm $(\frac{3a}{2}\Delta u^2 + K_T - \frac{u^2}{r})$
PH	8.41	1.300	0.797
PF	4.04	0.264	0.158
SP	3.89	0.192	0.112
FF	7.38	0.200	0.000
SF	7.44	0.040	-0.150
SH	10.90	0.620	0.200
FH	11.84	0.770	0.150

(b) Microwave

	B_o	Correction	B_z*	B_{calc}**
$A(MH_z)$	8336.572	-16.980	8319.59(170)	8319.07
$B(MH_z)$	3725.667	- 5.485	3720.18(55)	3720.06
$C(MH_z)$	2805.302	- 1.260	2804.04(13)	2804.15

(c) L.C.N.M.R.

	D_{obs}	Correction	D_α^o *	D_{calc}**
PF	71.0(7)	0.7	71.7(7)	71.76
PH	632.5(10)	24.2	656.7(25)	656.96
FH	437.8(7)	1.7	439.5(8)	439.53
FF	263.1(5)	0.7	263.7(6)	263.74

* An uncertainty of 10% was assumed for vibrational corrections

** Calculated from Refinement E

Table 7.9 Molecular Parameters for PF_2HS (r_α^o structures)

	A E.D. only	B Microwave only (r_z)	C E.D.+M.W.	D E.D. +L.C.	E E.D.+L.C.+M.W.
Distances/pm					
P-H	139.2(fixed)	139.2(15)	138.6(16)	140.9(20)	141.1(13)
P-F	154.7(2)	155.0(2)	154.7(2)	154.7(2)	154.6(2)
P=S	187.6(3)	187.3(3)	187.5(3)	187.5(3)	187.5(3)
Angles/^{o}					
<FPF	99.3(5)	98.7(2)	99.0(2)	99.4(5)	99.1(1)
<HPS	117.0(fixed)	119.2(10)	114.3(20)	118.4(8)	116.8(6)
<FPS	116.2(2)	117.1(2)	117.0(2)	116.2(2)	117.0(2)

Table 7.10 Least Squares Correlation Matrix x100 for PF_2HS (Refinement E)

PF	<FPF	<HPS	<FPS	S_{xx-yy}	S_{xy}	u(PS)	k1	k2	k3	
-70	64	-96	84	98	-75				-51	PH
	-95	61		-63						PF
		56	-80	-54	77				51	PS
		-59		57						<FPF
			-91	-97	86				53	<HPS
				87	-92				-57	<FPS
					-80				-54	S_{xx-yy}
									53	S_{xy}
						54	77	50		u(PF)
							71			u(PS)
							56			u(SF)
								63		k1

Note: Only |elements| > 50 included

Table 7.11 Parameters for Some Compounds Related to PF_2HS

	P-F	P=S	<FPF	<FPS	Ref.
SPF_2H	154.6(2)	187.5(3)	99.1(1)	117.0(2)	this work
SPF_3	153.8(3)	186.6(5)	99.6(3)		188
SPF_2Cl	153.7(2)	186.5(8)	100.5(8)	116.2(9)	45
$SPCl_3$		188.5(5)			189
SPF_2Br	154.4(3)	188.2(4)	98.3(10)	118.2(10)	45
$SPBr_3$		189.4(4)			190
SPF_2I	154.6(5)	190.2(6)			45
OPF_2H	153.9(3)		99.8(5)	[116.3(10)]	191
$SePF_2H$	155.7(3)		98.1(7)	[116.8(3)]	124
PF_3	156.5(1)		97.8(2)		192
PF_5	153.4(4)*				193

* Equatorial P-F distance, the axial P-F is slightly longer

Table 7.12 Examples of P-H Bond Lengths

Compound	Distance/pm	Structure	Reference
SPF_2H	141.1(13)	r_α^o	This work
$SePF_2H$	142.2(7)	r_a	124
OPF_2H	138.7(10)	r_o	191
$MePH_2.BH_3$	140.4(15)	r_o	194
$Me_2PH.BH_3$	141.4(12)	r_o	195
PF_2H	141.2(6)	r_a	185
PH_3	142.0(5)	r_o	196
$PH_2(CH_3)$	142.3(7)	r_a	197
$PH(CH_3)_2$	144.5(20)	r_a	197
$PH_2(SiH_3)$	143.8(20)	r_a	198
$PH_2(CF_3)$	143.0(30)	r_o	199
P_2H_4	141.7(2)	r_o	200
P_2H_4	145.1(7)	r_a	201

Figure 7.1 Liquid Crystal N.M.R. Spectra for PF_2HS

(a) ^1H isotropic ($CDCl_3$ solvent)

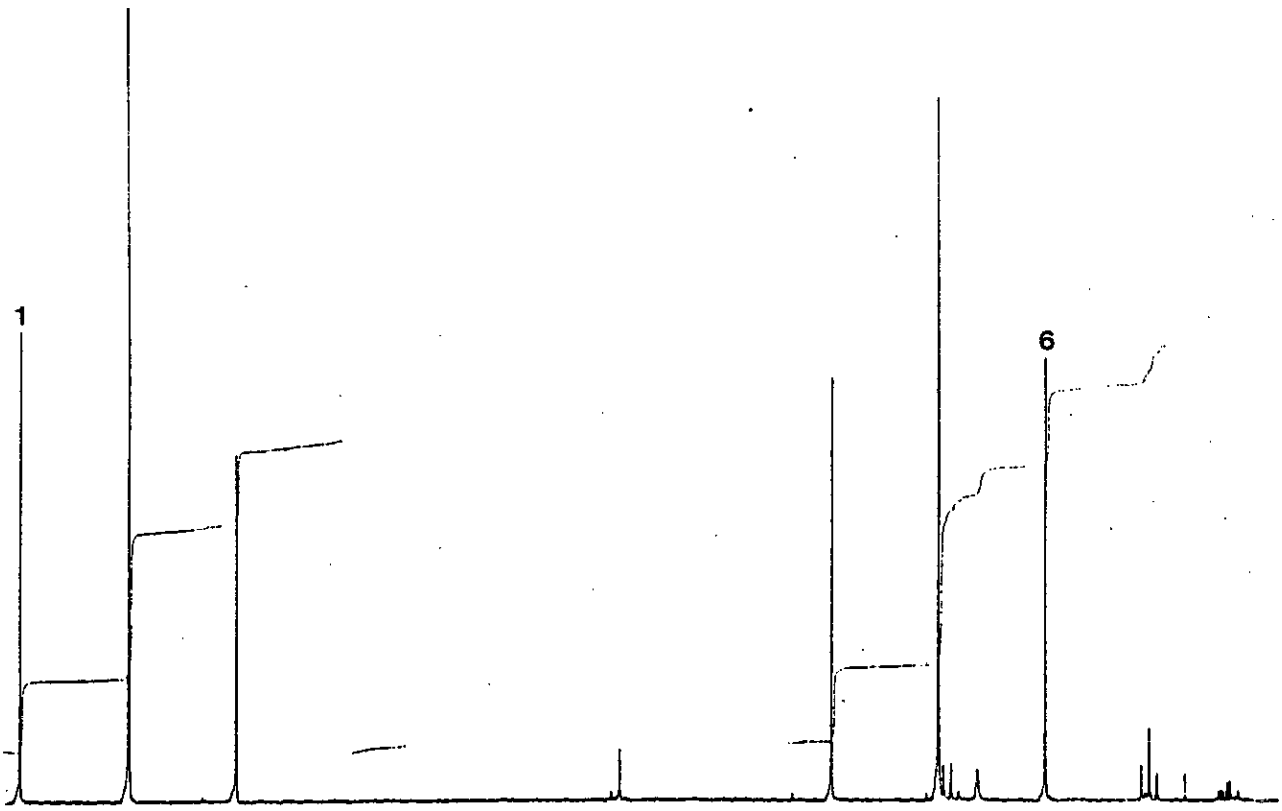

(b) ^1H isotropic (showing additional E5 resonances)

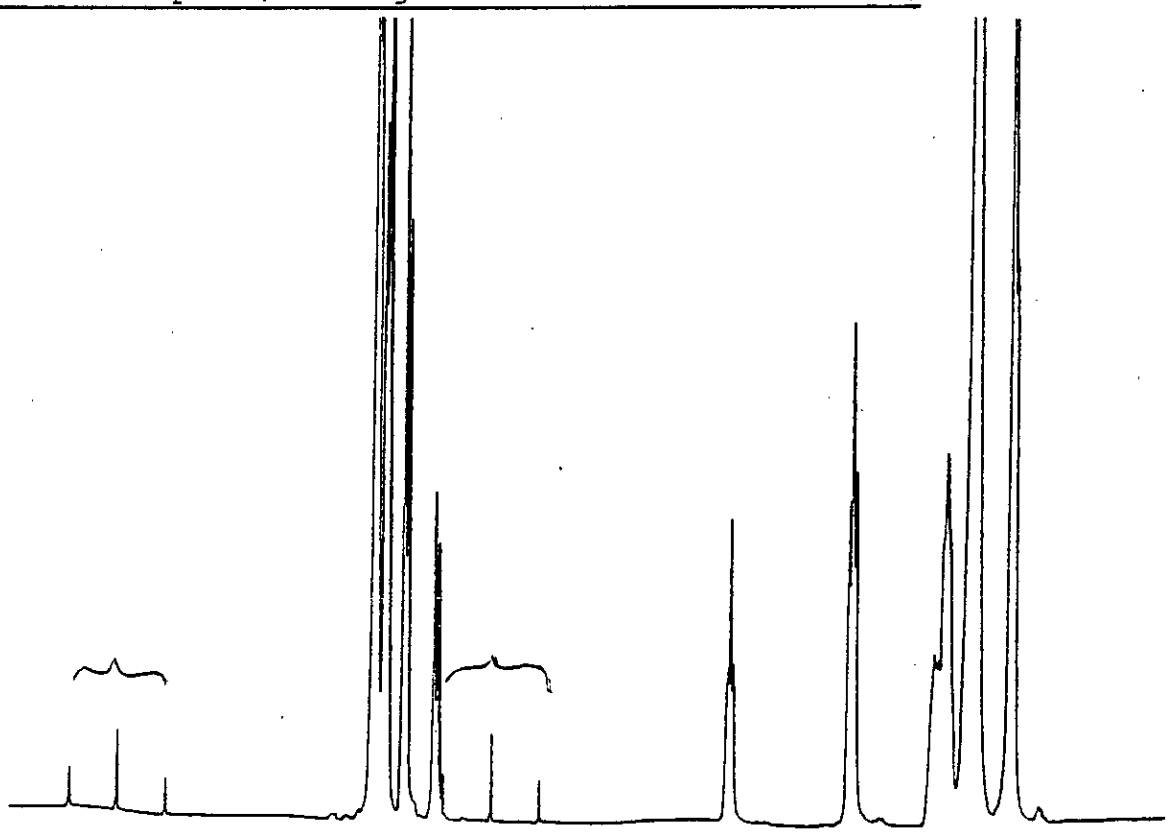

Figure 7.1 (contd.)

(c) ^{19}F isotropic

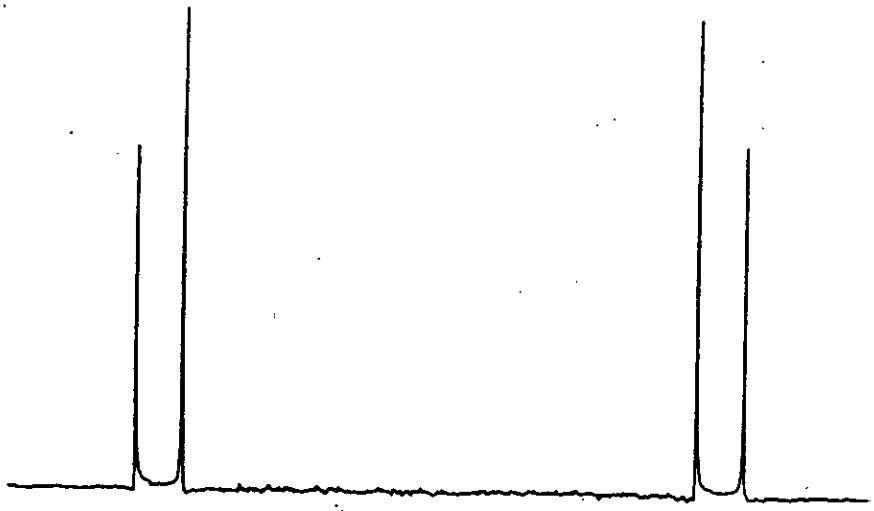

(d) ^{31}P isotropic

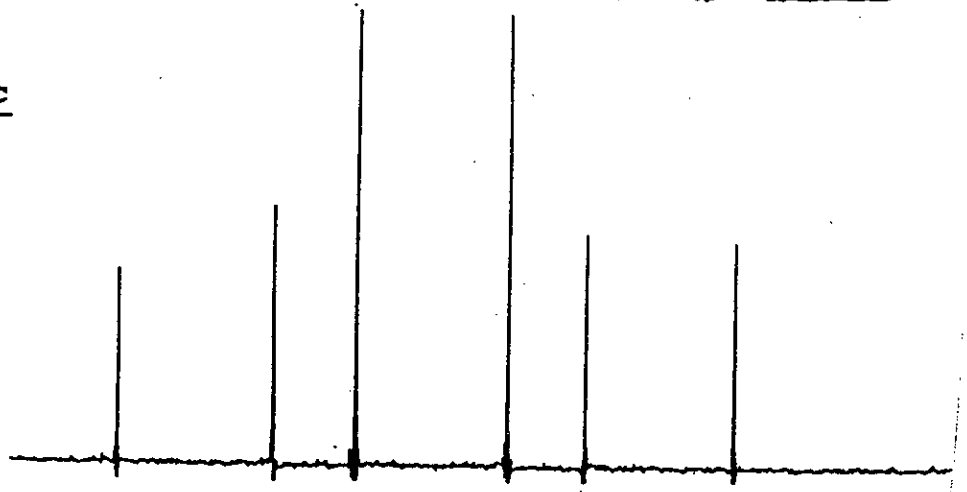

(e) ^{19}F (253 K)

(f) ^{31}P (253 K)

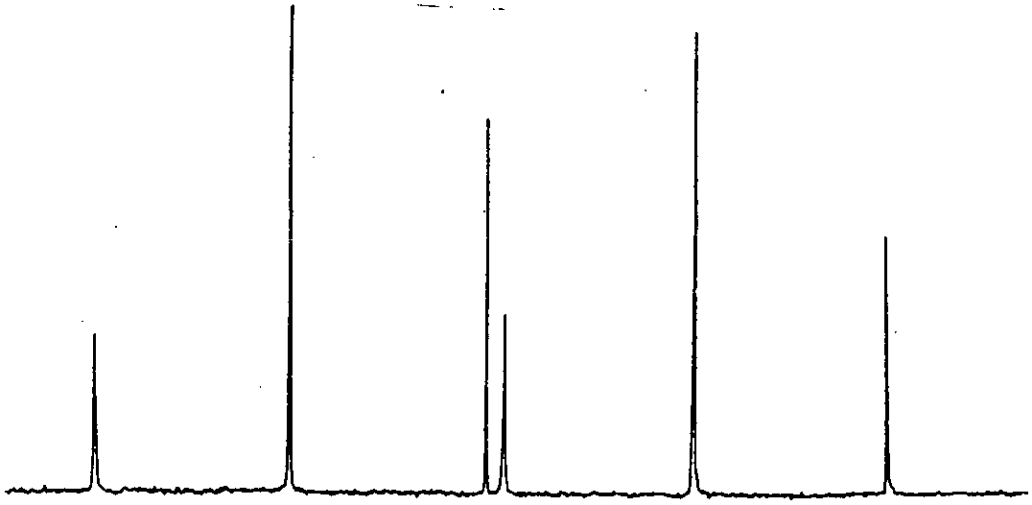

Figure 7.1 (contd.)

(g) F{H} Double Resonance Experiment (isotropic)

(i) Irradiating high frequency triplet in ^{1}H spectrum

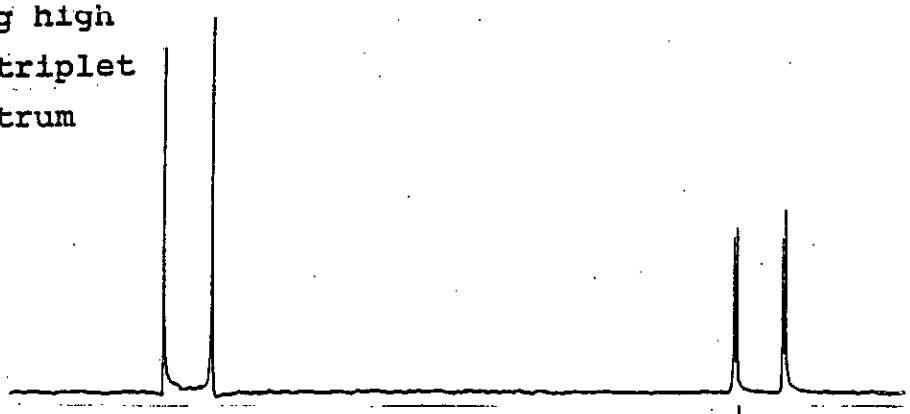

(ii) Irradiating low frequency triplet in ^{1}H spectrum

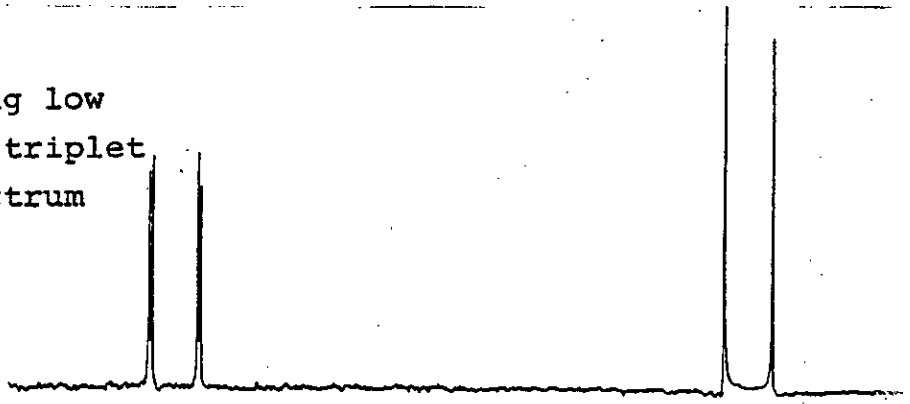

(h) F{P} Double Resonance Experiment (isotropic)

(i) Irradiating first peak in ^{31}P spectrum

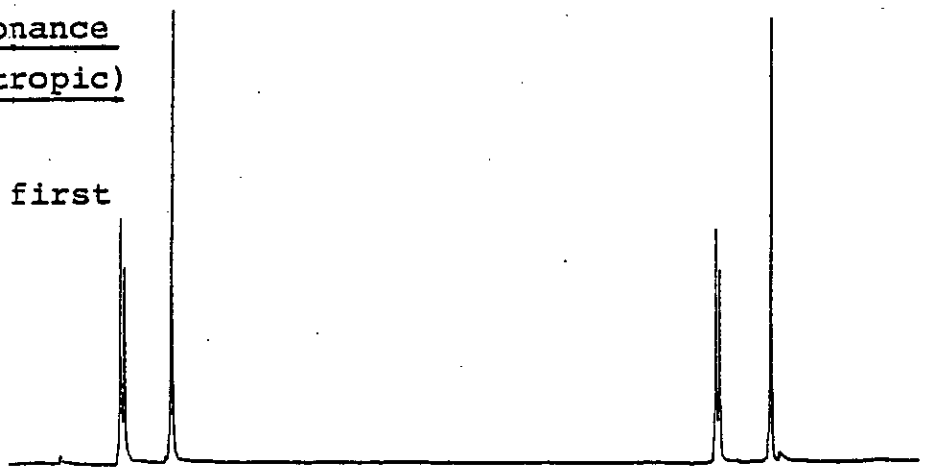

(ii) Irradiating last peak in ^{31}P spectrum

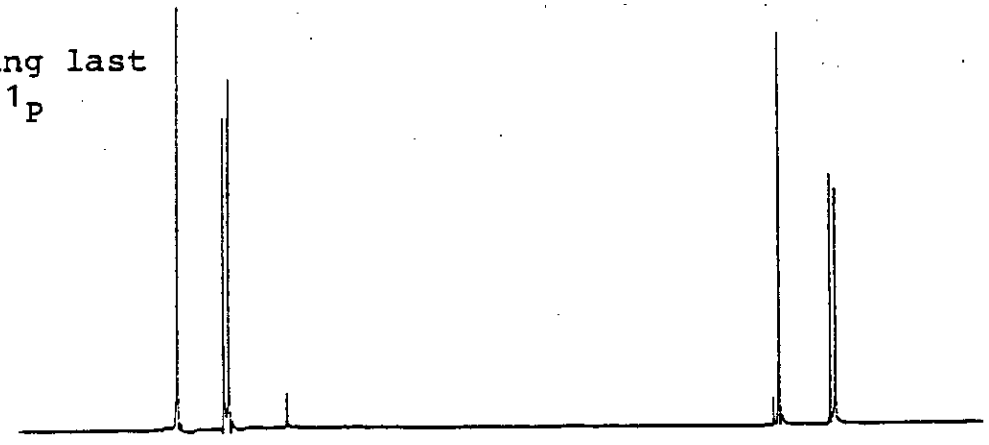

(i) F{H} Double Resonance Experiment (253 K)

(i) Irradiating on Peak 1 in ^{1}H spectrum

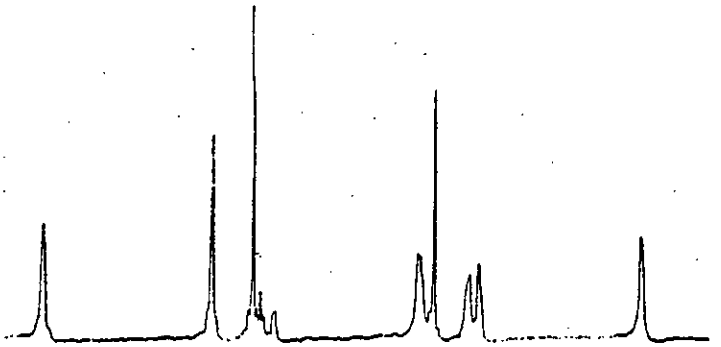

(ii) Peak 2

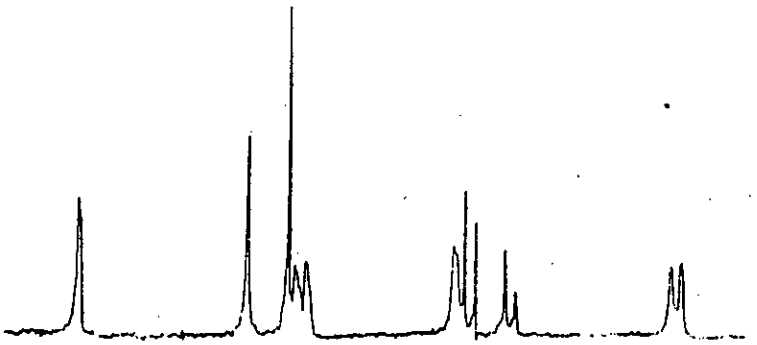

(iii) Peak 3

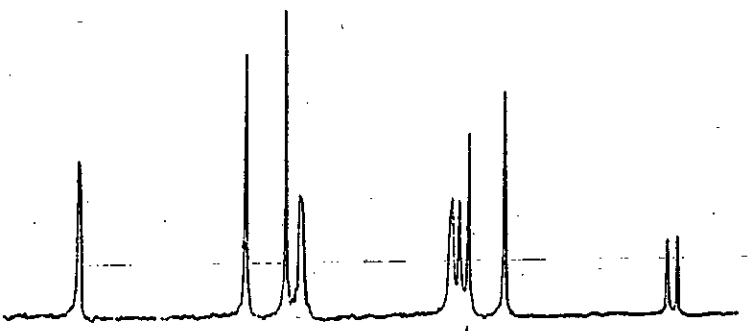

(iv) Peak 4

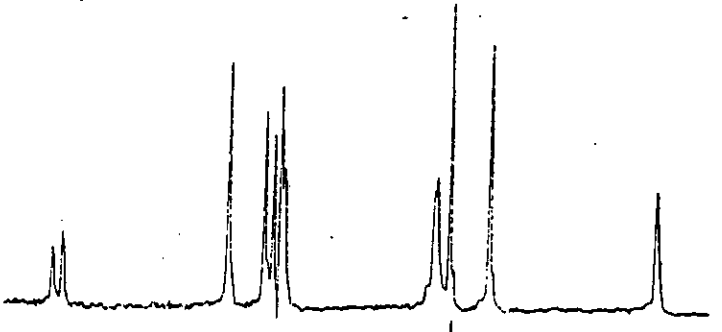

(v) Peak 5

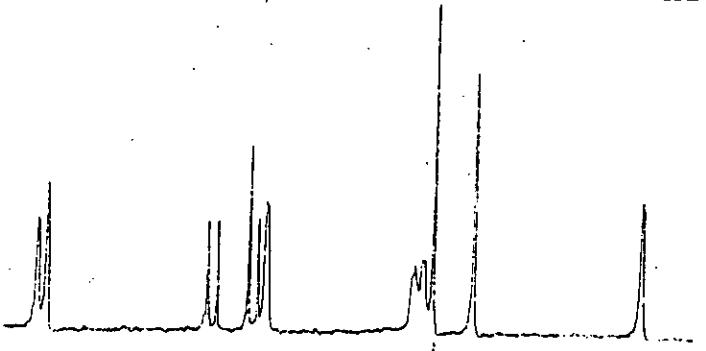

(vi) Peak 6

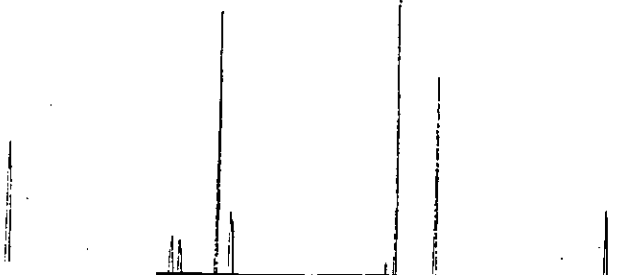

Figure 7.2 Two-dimensional N.M.R. spectrum for PF_2HS (proton decoupled)

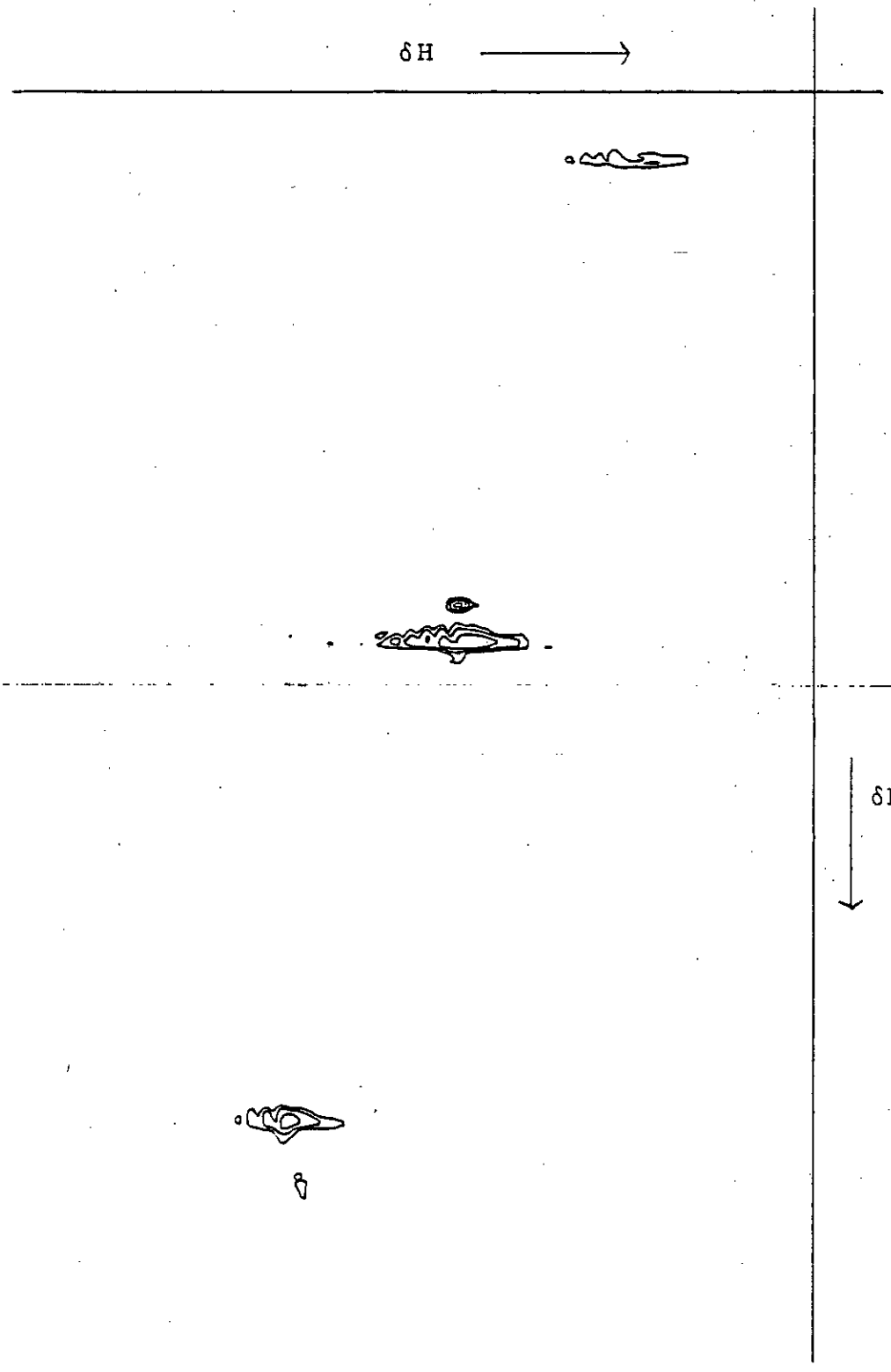

Figure 7.3 Observed and Weighted Difference Molecular Scattering Intensities for PF_2HS

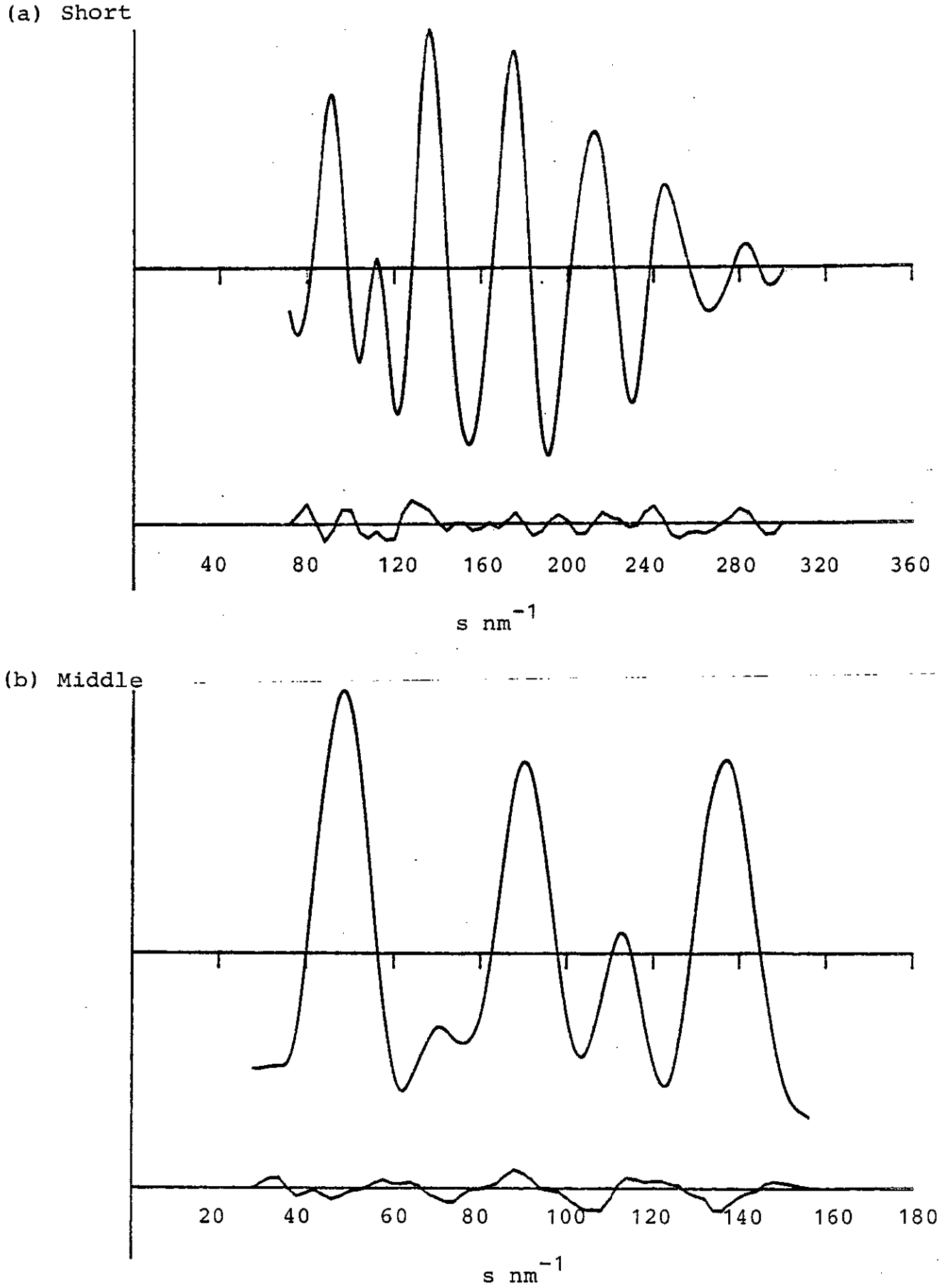

Figure 7.3 (contd.)

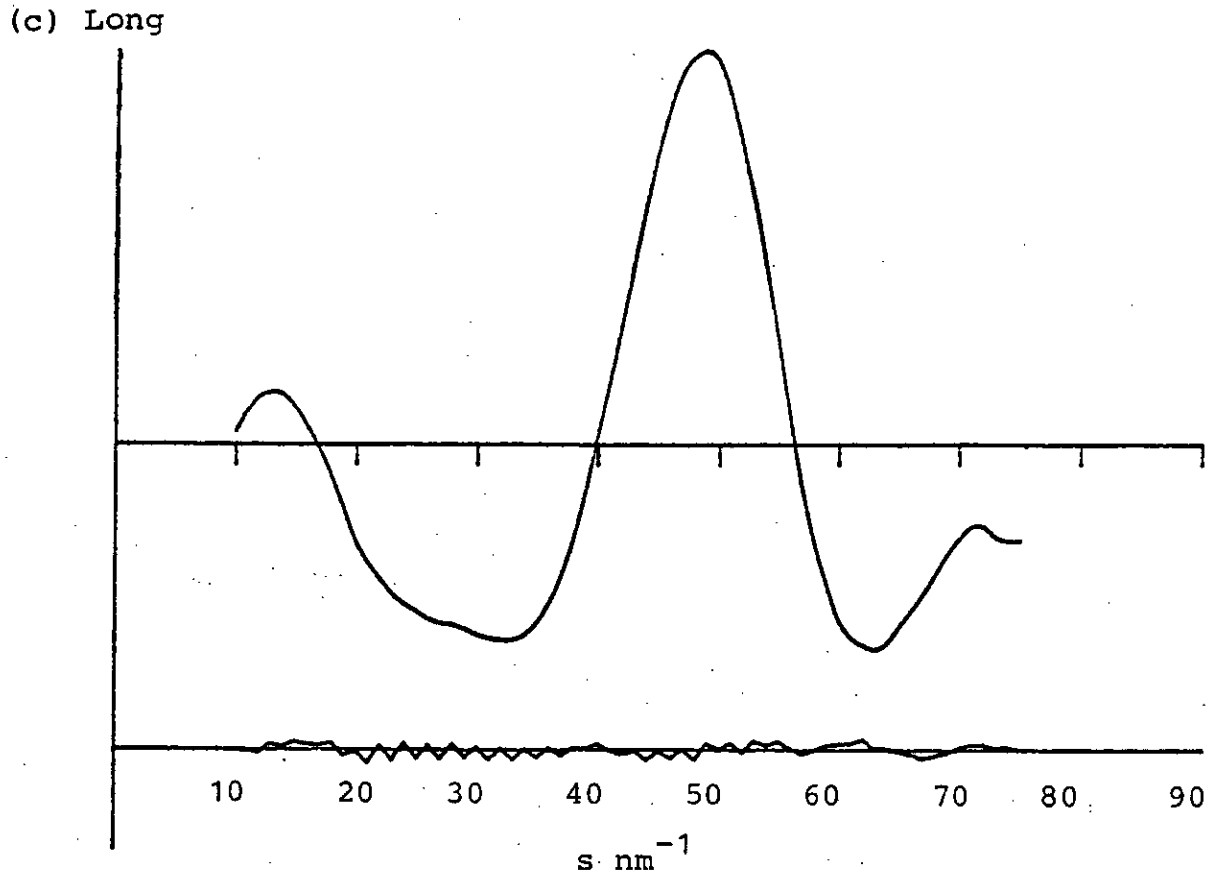

Figure 7.4 Observed and Difference Radial Distribution Curves for PF_2HS

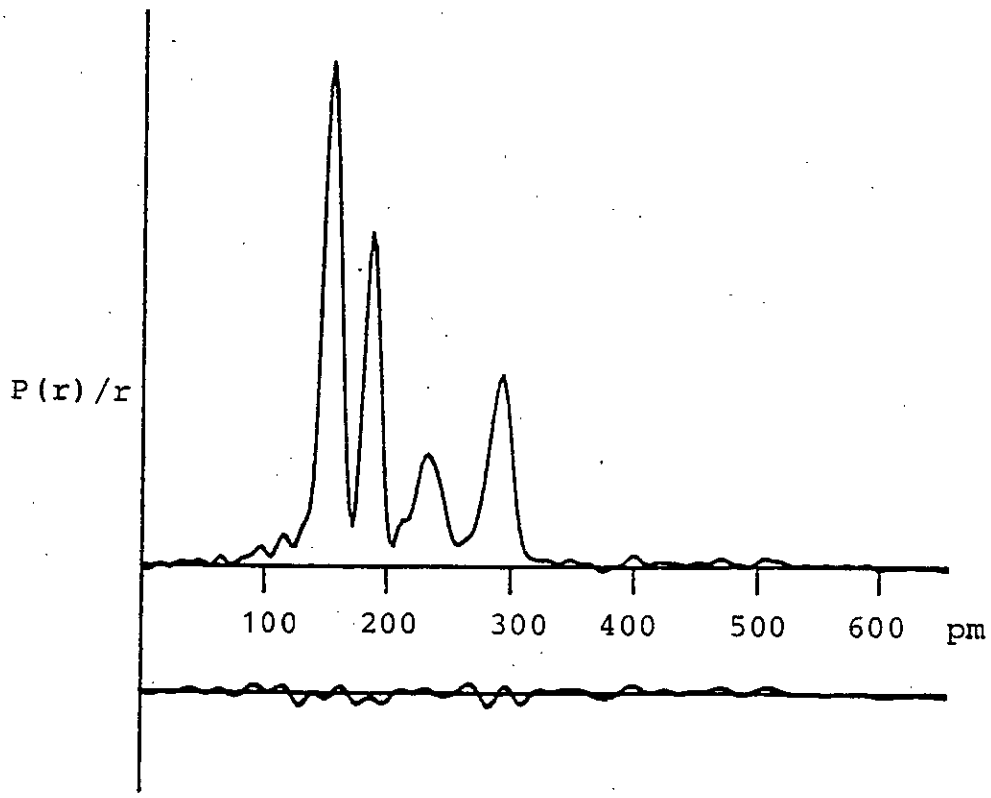

CHAPTER EIGHT

THE MOLECULAR STRUCTURE OF SILYL CYANIDE, DETERMINED BY LIQUID CRYSTAL N.M.R. SPECTROSCOPY

8.1 Introduction

It was noted in Chapter 2 that the amount of structural information available from Liquid Crystal N.M.R. Spectroscopy (L.C.N.M.R.) was dependent upon the number of observable couplings and the geometry of the molecule under study. Silyl cyanide is an eminently suitable compound for study by this technique. It possesses C_{3v} symmetry, and so requires only one parameter to define the orientation of the threefold symmetry axis with respect to the applied field (see Table 2.1), and by using isotopic enrichment of the carbon-13 and nitrogen-15 species, couplings to each of the nuclei can be observed. It is therefore possible to refine a structure from the L.C.N.M.R. data alone although an overall multiplicative scaling factor is required.

The structure of silyl cyanide in the liquid crystal solution is compared with that obtained in the gas phase from Electron Diffraction (E.D.) and Microwave Spectroscopy, and with that obtained in the solid phase from X-ray Crystallography. The observed differences in the various structures are discussed.

8.2 Experimental

A sample of silyl bromide was prepared by a variation of the standard method[202] from phenyl silane and hydrogen bromide:

$$C_6H_5SiH_3 + HBr \rightarrow C_6H_6 + SiH_3Br$$

A sample of silyl cyanide was prepared by the reaction between silyl bromide and silver cyanide. The silver cyanide salt (30 mmol) was prepared from silver nitrate and potassium cyanide solutions:

$$AgNO_3 + KCN \rightarrow AgCN\downarrow + KNO_3$$

The precipitate was filtered off and washed with deionised water, alcohol then dry ether, then transferred to an ampoule and pumped dry overnight on a vacuum line.

Portions of silyl bromide (∿5 mmol) were condensed onto the large excess of silver cyanide, and allowed to warm to room temperature for five minutes:

$$SiH_3Br + AgCN \rightarrow SiH_3CN + AgBr$$

The product was fractionated and its purity checked by infrared spectroscopy.

A sample of $SiH_3\ ^{13}C^{15}N$ was produced from the doubly labelled potassium cyanide salt for use in the N.M.R. experiments. A yield of 80% was recorded.

8.3 Data Collection

8.3.1 Electron Diffraction

A sample of silyl cyanide was run on the Edinburgh Electron Diffraction Apparatus (see Chapter 1.3). The plates obtained were traced by the microdensitometry service at Daresbury. The relevant experimental details are listed in Table 1.1.

8.3.2 Liquid Crystal N.M.R. Spectroscopy

Samples were prepared containing 0.3 mmol of the doubly labelled $SiH_3\ ^{13}C^{15}N$ in 0.4 ml of 'E5' liquid crystal as solvent in 5 mm N.M.R. tubes. These solutions were found to become isotropic around 310 K.

A sample was also prepared containing 0.3 mmol of $SiH_3\ ^{13}C^{15}N$ in 0.4 ml of $CDCl_3$ solvent.

Spectra were obtained through the departmental service on the Bruker WP200SY and WH360 spectrometers.

It was found that, in the case of the proton and carbon-13 isotropic spectra of the liquid crystal solutions, the solvent resonances completely masked those from the solute itself. The isotropic indirect J couplings (Table 8.2) have, therefore, been measured in the $CDCl_3$ solution.

A series of double resonance experiments (Table 8.1) was carried out in order to determine the relative signs of the couplings. These were later assigned absolute values by inspection, allowing for the fact that these experiments

relate the signs of the reduced K coupling constants (see Chapter 2.6), which have opposite signs from the indirect J couplings when nitrogen-15 or silicon-29 are involved.

Table 8.1 Isotropic Double Resonance Experiments on $SiH_3\ ^{13}C^{15}N$ in $CDCl_3$ Solution

Experiment	Couplings Related	Relative Signs	
		K	J
$^{15}N-\{^1H\}$	NC and CH	equal	opposite
$^{13}C-\{^1H\}$	CSi and SiH	equal	equal
	CN and NH	equal	equal

The direct D couplings (Table 8.2) were measured over a range of temperatures. Double resonance experiments were not required as the signs of the direct couplings are defined by the molecular geometry. A selection of the spectra obtained are shown in Figure 8.1.

An additional sample was made up containing 0.3 mmol of $SiH_3\ ^{13}C^{15}N$ in 0.5 ml of 'MBBA' liquid crystal as solvent. N.M.R. spectra obtained from this sample indicated that the solute had reacted with the solvent and decomposed. This problem has been previously discussed in Chapter 2.1.

8.4 Structural Refinements

8.4.1 Electron Diffraction

In all structural refinements it was assumed that the silyl cyanide molecule possesses C_{3v} symmetry. A model program was written with four independent parameters, the SiH, SiC and CN bond lengths and the <HSiC angle.

A normal co-ordinate analysis using the GAMP routine (see Chapter 3.6) was carried out to determine the amplitudes of vibration. A harmonic force field was developed which exactly fitted the observed vibrational frequencies[203] which are listed in Table 8.3 with their assignments. The calculated amplitudes of vibration were used as starting values in the E.D. refinement and to calculate the vibrational corrections (Table 8.5) as outlined in Chapter 3.

The r_{α}^{o} structure (see Table 8.7) was refined from the E.D. data. All parameters were allowed to refine except the H...H amplitude of vibration which was fixed at the value obtained from the normal co-ordinate analysis.

The final R_{gen} factor obtained was 8.4%.

8.4.2 Microwave Spectroscopy

The rotational constants for the various isotopic species of silyl cyanide were measured by Careless and Kroto[204]. These were corrected for harmonic vibrations and converted into an r_z structure (see Table 8.7) using a least-squares refinement method in Edinburgh by Cradock.

8.4.3 X-Ray Crystallography

The solid state crystal and molecular structures (see Table 8.7) of silyl cyanide have been investigated previously at Edinburgh by Barrow[205]. A monoclinic crystal was studied by X-ray diffraction at a temperature of 150 K. The results were analysed by Fourier methods and least-squares refinement, making allowance for the complex nature of the anomalous dispersion effects for the Si, C and N nuclei. A symmetry space group of $P2_1/m$ was assumed and a final R factor of 3.5% attained.

8.4.4 Liquid Crystal N.M.R. Spectroscopy

A model program was written to extract the structural information from the L.C.N.M.R. data, according to equation 2.18. Only one parameter was required to define the orientation (C_{3v} symmetry, Table 2.1). The direct coupling constants were included in the E.D. refinement routine with weights inversely proportional to the square of their uncertainties. The E.D. r_α^o structure was taken as a starting set of parameters, but the E.D. data were ignored.

The orientation parameter can be calculated for the couplings at each temperature from the HH coupling, which is known absolutely, having no component of indirect J coupling. Only the zz element of the orientation matrix is required for a molecule of C_{3v} symmetry, defining the orientation of the molecular z-axis, which in this case lies along the SiC and CN bonds. According to equation 2.3 the orientation, S, of any bond is given by

$$S = \tfrac{1}{2} \langle 3\cos^2\theta - 1 \rangle \qquad 8.1$$

where θ is the angle between the bond and the applied field.

If the orientation of the SiC and CN bonds is defined as S_{zz}, then the orientation of the HH distance, which lies perpendicular to the z-axis, is given by

$$S_{HH} = \tfrac{1}{2}(3\cos^2 \tfrac{\pi}{2} - 1) S_{zz} = -\tfrac{1}{2} S_{zz} \qquad 8.2$$

The S_{zz} orientation can then be calculated from the equation

$$D_{HH} = \frac{-h\ \gamma_H \gamma_H}{4\pi^2 r_{HH}^3} \cdot (-\tfrac{1}{2}\ S_{zz}) \qquad 8.3$$

Since S_{zz} is positive, as the molecules of silyl cyanide preferentially align themselves with their long axis parallel to the liquid crystal solvent molecules, the signs of the direct couplings can all be determined from equation 8.3. However, because of an incomplete series of double resonance experiments, the indirect J coupling signs are not known. It can be shown, by considering both signs alternately in the refinement, that a negative value for the large HSi indirect J coupling is the only sensible result.

Therefore, from Table 8.1, it can be seen that the CSi coupling is also negative.

The observed coupling in the nematic mesophase, Δ, is of magnitude $J + 2D$ (except for the HH coupling, $\Delta = 3D$), therefore, if measurements are made at two different temperatures and the couplings subtracted, then the J dependence is lost (see Chapter 4.4.2). This differences method is valid in the C_{3v} symmetry case, as the couplings vary linearly with orientation.

The pseudo-couplings derived by this method are listed in Table 8.4 and the structure refined from them is listed as Refinement A in Table 8.6. Vibrational corrections have not been applied as the physical significance of the pseudo-couplings is not yet fully understood.

In refinements of the conventional couplings measured at temperatures of 264 K and 295 K, the signs of the J components were varied according to the constraints imposed by the relationships established by the double resonance experiments (Table 8.1). The structures derived were compared to that from the differences method, (Table 8.6) and the absolute signs of the indirect J couplings were thus established.

Using the program VIBR[146], vibrational corrections (Table 8.5) were applied to the couplings (see Chapter 3.6). The structures, with and without vibrational corrections, are listed in Table 8.6 and the corrected r_α^o structures are listed in Table 8.7 for comparison with the structures determined in different phases.

The application of vibrational corrections has produced a more self-consistent structure, with greatly reduced uncertainties. The parameters listed have been arbitrarily scaled to the E.D. r_{α}^{o} CN bond length, and the stated uncertainties do not allow for any scaling error.

The excellent agreement between the corrected and calculated couplings (Table 8.5(b)), the improvement in the uncertainties and the magnitude of the resultant structural changes all emphasize the importance of the vibrational corrections.

8.5 Discussion

The molecular structure of silyl cyanide has been determined in the gas, liquid and solid phases (Table 8.7).

In the solid phase there was noted a short contact interaction between the silicon and the nitrogen of adjacent molecules, which tended to align in a sort of co-ordinated linear chain. The proximity of the nitrogen atom would be expected to shorten the silicon-hydrogen bondlength and widen the <HSiH angle, and this is the observed effect, although the hydrogen positions are only poorly resolved by X-ray crystallography.

The structure in the liquid phase is seen to lie somewhere between the gas and the solid phase structures. The 'E5' liquid crystal solvent contains cyanide groups, therefore, a co-ordination effect similar to that in the solid phase may be occurring. The fact that the <HSiH angle becomes wider at the lower temperature, at which greater solvent-solute interaction would be expected, gives further evidence for this. The liquid phase structure has been scaled to the Electron Diffraction CN bondlength as the co-ordination effect would be expected to increase the SiC bondlength and this is also noticed in comparison to the gas phase structure. It was attempted to analyse the structure in an alternative liquid crystal, 'MBBA', however this solvent proved too reactive and the solute decomposed.

Although changes in structure with phase can be explained by the specific interaction of the molecule with other cyanide groups, the differences between the gas phase structures determined by Electron Diffraction and Microwave Spectroscopy are more difficult to explain. Each technique gives a well-resolved structure, however, when vibrational corrections are applied to give the r_z and r_α^o structures (which should be equivalent), the sets of parameters derived by each technique are incompatible. This problem is as yet intractable.

The most interesting structural feature of the silyl cyanide molecule is the Si-C bond length (Table 8.8). As expected it is shorter than in the sp^3-hybridized case, for example in methyl silane, however, it is much longer than in other compounds with silicon bonded to formally sp-hybridized carbon.

Very short Si-C bond lengths have previously been tentatively explained by (p-d)π bonding[208], and by resonance structure effects[209]. Perhaps the low electron releasing tendency of the cyanide group reduces any contribution from these effects. For instance a configuration of the resonance structure of the type:

$$H_3 - Si^- = C = N^+$$

would not be favoured.

Table 8.2 Observed Couplings (Hz) for $SiH_3\,{}^{13}C^{15}N$

	J	$\Delta_{264\ K}$	$D_{264\ K}$	$\Delta_{295\ K}$	$D_{295\ K}$	$\Delta_{273\ K}$	$D_{273\ K}$
HN	- 1.16(2)	94.5(2)	47.9(2)	67.4(5)	34.3(5)	80.0(6)	40.6(6)
HC	- 14.72(2)	-450.7(2)	-227.7(2)	-321.8(3)	-163.3(3)	-379.0(4)	-191.9(4)
HSi	-239.09(2)	-1711.0(15)	-736.0(15)	-1284.7(5)	-522.8(5)	-	-
SiN	- 2.14(3)	-	-	-	-	-37.5(6)	-17.7(6)
SiC	- 61.90(5)	-	-	-	-	310.0(5)	186.0(5)
CN	- 12.82(2)	915.7(8)	464.3(8)	650.7(5)	331.8(5)	-	-
HH	-	2981.0(10)	993.7(10)	2143.5(2)	714.5(2)	-	-

Table 8.3 Observed Vibrational Frequencies and their Assignments for SiH_3CN

Symmetry Species	Frequency/cm^{-1}	Assignment
A'	2232	ν(C-H) symmetric
	2200	ν(C≡N)
	914	SiH_3 symm. deformation
	601.5	ν(Si-C)
E''	2245	ν(C-H) assymmetric
	933	SiH_3 asymm. deformation
	682	SiH_3 rock
	248	<Si-C-N

Table 8.4 SiH_3CN Coupling Differences (Hz)

	Δ_{264K}	Δ_{295K}	Difference	Difference/2*
HH	2981.0(10)	2143.5(2)	837.5	279.2(10)
HC	-450.7(2)	-321.8(3)	-128.9	-64.5(4)
HN	94.5(2)	67.4(5)	27.1	13.6(5)
HSi	-1711.0(15)	-1284.7(5)	-426.3	-213.2(16)
CN	915.7(8)	650.7(5)	265.0	132.8(9)

* For HH coupling Difference/3

Table 8.5 Vibrational Corrections for SiH_3CN

(a) Electron Diffraction

Distance	u_T/pm	r_α^o correction $(\frac{3}{2}a\Delta u^2 + K_T - \frac{u^2}{r})$
HH	14.96	0.77
HSi	8.79	1.04
HC	13.18	0.46
HN	16.37	-0.37
SiC	4.84	0.35
SiN	5.09	-0.03
CN	3.47	1.33

(b) Liquid Crystal N.M.R. Spectroscopy

264 K	D_{obs}	Correction	D_α^o	D_{calc}
HH	993.7(10)	24.0	1017.7	1017.7
HC	-227.7(2)	-4.6	-232.3	-232.2
HN	47.9(2)	-0.1	47.8	47.7
HSi	-736.0(15)	-37.1	-772.9	-772.9
CN	464.3(8)	35.2	499.5	499.5
295 K				
HH	714.5(2)	17.3	731.8	731.8
HC	-163.3(3)	-3.3	-166.6	-166.6
HN	34.3(5)	-0.1	34.2	34.1
HSi	-522.8(5)	-26.5	-549.3	-549.3
CN	331.8(5)	25.3	357.1	357.1

Table 8.6 Structural Refinements for SiH_3CN from Liquid Crystal N.M.R. Data*

Distances/pm	A/Differences	B/ 264 K	C/ 264 K + vibn. corrections	D/ 295 K	E/ 295 K + vibn. corrections
SiH	144.85(6)	144.54(6)	146.58(1)	144.42(6)	146.44(1)
CSi	182.73(130)	181.71(142)	187.40(9)	181.19(144)	186.81(7)
CN	115.50(12)	115.50(13)	115.50(1)	115.50(14)	115.50(1)
Angle/^{o}					
<HSiC	104.41(5)	105.07(6)	104.53(1)	105.33(6)	104.79(1)

* All scaled to CN bond length of 115.50 pm

Table 8.7 Comparison of the Structure of SiH_3CN in the Gas, Liquid and Solid Phase

	1/ Gas Phase		2/ Liquid Phase*		3/ Solid Phase
	a. Microwave	b. E.D.	a. 295 K	b. 264 K	X-ray Crystallography
Distances/pm					
SiH	148.10(5)	147.3(3)	146.44(1)	146.58(1)	133.0(60)
CSi	184.93(3)	185.2(1)	186.81(7)	187.40(9)	184.0(9)
CN	115.65(1)	115.5(1)	115.50(1)	115.50(1)	116.3(7)
Angle/^{o}					
<HSiC	107.1(1)	109.3(8)	104.79(1)	104.53(1)	102.0(40)

* Scaled to CN bond length of 115.5 pm

Table 8.8 Examples of SiC bondlengths

Compound	Distance/pm	Structure	Reference
SiH_3CH_3	186.7(1)	r_s	206
SiH_3CN	185.2(1)	r_α^o	this work
SiH_3CCH	182.6(3)	r_s	207
SiH_3CCCl	181.2(5)	r_α	208
SiH_3CCCH_3	180.2(4)	r_α^o	37
SiH_3CCCF_3	182.5	r_a	208

Figure 8.1 Selected L.C.N.M.R. Spectra for SiH_3CN

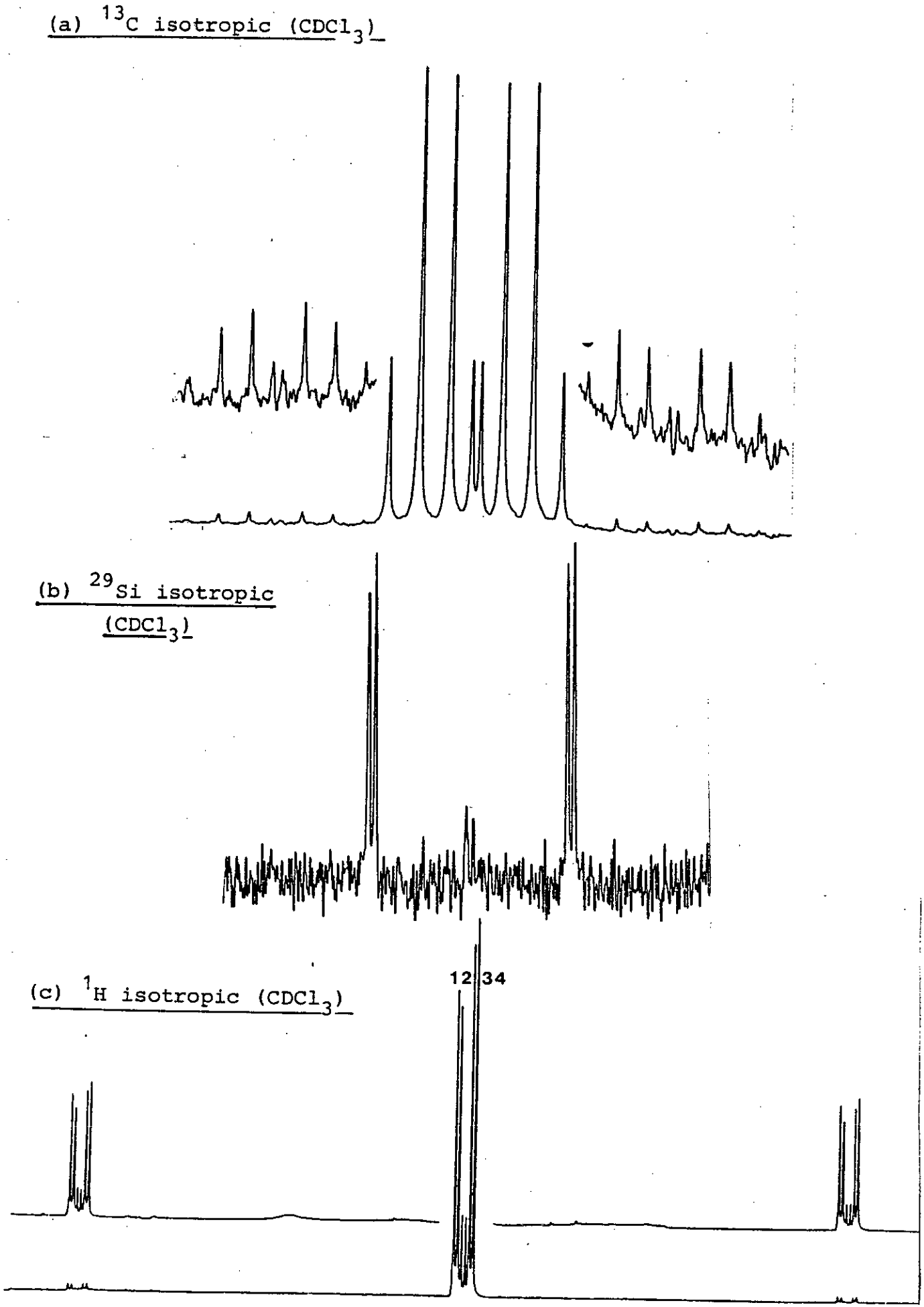

Figure 8.1 (contd.)

(d) ^{15}N (264 K)

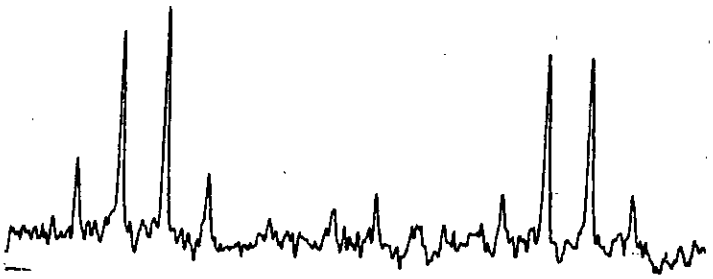

(e) ^{13}C (264 K)

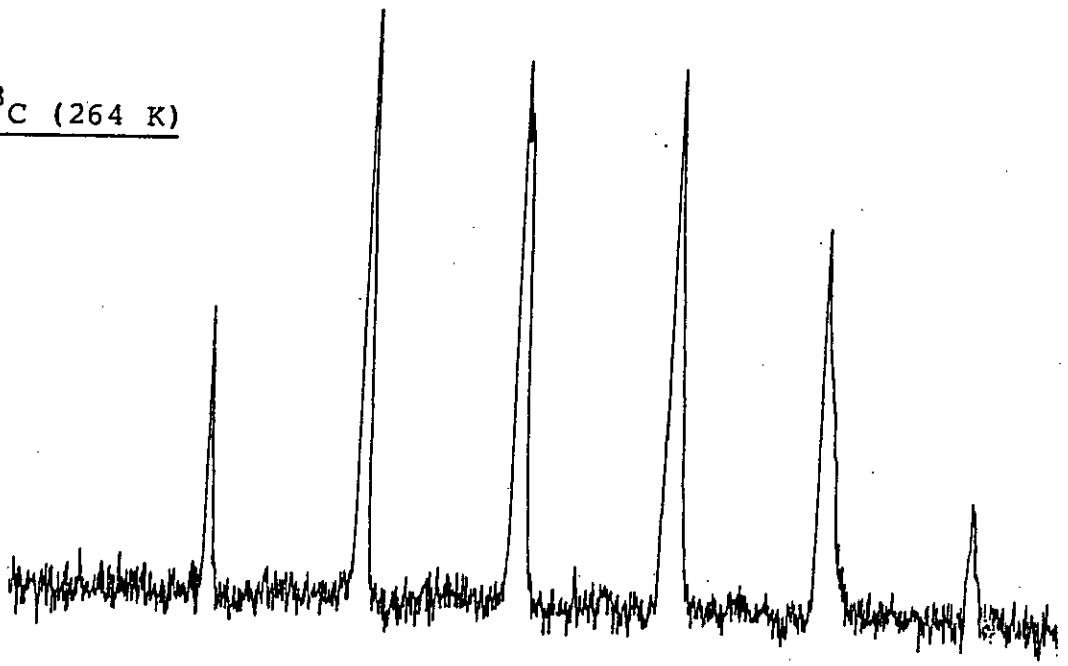

(f) ^{1}H (264 K)

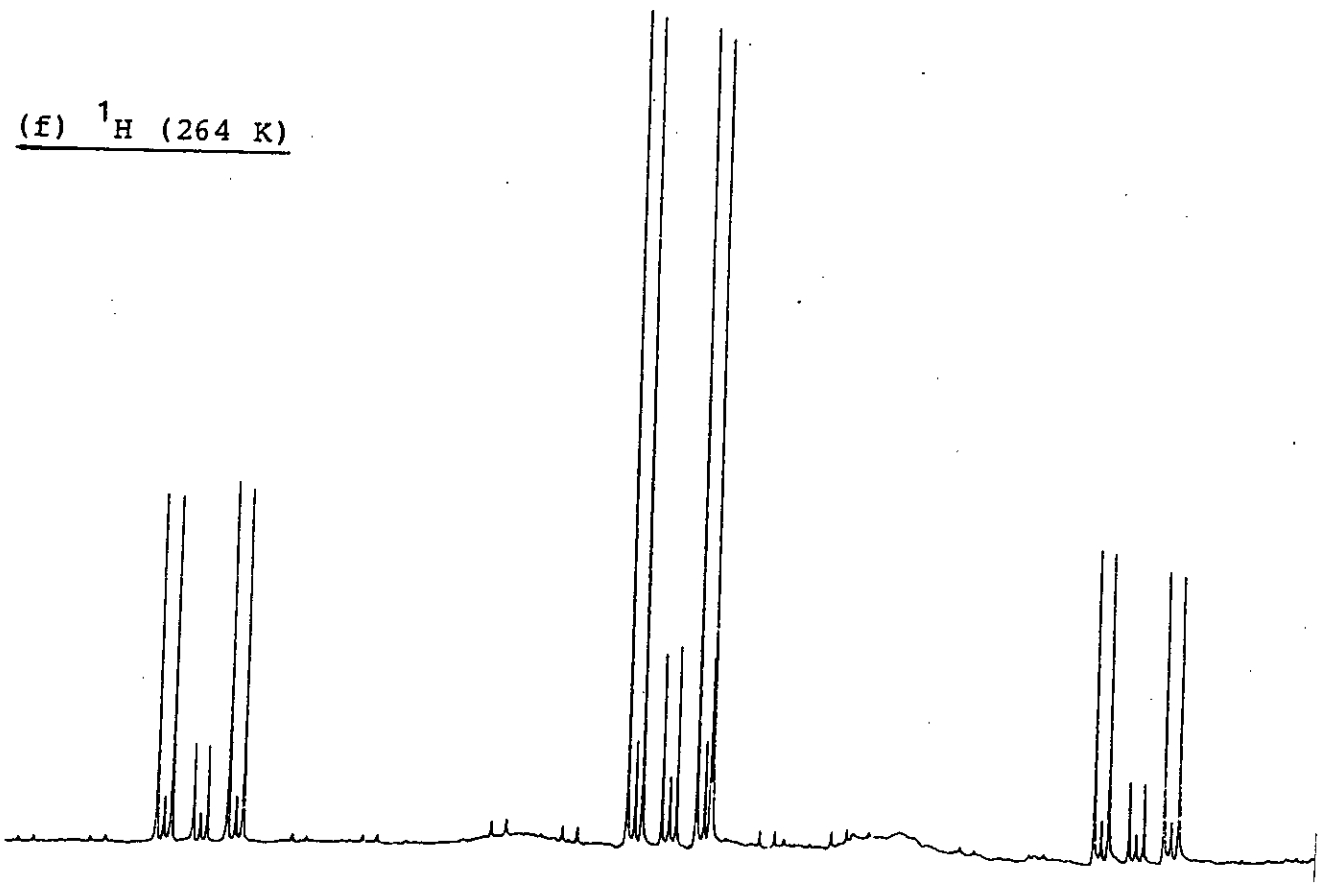

Figure 8.1 (contd.) $^{15}N\{^{1}H\}$ Double Resonance Experiment

(i) No irradiation

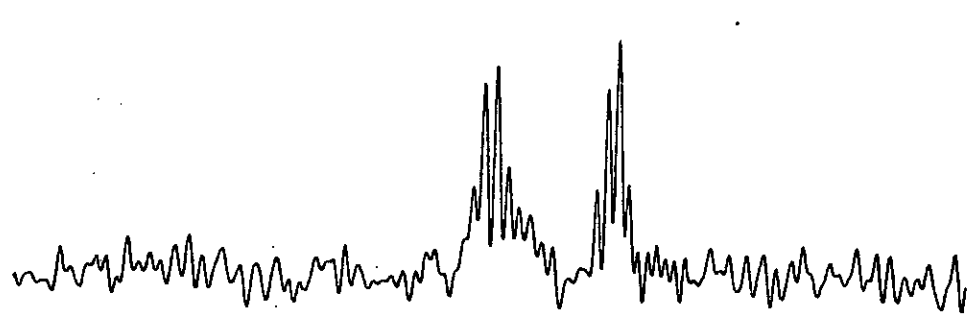

(ii) Irradiating on Peak 3 in ^{1}H spectrum

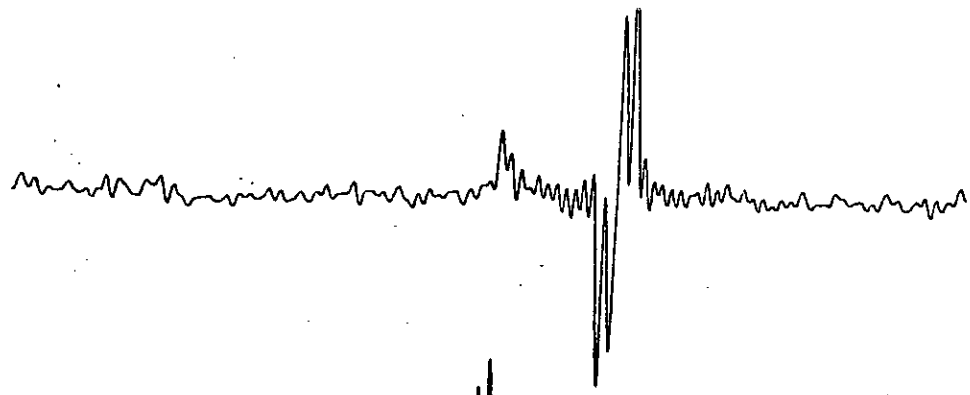

(iii) Irradiating on Peak 2 in ^{1}H spectrum

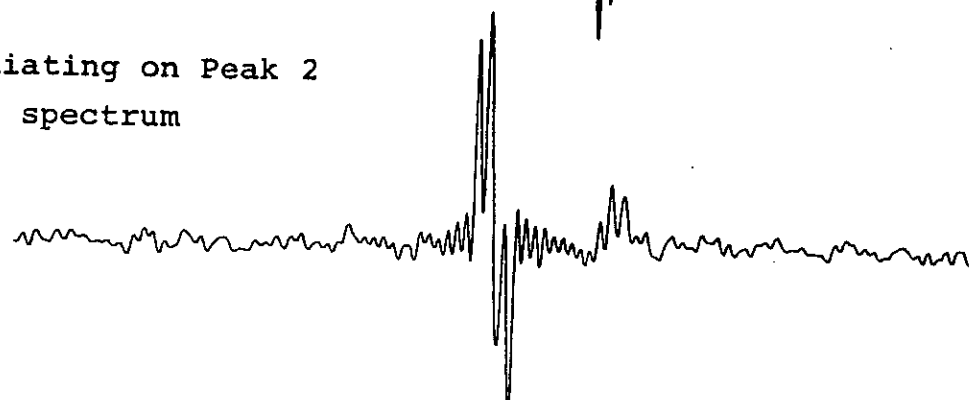

(iv) Irradiating on Peak 1 in ^{1}H spectrum

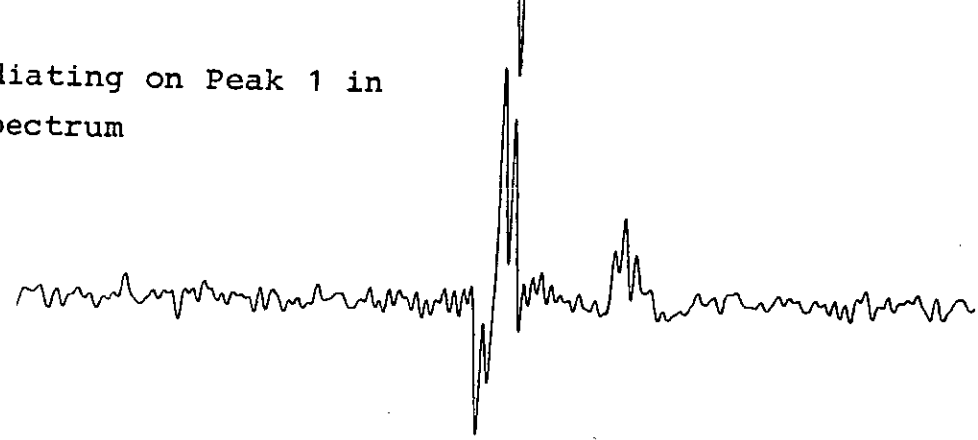

Figure 8.1 (contd.) $^{13}C\{^{1}H\}$ Double Resonance Experiment

(i) Irradiating on Peak 4 in ^{1}H spectrum

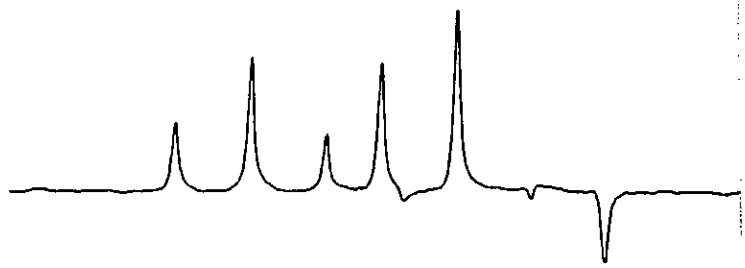

(ii) Irradiating on Peak 3 in ^{1}H spectrum

(iii) Irradiating on Peak 2 in ^{1}H spectrum

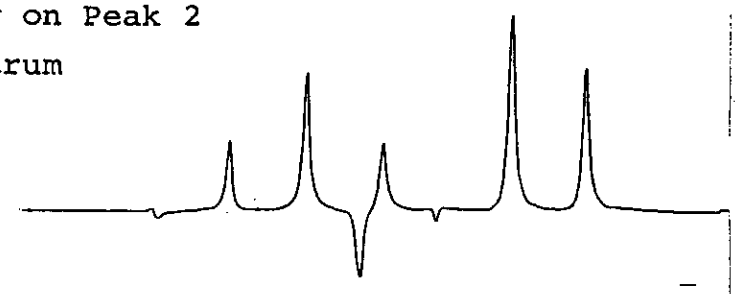

(iv) Irradiating on Peak 1 in ^{1}H spectrum

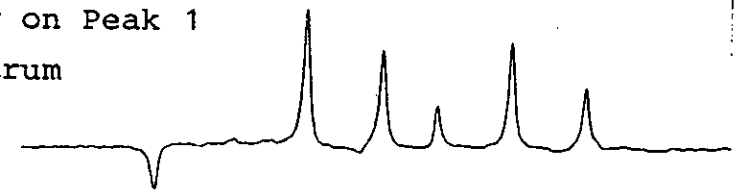

Figure 8.1 (contd.) $^{13}C\{^{1}H\}$ Double Resonance Experiment

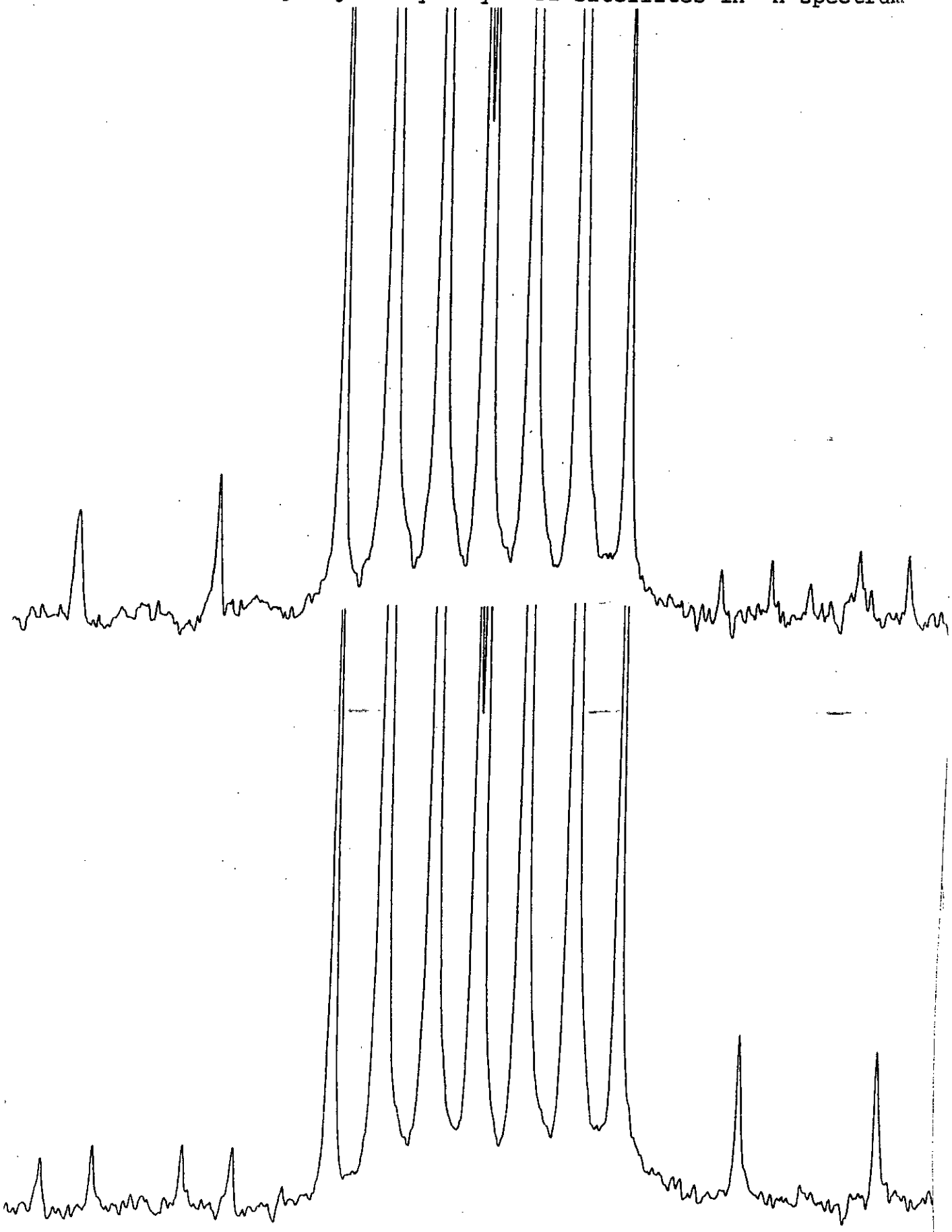

(i) Irradiating high frequency ^{29}Si satellites in ^{1}H spectrum

(ii) Irradiating low frequency ^{29}Si satellites in ^{1}H spectrum

References

1. L. de Broglie, Phil. Mag., 47, (1924), 446.
2. C. Davisson and L.H. Germer, Nature, 119, (1927), 558; Phys. Rev., 30, (1927), 705.
3. G.P. Thomson and A. Reid, Nature, 119 (1927), 890; G.P. Thomson, Proc.Roy.Soc. A., 117 (1928), 600; G.P. Thomson, Proc.Roy.Soc. A., 119 (1928), 651; A. Reid, Proc.Roy.Soc. A., 119 (1928), 663.
4. M. Jammer, "The Conceptual Development of Quantum Mechanics", McGraw-Hill, N.Y., (1966).
5. H. Mark and R. Weirl, Naturwiss., 18 (1930), 205; R. Weirl, Ann.Physik., 8 (1931), 521.
6. F. Trendelenburg, Naturwiss., 8 (1933), 173.
7. P.P. Debye , Phys.Z., 40 (1939), 66; P.P. Debye, Phys.Z., 40 (1939), 404.
8. H. Fetzer, Ph.D. Dissertation, University of Texas, Austin, (1966).
9. D.A. Swick and J. Kasle, Abstract American Crys. Ass., Annual Conf., (1964).
10. Molecular Structure by Diffraction Methods, Vol. 6, (1978), The Chem. Soc. Specialist Periodical Reports.
11. R.E. Hilderbrandt, Ph.D. Thesis. Cornell University, 1969.
12. B. Cagnac and J.C. Pebay-Peyroula, "Modern Atomic Physics - Fundamental Principles", MacMillan, London (1975).
13. P.M. Morse, Phys.Z., 33 (1932), 443.
14. R.A. Bonham, J.Chem.Phys., 36 (1962), 3260.
15. E. Rutherford, Phil.Mag., 21 (1911), 669.
16. P. Debye, Ann.Physik., 46 (1915), 809; P. Debye, Phys. Z., 31 (1930), 419.

17. P. Ehrenfest, Amsterdam Acad., 23 (1915), 1132.

18. M. Born, Z. Physik., 38 (1926), 803.

19. V. Schomaker and R. Glauber, Nature, 170 (1952), 290; R. Glauber and V. Schomaker, Phys.Rev., 89 (1953), 667.

20. H. Faxen and J. Holtsmark, Z. Physik., 45 (1927), 307.

21. E. Schroedinger, Ann.Physik., 79 (1926), 372; 734.

22. Molecular Structure by Diffraction Methods, Vol. 1 (1972), The Chem.Soc. Specialist Periodical Reports.

23. M. Davis, "Electron Diffraction in Gases", Marcel Dekker, (1971).

24. L.S. Bartell, J.Chem.Phys., 23 (1955), 1219.

25. P.M. Morse, Phys.Rev., 34 (1929), 57.

26. J. Karle and R.A. Bonham, J.Chem.Phys., 40 (1964), 1396; J. Peacher and J.C. Wills, J.Chem.Phys., 46 (1967), 4809; H.L. Cox and R.A. Bonham, J.Chem.Phys., 47 (1967), 2599.

27. L. Schafer, A.C. Yates and R.A. Bonham, J.Chem.Phys., 55 (1971), 3055.

28. L. Pauling and L.O. Brockway, J.Am.Chem.Soc., 57 (1935), 2684.

29. P. Debye, J.Chem.Phys., 9 (1941), 55.

30. V.P. Spiridinov, Z.G. Maimin and A.G. Gershikov, Chem.Phys.Letters, 65 (1979), 89; V.S. Luytsarev, V.P. Spiridinov and B.S. Butayev, J.Mol.Struc., 101 (1983),173

31. "Molecular Structure by Diffraction Methods", Vol. 3 (1974), The Chem.Soc. Specialist Periodical Reports.

32. B. Beagley, A.H. Clark and T.G. Hewitt, J.Chem.Soc. A, (1968), 658.

33. W.V.F. Brooks, S.J. Cyvin and P.C. Kvande, J.Phys.Chem., 69, (1965), 1489.; T. Iijima, M. Kimura and K. Tamagawa, J.Mol.Struc., 36, (1976), 243.

34. I. Hargittai, J.Mol.Struc., 100 (1983), 129.

35. S.H. Bauer, J.Am.Chem.Soc., 59 (1937), 1096.

36. R.L. Hilderbrandt and S.H. Bauer, J.Mol.Struc., 3 (1969), 325.

37. S. Cradock, J. Koprowski and D.W.H. Rankin, J.Mol.Struc., 77 (1981), 113.

38. D.M. Bridges, J.M. Freeman, G.C. Holywell and D.W.H. Rankin, J.Organomet.Chem., 32 (1971), 87.

39. B. Beagley, J.M. Freeman, G.C. Holywell and D.W.H. Rankin, J.Chem.Soc. A., (1971), 785.

40. M.G. Cox and J.G. Hayes, Report NAC26, Nat.Phys.Lab., (1973).

41. Y. Murato and Y. Morino, Acta.Cryst., 20 (1966), 605.

42. K. Kuchitsu, "Molecular Structures and Vibrations", Chapt. 10, Ed., S.J. Cyvin, Elsevier (1972), Amsterdam.

43. L.S. Bartell and L.O. Brockway, J.Appl.Phys., 24 (1953), 656; 1523.

44. S.H. Bauer, J.Chem.Phys., 18 (1950), 27.

45. L. Acha, E.R. Cromie and D.W.H. Rankin, J.Mol.Struc., 73 (1981), 111.

46. A.H. Clark, B. Beagley, D.W.J. Cruikshank and T.G. Hewitt, J.Chem.Soc. A., (1970), 872.

47. D.E.J. Arnold and D.W.H. Rankin, J.Fluor.Chem., 2 (1972),405.

48. D.W.H. Rankin and S.J. Cyvin, J.Chem.Soc. Dalton, (1972), 1277.

49. Y. Morino, Acta Cryst., 13 (1960), 1107; O. Bastiansen and M. Traette berg, Acta Cryst., 13 (1960), 1108.

50. D.W.H. Rankin, J.Mol.Struc., 97 (1983), 129.

51. K. Kuchitsu and S. Konaka, J.Chem.Phys., 45 (1966), 4342.

52. K. Kuchitsu, J.P. Guillory and L.S. Bartell, J.Chem.Phys., 49, (1968), 2488.

53. Y. Morino, K. Kuchitsu, Y. Mori and M. Tanimoto, Bull.Chem.Soc. Japan, 41 (1968), 2349.

54. K. Kuchitsu, T. Fukuyama and Y. Morino, J.Mol.Struct., 1 (1968), 463.

55. E.J. Jacob, H.B. Thompson and L.S. Bartell, J.Mol.Struc., 8 (1971), 383.

56. S. Tsuchiya and T. Iijima, J.Mol.Struc., 13 (1972), 327.

57. S.J. Cyvin (ed.), "Molecular Structures and Vibrations", Elsevier (1972), Amsterdam.

58. F. Reinitzer, Monatsh., 9 (1888), 421.

59. O. Lehmann, "Flussige Kristalle", Engelmann (1904), Leipzig.

60. G. Friedel, Ann.Phys., 18 (1922), 273.

61. E. Bose, Z.Physik, 10 (1909), 32.

62. H. Zocher, Trans.Faraday Soc., 29 (1933), 945.

63. G.R. Luckhurst, Mol.Cryst., 2 (1967), 363.

64. W. Maier, Z.Naturforsch, 2a (1947), 458.

65. W.M. Gelbart, J.Phys.Chem., 86 (1982), 4298.

66. G. Meier, E. Sackmann and J.G. Grabmeier, "Applications of Liquid Crystals", Springer-Verlag (1975), Berlin.

67. A.D. Buckingham and J.A. Pople, Trans.Faraday Soc., 59 (1963), 2421.

68. P. Ducros, Bull.Soc. Franc.Min.Crys., 83 (1960), 85.

69. A. Saupe and G. Englert, Phys.Rev.Letts., 11 (1963), 462.

70. G. Englert and A. Saupe, Z.Naturforsch, 19a (1964), 172.

71. G.S. Laurenson, Ph.D. Thesis, University of Edinburgh (1983).

72. P.D. Blair and D.W.H. Rankin, unpublished observations.

73. G.W. Gray, "Advances in Liquid Crystal Materials for Applications", (1978), B.D.H. Chemicals Ltd.

74. P. Diehl, "Nuclear Magnetic Resonance", Chapt. 12, Vol.5, (1975), The Chem.Soc. Specialist Periodical Reports.

75. J. Bulthuis and C. MacLean, Chem.Phys.Lett., 7 (1970), 242.

76. P. Diehl, H. Bosiger and H. Zimmerman, J.Mag.Res., 33 (1979), 113.

77. J.W. Elmsley and J.C. Lindon, Mol.Phys., 29 (1975), 2; 531.

78. P. Diehl, J. Jokisaari and F. Moia, J.Mol.Struc., 96 (1982), 107.

79. E.E. Burnell, J.R. Council and S.E. Ulrich, Chem.Phys. Letts., 31 (1975), 295.

80. P. Diehl, M. Reinhold, A.S. Tracey and E. Wullschleger, Mol.Phys., 30 (1975), 1781.

81. P.K. Bhattacharyya and B.P. Dailey, Mol.Phys., 26 (1973),137

82. P.K. Bhattacharyya and B.P. Dailey, J.Mag.Res., 13 (1974), 317.

83. J. Jokisaari, T. Vaananen and J. Lounila, Mol.Phys., 45 (1982), 141.

84. T. Vaananen, J. Jokisaari and J. Lounila, J.Mag.Res., 49 (1982), 73.

85. T. Vaananen, J. Jokisaari, A. Kaariainen and J. Lounila, J.Mol.Struc., 102 (1983), 175.

86. G. Dombi, J. Amrein and P. Diehl, Org.Mag.Res., 13 (1980), 224.

87. A. Saupe, Mol.Crys., 1 (1966), 527.

88. J.C. Robertson, C.T. Yim and D.F.R. Gilson, Can.J.Chem., 49 (1971), 2345.

89. L.C. Snyder and E.W. Anderson, J.Am.Chem.Soc., 86 (1964), 5023.

90. L.C. Snyder, J.Chem.Phys., 43 (1965), 4041.

91. A. Saupe, G. Englert and A. Pouh, Adv. in Chem. Series, 3 (1967), 51.

92. A. Saupe, Z.Naturforsch, 19a (1964), 161.

93. J.W. Emsley, Private correspondence, (1983).

94. J.W. Emsley and J.C. Lindon, "N.M.R. Spectroscopy using Liquid Crystal Solvents", (1975), Pergamon Press.

95. P. Diehl and C.L. Khetrapal, "N.M.R. Studies of Molecules Oriented in the Nematic Phase of Liquid Crystals".

96. B.P. Dailey and N. Zumbulyadis, Mol.Phys., 26 (1973), 777.

97. D.W.H. Rankin, personal communication (1983).

98. J.I. Musher, J.Chem.Phys., 46 (1967), 1537.

99. C.M. Woodman, Mol.Phys., 13 (1967), 365.

100. P.K. Bhattacharyya and B.P. Dailey, Mol.Phys., 28 (1974), 209.

101. I.W. Anderson, J.E. Bentham and D.W.H. Rankin, J.C.S. Dalton (1973), 1215.

102. J.A. Pople and D.P. Santry, Mol.Phys., 8 (1964), 1.

103. A.V. Cunliffe, E.G. Finer, R.K. Harris and D.D. Elleman, Mol.Phys., 12 (1967), 497.

104. D.L. Van der Hart and H.S. Gutowsky, J.Chem.Phys., 50 (1969), 1058.

105. B. Pedersen, J. Schaug and H. Hopf, Acta.Chem.Scand., 28 (1974), 846.

106. P. Diehl, S. Sykora and J. Vogt, J.Mag.Res., 19 (1975), 67.

107. D.S. Stephenson and G. Binsch, "DAVINS", Q.C.P.E., Indiana University.

108. R. Poupko, Z. Luz and H. Zimmerman, J.Am.Chem.Soc., 104, (1982), 5307.

109. P. Diehl, T. Bjorholm and H. Bösiger, J.Mag.Res., 42 (1981), 390.

110. J. Courtieu, D.W. Alderman and D.M. Grant, J.Am.Chem.Soc., 103, (1981), 6783.

111. A. Saupe, Z.Naturforsch., 20a (1965), 572.

112. G.R. Luckhurst, Quart.Rev., 22 (1968), 179.

113. "Nuclear Magnetic Resonance", Vol. 1,3,5,7, The Chem.Soc. Specialist Periodical Reports.

114. P. Diehl, S. Sykora, W. Niederberger and E.E. Burnell, J.Mag.Res., 14 (1974), 260.

115. L.C. Snyder and E.W. Anderson, J.Chem.Phys., 42 (1965), 3336.

116. R. Ditchfield and L.C. Snyder, J.Chem.Phys., 56 (1972), 5823.

117. J. Bulthuis and C.A. de Lange, J.Mag.Res., 14 (1974), 13.

118. P. Diehl, S. Sykora and E. Wullschleger, Mol.Phys., 29 (1975), 305.

119. S. Meiboom, R.C. Hewitt and L.C. Snyder, Pure Appl. Chem., 32 (1972), 251.

120. C.W. Haigh and S. Sykes, Chem.Phys.Letts., 19 (1973), 571.

121. T.R. Krugh and R.A. Bernheim, J.Am.Chem.Soc., 91 (1969), 2385.

122. J. Gerritsen and C. MacLean, Rec.Trav.Chim., 91 (1972), 1393.

123. N. Suryaprakash, A.C. Kunwar and C.L. Khetrapal, J.Mol.Struc., 101 (1983), 121.

124. A.S.F. Boyd, G.S. Laurenson and D.W.H. Rankin, J.Mol.Struc., 71 (1981), 217.

125. T. Vaananen, J. Jokisaari and J. Lounila, J.Mag.Res., 54 (1983), 436.

126. W.G. Richards and J.A. Horsley, "Ab Initio Molecular Orbital Calculations for Chemists", Oxford Sci.Res. Papers (1970), Oxford.

127. M. Born and J.R. Oppenheimer, Ann.Physik., 84 (1927), 457.

128. P.R. Bunker, J.Mol.Spec., 42 (1972), 478.

129. E.W. Ng, L.S. Su and R.A. Bonham, J.Chem.Phys., 50 (1969), 2038.

130. A.R. Hoy, G. Strey and I.M. Mills, Mol.Phys., 24 (1972), 1265.

131. K. Kuchitsu and L.S. Bartell, J.Chem.Phys., 35 (1961), 1945.

132. K. Kuchitsu, J.Chem.Phys., 44 (1966), 906.

133. Y. Morino, S.J. Cyvin, K. Kuchitsu and T. Iijima, J.Chem.Phys., 36 (1962), 1109.

134. Y. Morino, K. Kuchitsu and T. Oka, J.Chem.Phys., 36 (1962), 1108.

135. L.S. Bartell and K. Kuchitsu, J.Chem.Phys., 68 (1978), 1213.

136. L.S. Bartell and K. Kuchitsu, J.Chem.Phys., 71 (1979), 1039.

137. L.S. Bartell, J.Chem.Phys., 70 (1979), 4581.

138. L.S. Bartell, S.K. Down and S.R. Goates, J.Chem.Phys., 70 (1979), 4585.

139. R. Stolevik, H.M. Seip and S.J. Cyvin, Chem.Phys. Letts., 15 (1972), 263.

140. A.G. Gershikov and V.P. Spiridinov, J.Mol.Struc., 75 (1981), 291.

141. E.E. Burnell, M.A.J. Sweeney and T.C. Wong, Chem.Phys.Letts., 39 (1976), 489.

142. A.D. Buckingham, E.E. Burnell and C.A. de Lange, Mol.Phys., 16 (1969), 299.

143. E.E. Burnell and C.A. de Lange, J.Mag.Res., 39 (1980), 461.

144. J.W. Emsley and G.R. Luckhurst, Mol.Phys., 41 (1980), 19.

145. N.J.D. Lucas, Mol.Phys., 22 (1971), 147; 233; Mol.Phys., 23 (1972), 825.

146. S. Sykora, J. Vogt, H. Bosiger and P. Diehl, J.Mag.Res., 36 (1979), 53.

147. P. Diehl and W. Niederberger, J.Mag.Res., 9 (1973), 495.

148. R. Chang, "Basic Principles of Spectroscopy", McGraw-Hill (1971), New York.

149. S.J. Cyvin, "Molecular Vibrations and Mean Square Amplitudes", Elsevier (1968), Amsterdam.

150. W.D. Gwinn, J.Chem.Phys., 55 (1971), 477.

151. K. Kuchitsu, Bull.Chem.Soc. Japan, 40 (1967), 498.

152. M. Nakata, K. Kohata, T. Fukuyama and K. Kuchitsu, J.Mol.Spec., 83 (1980), 105.

153. M. Nakata, S. Yamamoto, T. Fukuyama and K. Kuchitsu, J.Mol.Struc., 100 (1983), 143.

154. S. Cradock, G.S. Laurenson and D.W.H. Rankin, J.C.S. Dalton, (1981), 187.

155. J.H. Schachtschneider and R.G. Snyder, Spec.Acta, 19 (1963), 17.

156. R.L. Hiderbrandt and J.D. Wieser, J.Chem.Phys., 55 (1971), 4648.

157. G.C. Holywell and D.W.H. Rankin, J.Mol.Struc., 9 (1971), 11.

158.

159. R.W. Rudolph, R.C. Taylor and R.W. Parry, J.Am.Chem.Soc., 88 (1966), 3729.

160. G.G. Flaskerud, R.E. Pullen and J.M. Shreeve, Inorg.Chem., 8 (1969), 728.

161. E.L. Mutterties (ed.), Inorg.Synth., 10 (1967), 150.

162. H.S. Booth (Ed.), Inorg.Synth., 1 (1939), 150.

163. R.S. Reid, Chemistry IV Project, University of Edinburgh (1974).

164. N. Zumburlyadis and B.P. Dailey, Mol.Phys., 26 (1973), 777.

165. S. Cradock, E.A.V. Ebsworth, M.L. McConnell, D.W.H. Rankin, and M.R. Todd, J.C.S. Dalton, (1977), 1925.

166. P.L. Lee, K. Cohn and R.H. Schwendeman, Inorg.Chem., 11 (1972), 1917.

167. H.H. Anderson, J.Am.Chem.Soc., 69 (1947), 2495.

168. A. Murray and D.L. Williams, "Organic Syntheses with Isotopes", Interscience, 1 (1958), 574.

169. W.C. Hamilton, Acta Crys., 18 (1965), 502.

170. E.E. Haley and J.P. Lambooy, J.Am.Chem.Soc., 76 (1954), 2926.

171. K. Hedberg, J.Am.Chem.Soc., 77 (1955), 6491.

172. B. Beagley and A.R. Conrad, Trans.Far.Soc., 66 (1970), 2740.

173. J.D. Murdoch, D.W.H. Rankin and B. Beagley, J.Mol.Struc., 31 (1976), 291.

174. A.H. Brittain, J.E. Smith, P.L. Lee, K. Cohn and R.H. Schwendeman, J.Am.Chem.Soc., 93 (1971), 6772.

175. V. Schomaker and D.P. Stevenson, J.Am.Chem.Soc., 63 (1941), 37.

176. L. Pauling, "The Nature of the Chemical Bond", Cornell University Press (1960).

177. D.W.J. Cruikshank, J.Chem.Soc., (1961), 5486.

178. P. Paybutt, M.F. Guest and I.H. Hillier, Proc.Roy.Soc., London, A, (1973), 333.

179. C. Glidewell and H.D. Holden, J.Mol.Struc., 89 (1982), 325.

180. A. Wynd, Fourth Year Project, University of Edinburgh, (1983).

181. C.R. Nave and J. Sheridan, J.Mol.Struc., 15 (1973), 391.

182. L.F. Centofanti and R.W. Parry, Inorg.Chem., 9 (1970), 744.

183. D.W.W. Anderson, E.A.V. Ebsworth, G.D. Meikle and D.W.H. Rankin, Mol.Phys., 25 (1973), 381.

184. S.D. Ross, "Inorganic Infra-red and Raman Spectra", McGraw-Hill, London (1972).

185. R.L. Kuczkowski, J.Am.Chem.Soc., 90 (1968), 1705.

186. L.S. Bartell and K.W. Hansen, Inorg.Chem., 4 (1965), 1777.

187. L.S. Bartell, J.Chem.Phys., 32 (1960), 827.

188. K. Karakida and K. Kuchitso, Inorg.Chim.Acta, 16 (1976), 29.

189. T. Moritani, K. Kuchitsu and Y. Morino, Inorg.Chem., 10 (1971), 344.

190. E.J. Jacob, D.D. Danielson and S. Samdal, J.Mol.Struc., 62 (1980), 143.

191. L.F. Centofanti and R.L. Kuczkowski, Inorg.Chem., 7 (1968), 2582.

192. Y. Morino, K. Kuchitsu and T. Moritani, Inorg.Chem., 8 (1969), 867.

193. K.W. Hansen and L.S. Bartell, Inorg.Chem., 4 (1965), 1775.

194. P.S. Bryan and R.L. Kuczkowski, Inorg.Chem., 11 (1972), 553.

195. J.F. Durig, B.A. Hudgens, Y.S. Li and J.D. Odom, J.Chem.Phys., 61 (1974), 4390.

196. C.A. Burrus, J.Chem.Phys., 28 (1958), 427.

197. L.S. Bartell, J.Chem.Phys., 32 (1960), 832.

198. C. Glidewell, P.M. Pinder, A.G. Robiette and G.M. Sheldrick, J.C.S. Dalton, (1972), 1402.

199. I. Yang, C. Britt, A. Cowley and J. Boggs, J.Chem.Phys., 48 (1968), 812.

200. J.R. Durig, L.A. Carreira and J.D. Odom, J.Am.Chem.Soc., 96 (1974), 2688.

201. B. Beagley, A.R. Conrad, J.M. Freeman, J.J. Monaghan, B.G. Norton and G.C. Holywell, J.Mol.Struc., 11 (1972), 371.

202. G. Fritz and D. Kummer, Z.Anorg.Chem., 308 (1961), 105.

203. H.R. Linton and E.R. Nixon, Spec.Acta., 10 (1958), 299.

204. A.J. Careless and H.W. Kroto, J.Mol.Spec., 57 (1975), 198.

205. M. Barrow, Private Correspondence, (1979).

206. R.W. Kilb and L. Pierce, J.Chem.Phys., 27 (1957), 108.

207. J.S. Muenter and V.S. Laurie, J.Chem.Phys., 39 (1963), 1181.

208. S. Cradock, A. Fraser and D.W.H. Rankin, J.Mol.Struc., 71 (1981), 209.

209. N. Muller and R.C. Bracken, J.Chem.Phys., 32 (1960), 1577.

APPENDIX I

COMPUTING

(i) Example of a mathematical model routine called by the E.D. structural refinement program. COORD calculates the atomic co-ordinates, utilising a standard routine M80MX2. EXTRA calculates the dipolar coupling for each atom pair.

(ii) This routine utilises a Spline Function Algorithm to automatically subtract a background from the Electron Diffraction molecular scattering intensity curve. It has been incorporated in the E.D. refinement program as command 59.

(i)

```
      SUBROUTINE COORD(X,Y,Z)
C  MODEL FOR PF2NCO
C
C PARAMS   1     2     3     4      5      6     7     8      9
C         P-F   P-N   C-N   C-O   <FPF   <FPN   <PNC   <NCO   TORSION
C
C ATOMS    1     2,3    4     5     6
C
C          P      F     N     C     O
C
      IMPLICIT REAL*8(A-H,O-Z)
      REAL*4 RM
      COMMON/M80/PAR(20),R(100),RM(100),U(100)
      DIMENSION X(50),Y(50),Z(50)
      PI=3.141593
      RAD=PI/180.
      A5=PAR(5)*RAD
      A6=PAR(6)*RAD
      A7=PAR(7)*RAD
      A8=PAR(8)*RAD
      A9=PAR(9)*RAD
      CALL M80MX2(PAR(2),PAR(1),A6,A5,0.,0.,A9,1.,X,Y,Z)
      X(5)=-PAR(3)*DCOS(PI-A7)
      Y(5)=-PAR(3)*DSIN(PI-A7)
      X(6)=-PAR(3)*DCOS(PI-A7)-PAR(4)*DCOS(2*PI-A7-A8)
      Y(6)=-PAR(3)*DSIN(PI-A7)-PAR(4)*DSIN(2*PI-A7-A8)
      END


      SUBROUTINE EXTRA(X,Y,Z,E)
C
C     COUPLINGS
C      1     2     3     4     5     6     7
C      FF    FP    FC    FN    CP    CN    PN
C
C     PAR  1       2       3
C       Szz    Sxx-yy    Sxy
C
      IMPLICIT REAL*8(A-H,O-Z)
      REAL*4 RM
      COMMON/M80/PAR(20),R(100),RM(100),U(100)
      DIMENSION E(20),X(50),Y(50),Z(50),S(5),G(50)
      G(1)=9.919D1
      G(2)=2.30509D2
      G(3)=G(2)
      G(4)=-2.4832D1
      G(5)=6.1605D1
      S(1)=PAR(10)
      S(2)=PAR(11)
      S(5)=PAR(12)
      S(3)=0.0D0
      S(4)=0.0D0
      E(1)=ED8ONA(X,Y,Z,G,S,2,3)
      E(2)=ED8ONA(X,Y,Z,G,S,1,2)
      E(3)=ED8ONA(X,Y,Z,G,S,2,4)
      E(4)=ED8ONA(X,Y,Z,G,S,1,4)
      RETURN
      END


      DOUBLE PRECISION FUNCTION ED8ONA(X,Y,Z,G,S,I,J)
C  Calculates dipolar coupling between atoms I and J
C
      IMPLICIT REAL*8 (A-H,O-Z)
      DIMENSION X(50),Y(50),Z(50),S(5),G(50)
      R=DSQRT((X(I)-X(J))**2+(Y(I)-Y(J))**2+(Z(I)-Z(J))**2)
      CX=(X(I)-X(J))/R
      CY=(Y(I)-Y(J))/R
      CZ=(Z(I)-Z(J))/R
      ED8ONA=-G(I)*G(J)*(S(1)*(3.0D0*CZ*CZ-1.0D0)+S(2)*(CX*CX-CY*CY)
     £+2.0D0*S(3)*CX*CZ+2.0D0*S(4)*CY*CZ+2.0D0*S(5)*CX*CY)/R**3
      RETURN
      END
```

(ii)

```
C Subtract Automatic Background (Spline)
  590 CALL FFRMPT('Data set no.:',13)
      READ(5,6002)I
      IF(I.LE.2)GO TO 10
      IF(I.LE.NDS)GO TO 591
      WRITE(6,7002)I
      GO TO 590
  591 ION=SMIN(I)/DELS(I)-0.01
      IOFF=SMAX(I)/DELS(I)-0.01
      DO 1115 III=1,NR
      MI(III)=NK(MI(III))
 1115 MJ(III)=NK(MJ(III))
      CALL ED80RB(PA,PB,PC,PD)
      DO 1112 III=1,50
      X(III)=0.
      Y(III)=0.
      Z(III)=0.
 1112 CONTINUE
      CALL COORD(X,Y,Z)
      DO 1113 III=1,NR
      R(III)=ED80RJ(MI,MJ,X,Y,Z,M24,U,PK,III)
 1113 CONTINUE
      NM=IOFF-ION+1
      SC=DABS(SCF(I))
      S=SMIN(I)
      NCAP=7
      DO 1111 J=ION,IOFF
      TIS(J)=0
      L=S*S+1.0001
      DO 2222 KK=1,NR
      IF(ANR(KK).LT.0.001)ANR(KK)=0.
      ANR(KK)=ANR(KK)*U(KK)**4/6
      A=1
      IF(MI(KK).EQ.MJ(KK))GO TO 1114
      A=DCOS(PA(KK)+S*PB(KK)+S**2*PC(KK)+S**3*PD(KK))
 1114 TC(KK)=S*(R(KK)-ANR(KK)*S*S)
      BB=S
      IF(M25.NE.1)BB=1.
      TB(KK)=RM(KK)*(SF(1,MI(KK))-SF(L,MI(KK)))*(SF(1,MJ(KK))-
     *SF(L,MJ(KK)))*DEXP(-0.5*S*S*U(KK)**2)/(BB*R(KK))
      TA(KK)=TB(KK)*DSIN(TC(KK))
 2222 TIS(J)=TIS(J)+TA(KK)
      TIS(J)=TIS(J)*SC
      JJJ=J-ION+1
      XX(JJJ)=JJJ
      W(JJJ)=1.0
      EI(I,J)=EI(I,J)/2.
      YY(JJJ)=EI(I,J)-TIS(J)
      S=S-DELS(I)
 1111 CONTINUE
      WRITE(6,1120)(J,EI(I,J),TIS(J),J=ION,IOFF)
 1120 FORMAT(I5,2E20.5)
      MM=NM/5
      TP(5)=MM*0.3
      TP(6)=MM*0.6
      TP(7)=MM
      TP(8)=2*MM
      TP(9)=3*MM
      TP(10)=4*MM
      NCAP2=NCAP+2
      NCAP3=NCAP+3
      NCAP7=NCAP+7
      IFAIL=0
      CALL E02BAF(NM,NCAP7,XX,YY,W,TP,WORK1,WORK2,CCC,SS,IFAIL)
      IF(IFAIL.EQ.0)GO TO 1260
      WRITE(6,1990)IFAIL
 1990 FORMAT('     IFAIL=',I2)
 1260 MIDPT=.FALSE.
      WRITE(3,1996)
      M2=NM*2-1
      II=0
      DO 1340 I2=1,M2
        IF(.NOT.MIDPT)GO TO 1280
        XARG=0.5*(XX(II)+XX(II+1))
        IFAIL=1
        CALL E02BBF(NCAP7,TP,CCC,XARG,FIT,IFAIL)
        IF(IFAIL.NE.0)GO TO 1125
        GO TO 1320
 1125   WRITE(6,1992)XARG
        GO TO 1320
 1280   II=II+1
        IFAIL=1
        CALL E02BBF(NCAP7,TP,CCC,XX(II),FIT,IFAIL)
        IF(IFAIL.NE.0)GO TO 1300
        RES=FIT-YY(II)
        III=II+ION
        EI(I,III)=EI(I,III)-FIT
        WRITE(3,1993)III,EI(I,III),YY(II),FIT,RES
        EI(I,III)=EI(I,III)*2.
        GO TO 1320
 1300   WRITE(6,1994)R,XARG
 1320   MIDPT=.NOT.MIDPT
 1340 CONTINUE
 1992 FORMAT(5H      ,E20.5,' ARGUMENT OUTSIDE RANGE')
 1996 FORMAT('          EI                 XORD                FIT
     #                RES')
 1993 FORMAT(1H ,I3,4E20.5)
 1994 FORMAT(1H ,I3,E20.5,'ARGUMENT OUTSIDE RANGE')
      MDATA=1
```

APPENDIX II

PUBLISHED PAPERS

Journal of Molecular Structure, 97 (1983), 147-151.

COMBINED USE OF DATA FROM LIQUID CRYSTAL N.M.R. AND ELECTRON DIFFRACTION IN STRUCTURAL STUDIES OF FLUOROPHOSPHINE DERIVATIVES

PETER D. BLAIR
Department of Chemistry, University of Edinburgh, West Mains Road, Edinburgh, EH9 3JJ (Scotland)

ABSTRACT

Liquid Crystal Nuclear Magnetic Resonance was used to obtain structural information on certain difluorophosphine pseudohalides. This was combined with data from Electron Diffraction in a joint analysis. Some results are given and problems encountered discussed.

INTRODUCTION

The determination of molecular structure by electron diffraction can sometimes be limited by the overlapping of peaks in the radial distribution curve. This problem manifests itself in the study of the difluorophosphine pseudohalides, particularly in the cases of the isocyanate and the isothiocyanate (see Fig. 1), where several peaks overlap.

Fig. 1. E.D. Radial Distribution Curves
a) Isocyanate b) Isothiocyanate

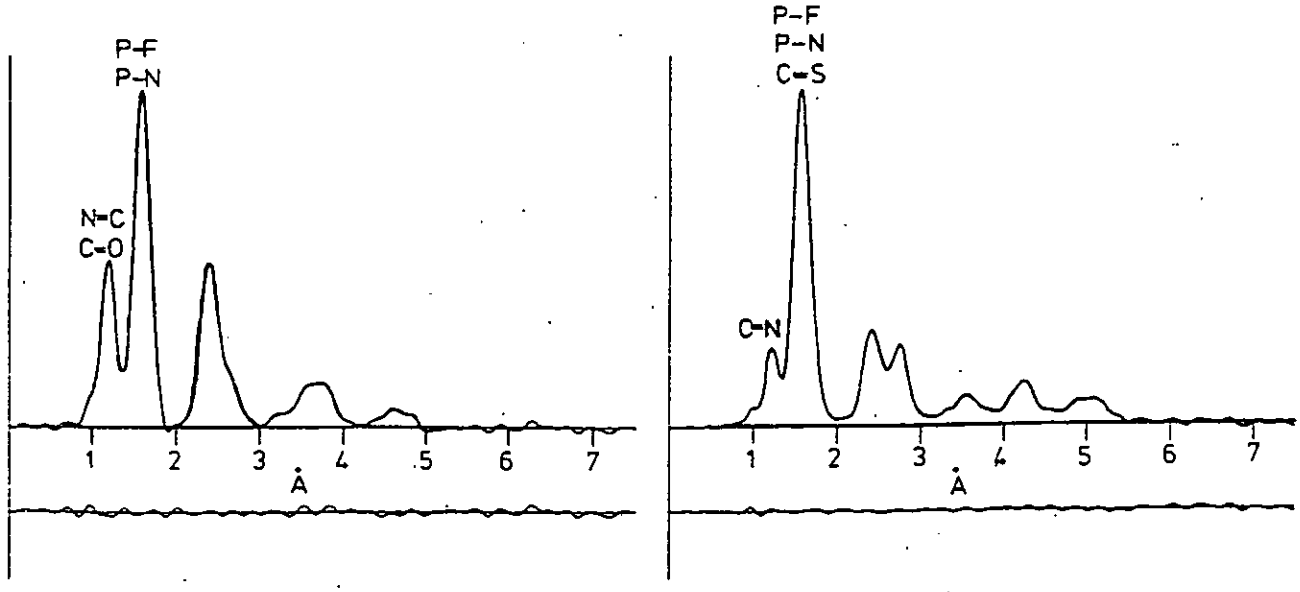

This results in it proving impossible to refine the entire structure and certain parameters have to be fixed at reasonable spectroscopic values (ref.1). This approach is unsatisfactory and it would be preferable to introduce extra structural information from an alternative source; for instance, use of rotational constants determined by microwave spectroscopy is well established (refs. 2,3). More recently it has been shown that structural information from Liquid Crystal N.M.R. can be utilised in a similar fashion (ref.4).

LIQUID CRYSTAL N.M.R.

Molecules dissolved in the nematic phase of a liquid crystal are constrained to align themselves on average in a particular orientation with respect to an applied field. The observable intramolecular couplings are dependant on the respective internuclear vectors, and therefore contain structural information (ref.5).

The difluorophosphine pseudohalides lend themselves to study by this technique because of the possibility of isotopic enrichment of the ^{13}C and ^{15}N nuclei, thus providing four spin-half nuclei (including ^{19}F and ^{31}P).

A total of seven couplings are observed: three parameters are required to define orientation, and therefore four extra pieces of structural information have been obtained.

Spectra were run on the University of Edinburgh Varian XL 100 spectrometer, in the nematic phase at 253K and 293K and in the isotropic phase at 313K. A series of double resonance experiments determined the signs of the couplings.

Fig. 2. The ^{19}F Spectrum of $PF_2{}^{13}C{}^{15}N$ in the Nematic Phase

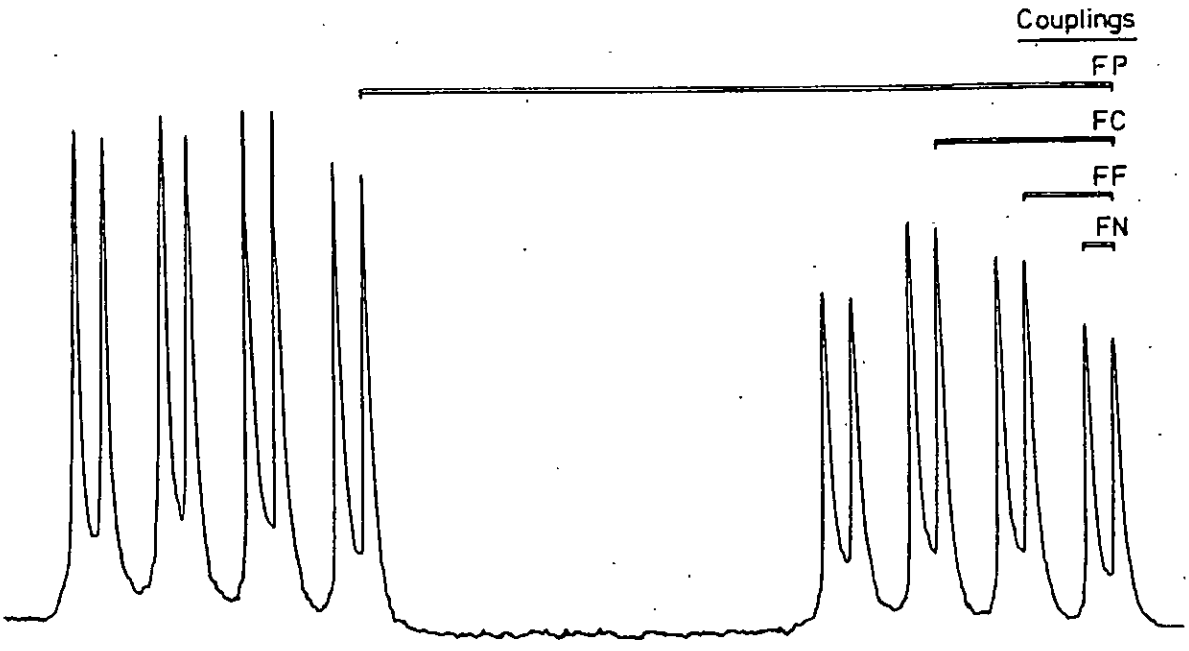

VIBRATIONAL CORRECTIONS

The isocyanate and isothiocyanate each possess a low-frequency, high-amplitude bend and torsion at the nitrogen atom (ref.6). These types of low frequency modes are always troublesome in structural work (ref.7) and in this case it was found that vibrational corrections to the couplings involving these modes seemed unreasonably large (ref.8).

RESULTS

In the case of the isothiocyanate, in the combined analysis it became possible to refine the previously fixed parameter; however it can be seen that the structure obtained is not compatible with that from E.D. data alone (Table 1).

TABLE 1

Structural Parameters for PF_2NCS

	ED	ED + LCNMR
r PF/Å	1.574(2)	1.584(2)
r PN/Å	1.669(5)	1.690(7)
r NC/Å	1.213(2)	1.248(4)
r CS/Å	1.553(F)	1.522(7)
<FPF/°	98.7(4)	98.0(6)
<FPN/°	98.4(4)	96.5(2)
<PNC/°	146.8(9)	138.7(6)

This could be explained by the questionable vibrational corrections and the fact that the refinement was heavily weighted toward the Liquid Crystal data, as is shown by the good agreement between observed and calculated direct couplings (Table 2).

TABLE 2

Direct Couplings for PF_2NCS (Hz)

	Observed	Calculated	Difference
D FF	196.0	195.9	0.1
D FP	33.9	34.0	-0.1
D FC	-76.3	-74.4	-1.9
D FN	75.9	74.2	1.7
D CP	-63.9	-62.2	-1.7
D CN	216.1	217.7	-1.6
D PN	42.1	43.2	-1.0

To attempt to overcome the difficulties associated with the low frequency modes it was decided to ignore the couplings involving ^{13}C in the isocyanate. Under these conditions the definition of the PF and PN band lengths is improve and the highly correlated angles at phosphorus become distinguishable (Table 3

TABLE 3

Structural Parameters for PF_2NCO
(Ignoring ^{13}C couplings)

	ED	ED + LCNMR
r PF/Å	1.572(2)	1.573(1)
r PN/Å	1.680(5)	1.678(4)
r NC/Å	1.219(6)	1.218(6)
r CO/Å	1.174(5)	1.175(5)
<FPF/°	97.6(8)	98.4(5)
<FPN/°	97.4(8)	97.3(3)
<PNC/°	133.1(14)	132.0(12)

DISCUSSION

The results for the isocyanate are promising when the couplings affected by the low frequency vibrational modes are neglected, and show that Liquid Crysta N.M.R. can be a useful source of extra structural information.

However much further attention must be focussed on problems such as

vibrational corrections before this type of combined analysis is standard practice.

REFERENCES

1 D.W.H. Rankin and S.J. Cyvin, J. Chem. Soc., Dalton Trans., (1972), 1277.
2 K. Kuchitsu, T. Fukuyama and Y. Morino, J. Mol. Struct., 1 (1968), 463.
3 E.J. Jacob, M.B. Thompson and L.S. Bartell, J. Mol. Struct., 8 (1971), 383.
4 A.S.F. Boyd, G.S. Laurenson and D.W.H. Rankin, J. Mol. Struct., 71 (1981), 217.
5 J.W. Emsley and J.C. Lindon, "N.M.R. Spectroscopy using Liquid Crystal Solvents".
6 S. Cradock, E.A.V. Ebsworth, M.L. McConnell, D.W.H. Rankin, M.R. Todd, J. Chem. Soc., Dalton Trans., (1977), 1925.
7 A.G. Gershikov and V. Spiridonov, J. Mol. Struct., 75 (1981), 291.
8 N.J.D. Lucas, J. Mol. Phys., 22 (1971), 233.

List of Courses and Conferences Attended

Teaching Quantum Mechanics to Chemists	(5)	Dr. K.P. Lawley
Electronics & Microprocessors	(5)	Mr. A. King
Homogenous Catalysts	(5)	Dr. T.A. Stephenson
Lasers in Chemistry	(5)	Professor R.J. Donovan
Crystallography	(5)	Dr. R.O. Gould

Fourier Transform I.R. Spectroscopy Seminar.

Aspects of Structural Chemistry	(5)	Dr. C. Glidewell

International Conference on Microwave Spectroscopy and Electron Diffraction, Tübingen, Germany - presented paper.

U.S.I.C. Conferences, Galashiels (3 years) - presented paper.